Fall 2011

Two-point bend studies of glass fibers

Zhongzhi Tang

Department: Materials Science and Engineering

TWO-POINT BEND STUDIES OF GLASS FIBERS

by

ZHONGZHI TANG

A DISSERTATION

Presented to the Faculty of the Graduate School of the

MISSOURI UNIVERSITY OF SCIENCE AND TECHNOLOGY

In Partial Fulfillment of the Requirements for the Degree

DOCTOR OF PHILOSOPHY

in

MATERIALS SCIENCE AND ENGINEERING

2011

Approved by

Richard K. Brow, Advisor
Gregory E. Hilmas
Wayne Huebner
Delbert E. Day
Lokeswarappa R. Dharani

PUBLICATION DISSERTATION OPTION

Part of the dissertation has been prepared in the format for publication in peer-reviewed journals. The first paper, 'Two-Point Bend Measurements of Failure Stress of Pristine Glass Fibers,' pages 25-52, was submitted to the *Journal of the American Ceramic Society* in August 2011. The second paper, 'Inert Failure Strain Measurements for Sodium Borate Glass Fibers,' pages 53-74, the third paper, 'Two-Point Bend Studies of Fatigue Effects in Silicate Glasses,' pages 75-112, and the fourth paper, 'Environmental Fatigue of Silicate Glasses in Humid Conditions,' pages 113-140, are to be submitted to the *Journal of Non-Crystalline Solids* in November 2011.

ABSTRACT

The principal objective of this research is to advance our understanding of how glass breaks. Glass, a material well known for its brittleness, has been used widely but within a frustrating limit of its strength. Generally, strength is not considered as an intrinsic property of glass, due to the difficulty of avoiding the presence of flaws on the sample surface. The fiber drawing system and two-point bending (TPB) equipment developed at Missouri S&T allow the fabrication of pristine glass fibers and failure strain measurements while minimizing the effects of strength limiting critical flaws. Several conditions affect the failure behavior of glasses, including glass composition, thermal history of melts and environmental conditions during the failure tests. Understanding how these conditions affect failure helps us understand how glass fails.

In this dissertation, failure strains for many different silicate and borate glasses were measured under a variety of experimental conditions. Failure stresses for various silicate glasses were calculated using values of the nonlinear elastic moduli reported in the literature. Inert intrinsic strengths for alkali silicate glasses were related to the structure and corresponding bond strengths, and the dependence of the inert strengths on faceplate velocity is discussed. Inert failure strains were also obtained for sodium borate glasses. Up to ~40% failure strain was measured for vitreous B_2O_3. The addition of soda to boron oxide increases the dimensionality and connectivity of the glass structure and hence increases its resistance to deformation, as was observed in elasticity and brittleness measurements reported in the literature. The increase in deformation resistance produces lower failure strains, a behavior also seen for alkali silicate and aluminosilicate glasses where the reduction of non-bridging oxygen increases the structure stiffness and leads to lower inert failure strain. Fatigue effects on silicate glasses were studied by measuring the failure strains in water at different temperatures and at different loading rates, and in air with a range of relative humidities. The dominant fatigue reaction for cross-linked network glasses is bond hydrolysis, whereas for alkali modified depolymerized glasses is ion-exchange reaction between alkali ions and water species. The fatigue mechanism difference results in the difference in the humidity sensitivity of the reaction rate. The dominant fatigue reaction also changes at around 50% relative humidity.

ACKNOWLEDGMENTS

My deepest thanks go to my advisor, Dr. Richard K. Brow, who provided opportunity, guidance, inspiration, encouragement and support throughout my entire study and research experience in Missouri University of Science and Technology. I could not ask for a better advisor.

I would like to thank Dr. Charles R. Kurkjian for lending his expertise in glass strength, and for providing advice and assistance in this research. Many thanks to Dr. Mary Reidmeyer. Her wisdom and practical experience has inspired and enlightened me on many occasions. I would also like to thank my committee members, Dr. Gregory E. Hilmas, Dr. Wayne Huebner, Dr. Delbert E. Day and Dr. Lokeswarappa R. Dharani for their time and guidance.

I wish to thank to Dr. Nathan P. Lower, who continuously devoted his time answering questions, giving instructions, and lending help. I wish to thank my lab mates in Dr. Brow's group. They are the best and the funniest colleagues one can wish for. I am also grateful to Ronald E. Haas, Jeff Wight, Brian Porter and other staffs members in the MRC for their technical support.

My sincere gratitude goes to my wife, Yaqin Lin, my parents, and all my friends for their love and support during the past four years.

Finally, I would like to acknowledge the NSF / University / Industry / Center for Glass Research / and the Department of Energy, through a sub-contract with Mo-Sci Corporation for their financial support.

TABLE OF CONTENTS

LIST OF ILLUSTRATIONS

Page

SECTION

PAPER 1

PAPER 2

PAPER 4

APPENDICES

LIST OF TABLES

Page

SECTION

PAPER 1

PAPER 2

PAPER 3

PAPER 4

APPENDICES

1. INTRODUCTION

1.1. OVERVIEW OF GLASS STRENGTH

Glass is found in many applications including windows, containers, insulation, lighting, etc. The transparency, luster and durability of glass have been appreciated for thousands of years [1]. However, the use of glass has been limited by its notorious brittleness. A common experience is to have glass objects that will readily break when subjected to a mechanical or a thermal shock. Typically, the practical strength of a glass is around 14-70 MPa [1], but the theoretical strength of glass is several orders of magnitude higher.

Assuming that glass is a flawless brittle solid, its theoretical strength is the amount of work done in pulling bonds apart and creating two new surfaces, and it was estimated to range from $E/10$ to E/π, where E is Young's modulus [2]. As for fused silica, E = 70 GPa, thus its theoretical strength is from 7 to 22 GPa. However, in the real world, most glasses are not 'flawless'. Practical strength is greatly reduced from its theoretical value due to strength-limiting flaws that form during processing or handling (for example, scratches or dents). In addition, glass strength is reduced due to environmental fatigue effects, which will be discussed later.

1.1.1. Effect of Flaws. Inglis [3] studied the stress concentration of an elliptical-shaped flaw in an infinite plate (Figure 1.1, [3]). He used the theory of elasticity, assuming that the material is linear elastic and obeys Hooke's law everywhere. He found that the maximum local stress depends on the shape and size of the flaw:

$$\sigma_{max} = \sigma_L \times 2\sqrt{c/\rho} \tag{1}$$

where σ_L is the remotely applied stress (GPa) on an infinite plate, σ_{max} is the maximum stress (GPa) at the edge of an elliptical flaw, c is the half crack length (mm) and ρ is the crack tip radius (mm). This equation has its limit when trying to answer such questions:

1) What is the maximum stress at the crack tip when the crack is extremely sharp (when ρ approaches 0)?
2) Why do large cracks tend to grow easier than small cracks?

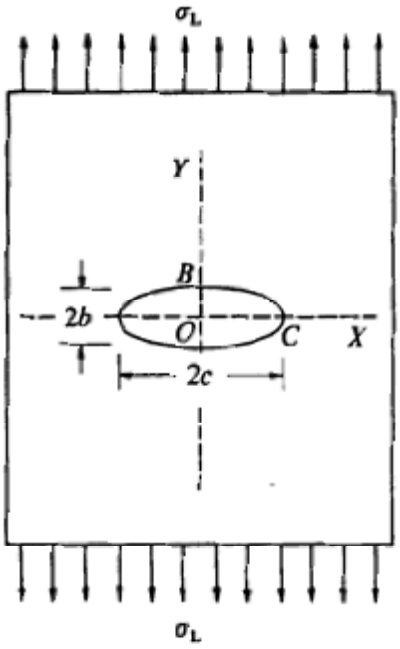

Figure 1.1. Remotely applied tension on an infinite plate with an elliptical-shaped flaw.

Griffith [4] advanced this study and suggested that having a maximum stress at the crack tip exceeding theoretical strength is not a sufficient criterion for failure. He considered energy conservation laws of mechanics and thermodynamics and proposed the energy-balance concept to relate the loss in strain energy to the gain in surface energy (γ, J/mm^2). Assuming an elliptical thorough crack in an infinite plate, Griffith developed his solution for strength (σ, GPa) of a flawed brittle solid:

$$\sigma = \sqrt{2E\gamma/\pi c} \tag{2}$$

in which, E is the Young's modulus (GPa). Since the flaw size c (mm) can vary by several orders of magnitude, the strength of glass was long considered to be an extrinsic property and depended on processing [1] (shown in Table 1.1).

Table 1.1. Typical strength for glass samples based on experience [1].

Sample Condition	Typical Strength
Freshly drawn, pristine fibers	~0.7-10 GPa
Handled fibers	~350-700 MPa
Freshly drawn rods	~70-140 MPa
Abraded rods	~14-35 MPa
Used glass products	~14-70 MPa

Considering a flawed brittle solid, generally, there are three modes (Figure 1.2) of crack-surface displacement used in fracture mechanics: Mode I is an opening (tensile) mode; Mode II is a sliding (in-plane shearing) mode; and Mode III is a tearing (torsional shearing) mode.

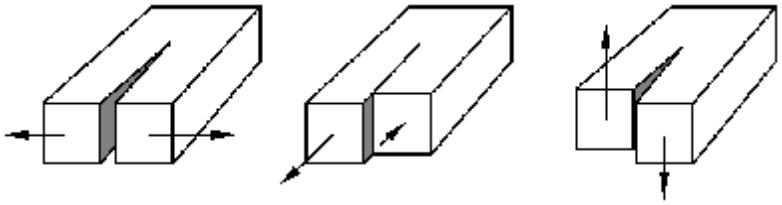

Mode I Mode II Mode III

Figure 1.2. Three modes of crack-surface displacement.

Mode I is the most common load type and its corresponding stress intensity factor is K_I (MPa·m$^{1/2}$). The stress intensity factors are used to predict the stress state (or 'stress intensity') near the crack tip caused by a remote load or residual stresses (σ, MPa):

$$K_I = \sigma\sqrt{\pi c} \tag{3}$$

in which c is the half size of crack (m). When this stress state becomes critical (K_{IC}), the crack will grow at its critical speed and the material will fail. The load at which this

failure occurs is referred to as the fracture strength. Thus, K_{IC} is an important property of a material in fracture mechanics, called fracture toughness. For silicate glasses, a typical value of fracture toughness falls in the range of 0.7 to 0.9 MPa·m$^{1/2}$ [5]. Equation (3) is often used in glass strength estimations. However, the validity of this equation in studies of 'flaw-free' glass samples is questionable.

1.1.2. Conventional Strength Measurement. Many efforts have been made to prepare flaw free glass samples [6]. Freshly drawn glass fibers (tested within hours after formation) are often used because they can be prepared and handled in such a way as to avoid damaging their surfaces (scratches or dents), and so pristine fibers usually give the greatest strength (Table 1.1). Conventional methods of measuring strength of glass include tensile tests [7-10], three-point bend tests [11] and four-point bend tests [12]

In a tensile test, a sample (usually in forms of a fiber or a rod) is gripped at both ends and pulled in tension until it fails. This technique provides information of deformation and applied load, which can be converted to strain and stress, based on the dimension of the sample. However, in a tensile test, the sample must be gripped on both ends and this may damage the sample surfaces causing a decrease in measured strength. Another disadvantage of the tensile test is that the test volume includes the entire length of the fiber between the grips, and this increases the probability of finding critical flaws and increases the scatter in measured values [13]. Three-point bend (Figure 1.3 (a)) and four-point bend tests (Figure 1.3 (b)), if performed on fibers, can significantly reduce the probability of encountering a critical surface defect, due to the smaller volume that is effectively under tension compared to typical tensile tests, but may create strength-limiting critical flaws where the testing fixtures touch the pristine surfaces.

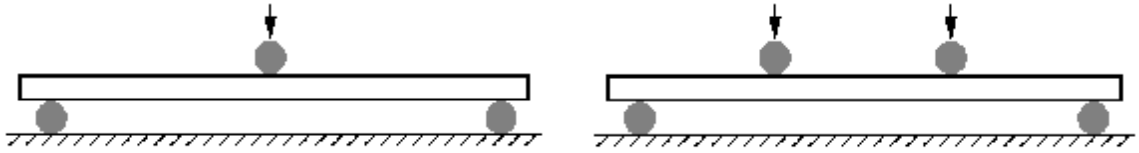

(a) (b)

Figure 1.3. Schematic diagram of (a) a three-point bend test, and (b) a four-point bend test.

1.1.3. Two-Point Bend Failure Strain Measurement. Although the two-point bending (TPB) technique was used as early as 1944 [14], its routine use in testing glass fibers began in 1980 [15]. In a TPB test (Figure 1.4), a section of glass fiber, diameter d (μm), is bent into a U-shape between two parallel faceplates, one of which travels towards the second at a constant faceplate velocity (v_{fp}), compressing the 'U' until failure. The gap distance at failure (D, μm) is recorded, and the failure strain (e_f) is then calculated from [16]:

$$\varepsilon_f = \frac{1.198 \times d}{(D - d)} \tag{4}$$

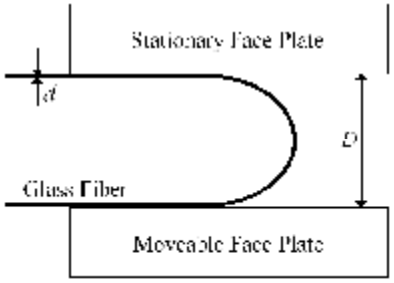

Figure 1.4. Schematic diagram of a two-point bend test.

The TPB test does not require the special grips needed for conventional tensile tests, and the relatively small gauge length (0.3-0.9 mm) in the region of highest tensile stress minimizes the probability of extrinsic flaws [15]. A more detailed gauge length calculation can be found in [16]. The TPB test does not require excessive handling of the glass samples. For example, in three-point bend test, acid-etched or polished samples are often used, whereas, the samples used in a TPB test are freshly-drawn fibers with pristine surfaces (tested within hours without touching the fiber surfaces). TPB can be used to measure the failure strains of pristine glass fibers in inert conditions (immersed in liquid nitrogen). The inert failure strains are considered to be inert intrinsic strength of glass, which is the closest measure of theoretical strength [13].

The application and possibilities of the TPB test are discussed in previous publications [17,18,19,20,21,22]. For example, Lower et al. used TPB to determine the inert intrinsic failure strains for sodium silicate glass (Figure 1.5, [19]) and sodium aluminosilicate glass (Figure 1.6, [20]).

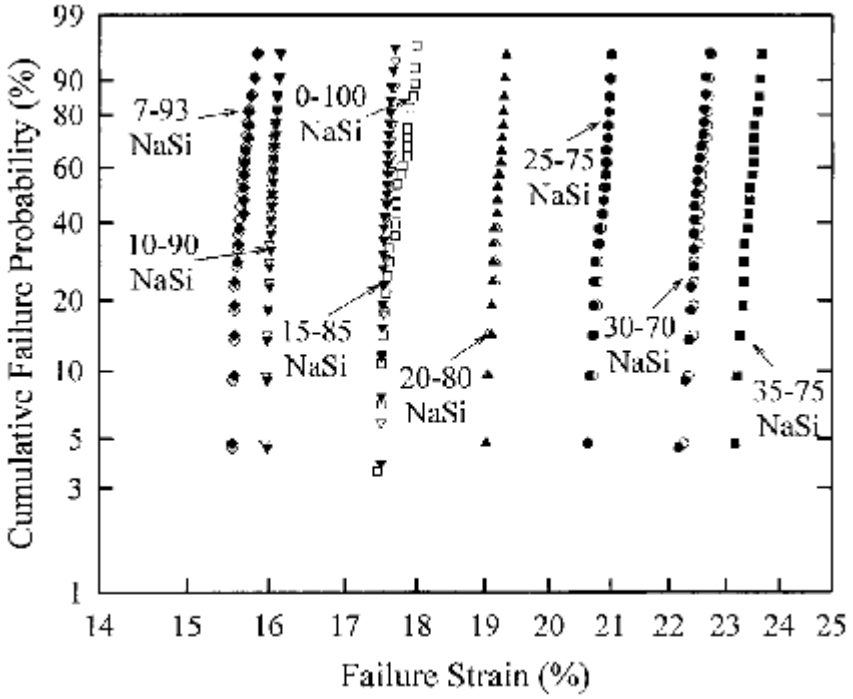

Figure 1.5. Weibull distributions of inert failure strains for sodium silicate glass fibers with compositions of xNa_2O-$ySiO_2$ (x+y=100, in mol%) [19].

These inert failure strains have been related to the silicate glass network [19]. It is interesting to see the compositional dependence of inert failure strains for other glass systems, for example, borate glasses. The study of inert failure strains for different glass systems might generate some general connection between inert intrinsic strength and glass structure.

The TPB test was also used to study the melt history effect [18]. Lower et al. reported that the failure strain distributions for E-glass were dependent on the melt time and temperature prior to the fiber drawing (shown in Figure 1.7)

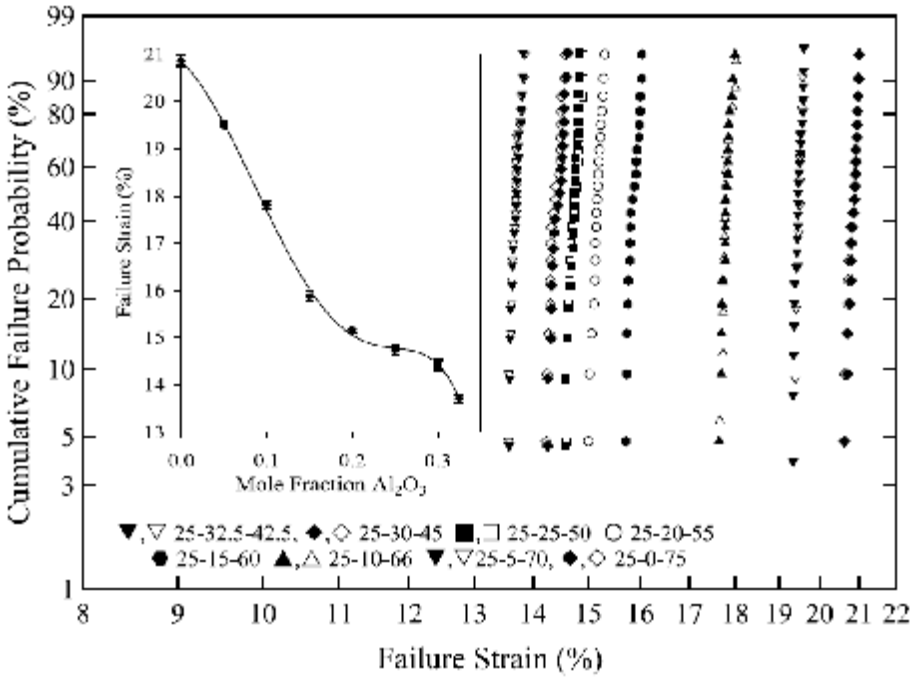

Figure 1.6. Weibull distributions of inert failure strains for sodium aluminosilicate glass fibers with compositions of $25Na_2O$-xAl_2O_3-$ySiO_2$ (x+y=75, in mol%) [20].

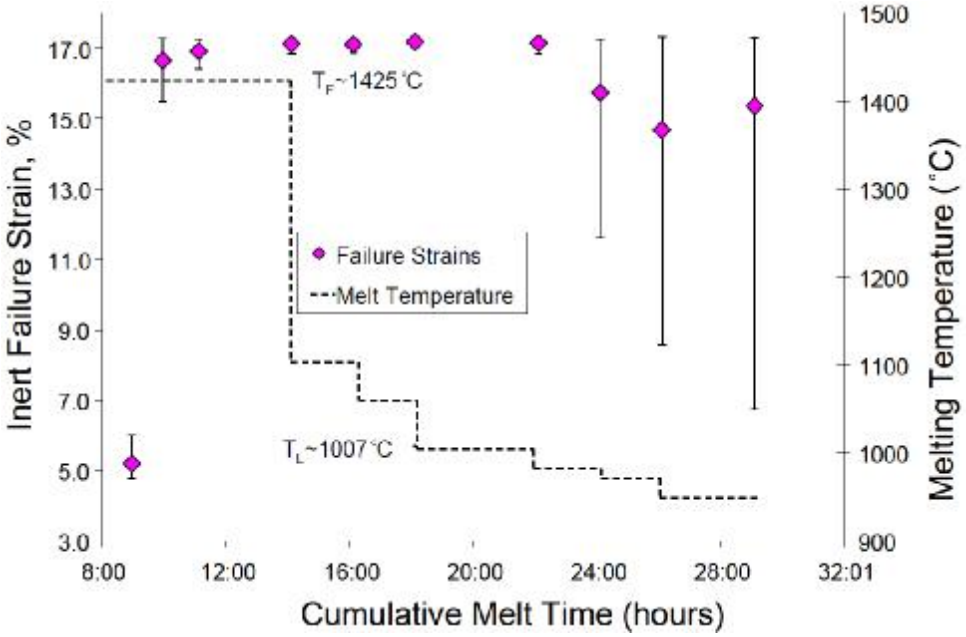

Figure 1.7. Inert failure strain distributions of soda-lime silicate fibers drawn from melts with consecutive thermal histories (time and temperature) indicated. Data points represent average failure strains and the 'uncertainty bars' represent the range from highest to lowest strain [18].

The melt history dependence of the inert failure strains indicates that some heterogeneities formed during the melting process serve as 'Griffith's flaws'. Attempts to detect the source of heterogeneities using optical microscopy, atomic force microscopy (AFM) and scanning electron microscopy (SEM) all failed [22]. The melt homogeneity study is of great interest to industry with regards to quality control.

One disadvantage of the TPB test is that it does not directly measure failure stress. Using zero-strain elastic modulus to calculate the failure stress from failure strain will lead to an incorrect estimation due to the non-linear elastic modulus [16].

1.2. ENVIRONMENTAL FATIGUE

The strength of glass is reduced not only by the effect of flaws but also by environmental fatigue. About a hundred years ago the strength of glass was found to be dependent on the loading time and loading rate in aqueous or humid environments [23]. Glass loaded at a fast rate or forced to support a load in a short time was relatively strong. The term 'fatigue' has been used to describe this phenomenon as early as the 1940s [24,25,26,27]. Charles [28,29,30] was the first who studied the fatigue effect thoroughly. Fatigue is usually categorized in two forms: static fatigue (a.k.a. delayed failure) and dynamic fatigue.

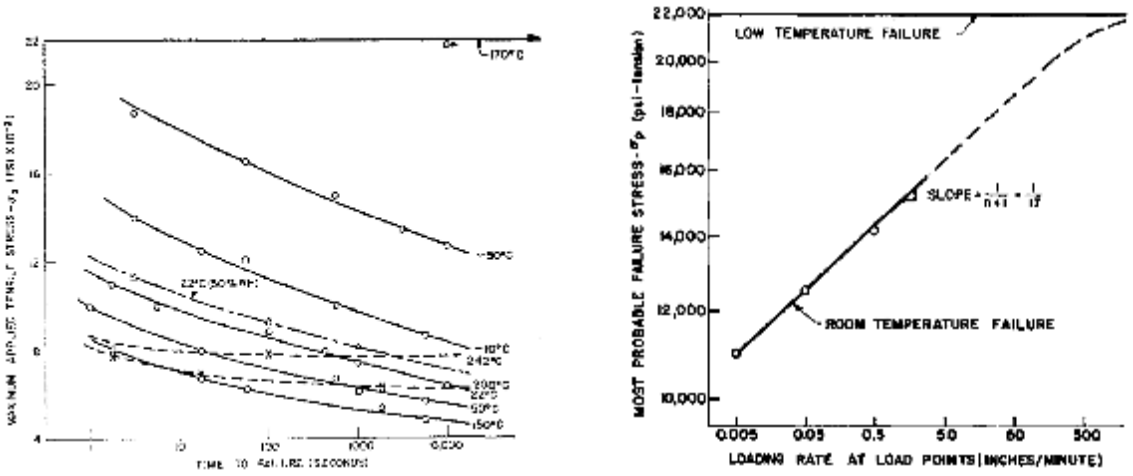

(a) (b)

Figure 1.8. Fatigue effect: (a) static fatigue (time to failure) and (b) dynamic fatigue for soda-lime silicate glass [29].

Static fatigue (Figure 1.8 (a), [29]) is measured by determining the time-to-failure of a sample under a constant applied stress or at a constant strain. Dynamic fatigue (Figure 1.8 (b), [30]) is usually measured by determining the failure stress or failure strain under different loading rates, from which the slope can be used to calculate the fatigue parameter n (will be introduced later).

Fatigue is important considering that most applications of glass involve some kind of applied force and some contact with air or aqueous environments. The fatigue of silica and silicate glass is of interest because of their wide applications. A well accepted concept is that the failure of glasses in wet environments is controlled by stress corrosion due to the chemical reaction between water and strained bonds at the crack tip [31]. Silica is considered inert to water at zero strain, but when the Si-O-Si bond is strained, it can hydrolyze by reacting with water [32,33]:

$$\begin{array}{c} | \\ -Si-O-Si- \\ | \end{array} + H_2O \longrightarrow 2\left[\begin{array}{c} | \\ -Si-OH \\ | \end{array}\right] \tag{5}$$

Silica is more susceptible to fatigue in the presence of basic solutions because hydroxyl ions further attack the glass network [34]:

$$\begin{array}{c} | \\ -Si-O-Si- \\ | \end{array} + OH^- \longrightarrow \begin{array}{c} | \\ -Si-O^- \\ | \end{array} + \begin{array}{c} | \\ -Si-OH \\ | \end{array} \tag{6}$$

The mechanism of fatigue in modified silicate glasses is different from that of silica. Alkali ions in a silicate glass can exchange with protons [29,35] or hydronium ions (H_3O^+) [36] in solution, increasing the pH value in the vicinity of the strained bond, increasing fatigue [29]:

$$\begin{array}{c} | \\ -Si-O-Si-ONa^+ \\ | \end{array} + H_2O \longrightarrow \begin{array}{c} | \\ -Si-O-Si-OH \\ | \end{array} + Na^+ + OH^- \tag{7}$$

Duncan and France et al [37] studied the fatigue of silica and sodium borosilicate glass in air and suggested that sodium borosilicate is more susceptible to fatigue than silica. They [38] also studied the fatigue of sodium borosilicate with different soda content in water and recognized that reducing soda caused an increase in the stability of glass, and hence low-soda borosilicate glass is less susceptible to fatigue. Wiederhorn and Bolz [39] studied stress corrosion behavior (another form of fatigue) for several silicate glasses. Among those glasses, silica glass had the greatest stress corrosion resistance, followed by low-alkali aluminosilicate and borosilicate glass. Soda-lime silicate glass however, was sensitive to stress corrosion, indicating that alkali ions play a detrimental part in fatigue.

1.3. SLOW CRACK GROWTH STUDY

In fracture mechanics, fatigue of glass has been studied by measuring slow crack growth (a.k.a. subcritical crack growth). A typical experiment is a double cantilever beam test, shown in Figure 1.9 (a) [31]. A crack of a predetermined length is introduced to a glass sample. A constant force is applied to the cracked ends of the sample. The crack velocity is measured using an optical microscope and recorded as a function of applied stress and environment Figure 1.9 (b) [31]. The curve shows three regions. In general, the crack extension in region I is due to the stress-assisted corrosive reaction between water and the strained bonds at the crack tip (for example reaction equation (5) to (7)). The plateau in region II shows that crack speed is independent of applied force. In this region, water migration becomes the limitation for crack velocity. The beginning of region III initiates a 'spontaneous' crack growth.

The slow crack velocity tests are usually shown in a more appropriate '*K*-*V*' curve (Figure 1.10), in which the applied force is converted to the stress intensity factor (*K*). In most stress corrosion studies, only region I crack growth is observed (see Figure 1.10 from Wiederhorn and Bolz [39]). In region I the crack growth behavior depends on the composition of the glass.

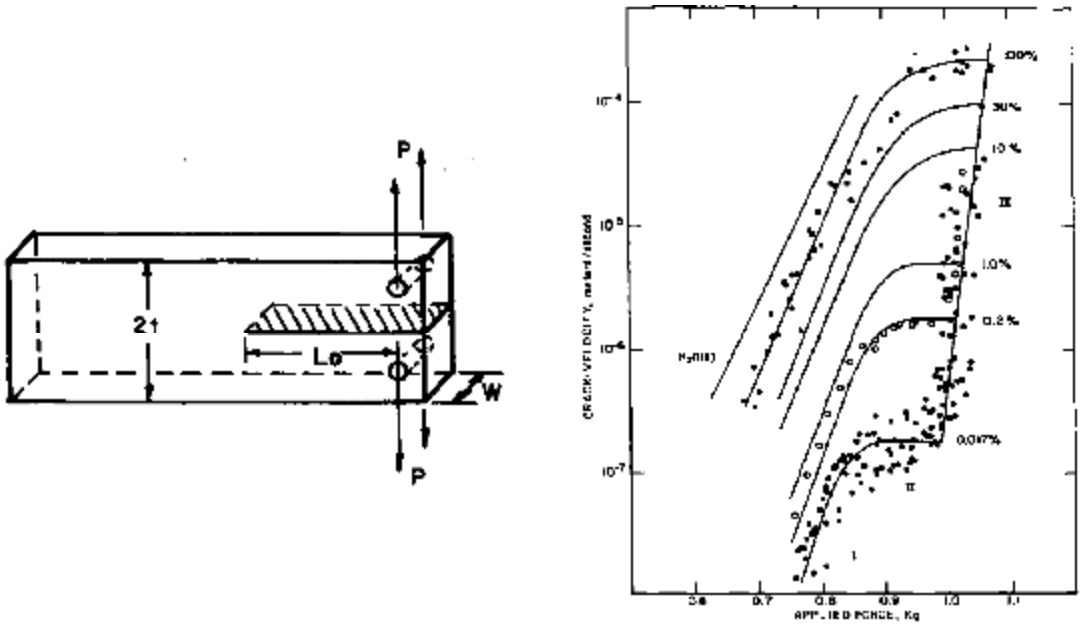

(a) (b)

Figure 1.9. Slow crack growth study: (a) typical experiment configuration and (b) typical result of slow-crack growth [31].

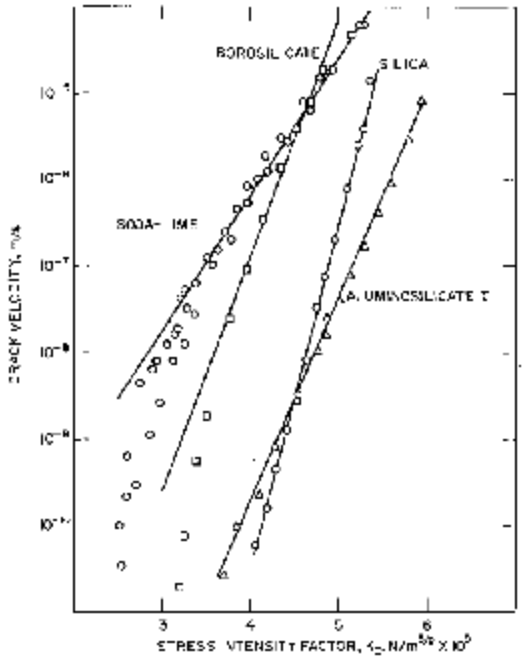

Figure 1.10. *K-V* curve for several silicate glasses in 25°C water [39].

The most widely used model to describe the *K-V* curve is based on an empirical power law [40,41]:

$$V = A(K_I/K_{IC})^n \tag{8}$$

where V is the crack growth velocity (μm/s), n is termed the stress corrosion susceptibility parameter, or the fatigue parameter, and A is the environmental parameter (μm/s) which has an Arrhenius temperature dependence. In addition to this model, an activation volume model [39] based on exponential law was proposed:

$$V = A \exp(n K_I/K_{IC}) \tag{9}$$

Other models based on exponential laws [42,43,44] have also been used, but their formulations are not very different. Shiue and Matthewson [45] compared several different models for fatigue and suggested that the power law fits the fatigue data the best, while the exponential law has a better physical meaning. Application wise, dynamic fatigue studies can also be described with the model using power law. The relationship between strength and stress rate can be derived analytically [46]:

$$\sigma_f = D\dot{\sigma}^{(1/n+1)} \tag{10}$$

where σ_f is the strength, or failure stress (GPa), D is a constant (s^{-1}), and $\dot{\sigma}$ is the applied stress rate (GPa/s). This equation allows direct comparison between slow-crack growth study and dynamic fatigue study. Thus most researchers prefer the power law model. Such relationship cannot be analytically derived from the exponential model and its application is thus much more limited.

1.4. TWO-POINT BEND STUDY OF FATIGUE

As mentioned before, dynamic fatigue [30] is usually measured by determining the failure stress or failure strain under different loading rates. The fatigue parameter, n, can be determined using Equation (10). The TPB test usually uses a measuring mode of constant faceplate velocity (v_{fp}), instead of constant stress rate or strain rate. Rondinella

and Matthewson [47] compared three different loading modes: constant strain rate, constant stress rate and constant faceplate velocity (v_{fp}) (shown in Figure 1.11). The power law model fits well for all three loading modes.

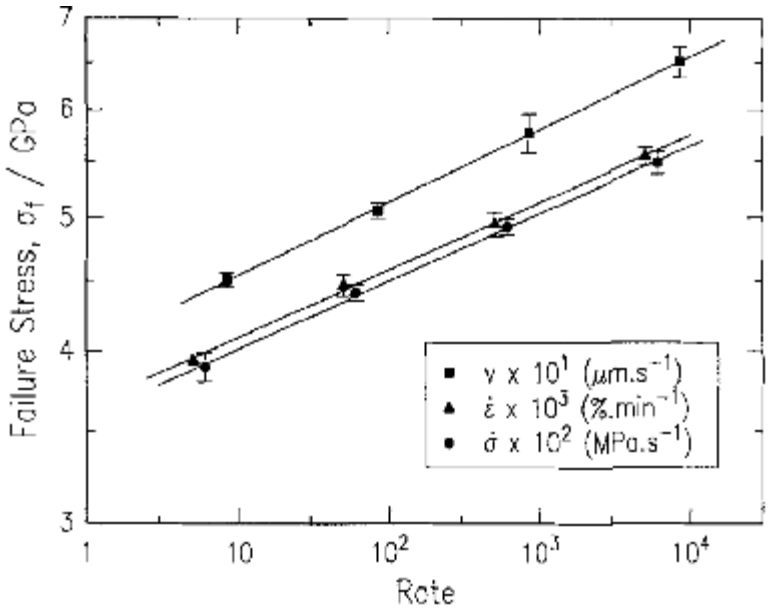

Figure 1.11. Dynamic fatigue results or coated fiber at constant velocity, constant strain rate, and constant stress rate loading modes [47].

The dynamic fatigue parameter, n, for constant faceplate velocity mode, can be calculated by:

$$n = 1 + 1/\frac{d\log(\varepsilon_f)}{d\log(v_{fp})} \tag{11}$$

There have been reports on the use of TPB to measure the fatigue for silica glass fibers [47,48,49,50,51] and sodium borosilicate fibers [38]. Except for dynamic fatigue [47], TPB has also been used in other forms of fatigue. For example, the failure strains in ambient conditions decrease systematically with increasing relative humidity [17], or with increasing temperature [52].

1.5. INERT STRENGTH AND INERT FATIGUE

In ambient conditions, glasses loaded at a rapid rate are relatively stronger due to the environmental fatigue effect. This is attributed to the stress corrosion reaction between water and strained glass bonds. To avoid environmental fatigue effects, strength measurements have been carried out in high vacuum (~10^{-8} Torr) [52], or at low temperatures (in liquid nitrogen or liquid helium), where the kinetics of the water degradation reactions are arrested [53]. Strengths of pristine glass fibers measured in such conditions are referred to as inert strength [13].

A number of researchers have reported the inert strength for fused silica. Proctor, et al. [53] reported a tensile strength of 11.8±2.2 GPa for 20 μm diameter silica fibers in liquid nitrogen. Pukh, et al. [54] used a three-point bending technique to measure the strength of a variety of compositions prepared as 100-150 μm fibers, under liquid nitrogen, and reported intrinsic strengths of 12.0 GPa for polymer coated silica glass. There are also reports of inert strengths for silica of 11-14 GPa measured in tensile test [55] and ~18% failure strain measured in two-point bend test [6], not measured under liquid nitrogen but in room temperature, high vacuum conditions (~10^{-8} Torr). These values fall in the range of 7-22 GPa, which is the theoretical strength for silica estimated using Orowan's theory [2].

Even though the water degradation reactions are believed to be arrested in inert conditions, fatigue has also been observed in pristine (flaw free) glass fibers measured in inert conditions, and referred to as inert fatigue [13, 53, 56]. Matthewson et al. [56] measured the fatigue effect of fused silica from 77 to 473K and showed that fatigue exists even at 77K (shown in Figure 1.12). Compared to room temperature fatigue, the fatigue parameter at 77K (calculated using equation (11)) is much higher (~400) but still measurable (Figure 1.13). Matthewson et al. did not differentiate inert fatigue and environmental fatigue and considered both processes to be caused by stress-induced reactions leading to weaker bonds at longer times.

Kurkjian, et al. [13] explained the inert fatigue effect as a consequence of the normal probability of failure due to thermal fluctuations of bond strengths under high stress, with longer times (slower loading) allowing weaker bonds to rupture and initiate

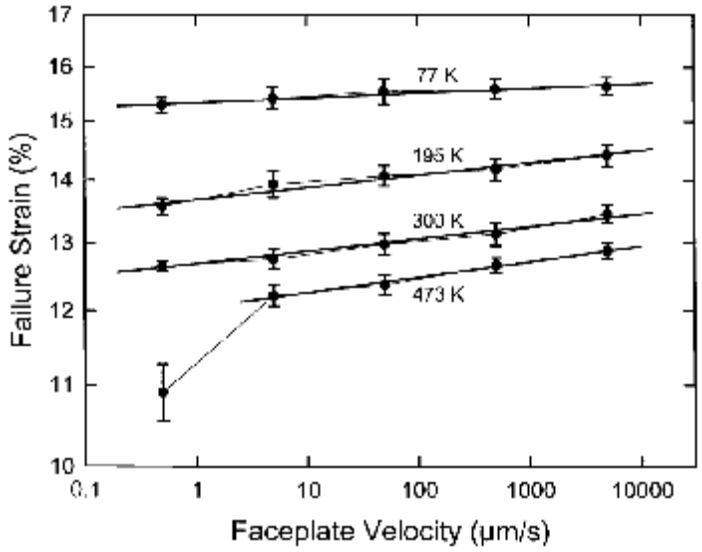

Figure 1.12. Dynamic fatigue observed from 77 to 473 K for fused silica fibers [56].

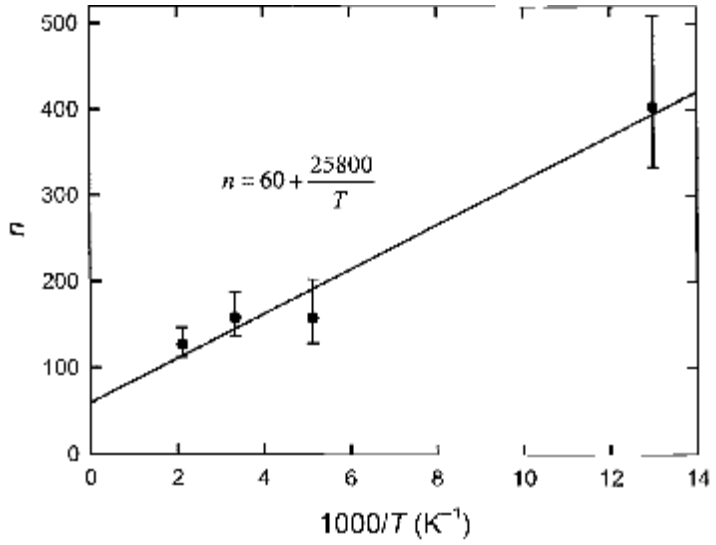

Figure 1.13. Fatigue parameter as a function of temperature for fused silica fibers [56].

failure. Kurkjian et al. viewed inert fatigue as a time dependent phenomena and suggested that the inert fatigue can be avoided by testing rapidly. Assuming the inert fatigue is due to the thermal fluctuation of bonds, if one can test the strength within the bond vibration time (τ_{vib}~10^{-13} s) the inert fatigue should be avoided. The inert fatigue was described by Kurkjian et al. using the equation:

$$\tau = \tau_{vib} \exp\left[\frac{E}{kT}\left(1 - \left\{\frac{\sigma}{\sigma_0}\right\}\right)\right] \tag{12}$$

where τ is the test time, τ_{vib} is the typical vibration time of bonds, E is the zero-stress environmental dependent activation energy, k is the Boltzmann's constant, T is the temperature, σ is the measured strength and σ_0 is the 'fatigue free' strength measured in time τ_{vib}.

Inert dynamic fatigue effect was also observed not only in silica, but also in E glass and some other glasses [19,20]. An interesting observation is that there is an inverse dependence of inert strength on loading rate for some glasses, that is, the inert failure strains increase with decreasing loading rate. For example, for some sodium silicate glasses, inert failure strain measured at a slow faceplate velocity (v_{fp} = 50 μm/s) is greater than that measured at a fast faceplate velocity (v_{fp} = 4000 μm/s), shown in Figure 1.14.

This effect is to the inverse of the 'normal' inert fatigue behavior of silica and E-glass, and has been referred to as the Inert Delayed Failure Effect (IDFE) [22]. One quantitative measure of IDFE is given by:

$$IDFE = 100 \times \frac{\left(\varepsilon_{f\cdot 50\mu m/s} - \varepsilon_{f\cdot 4000\mu m/s}\right)}{\varepsilon_{f\cdot 50\mu m/s}} \tag{13}$$

IDFE in Equation (13) is the relative difference in inert failure strains measured at a faceplate velocity of 50 and 4000 μm/s. Several glasses including silica and E-glass have a negative IDFE value, while some other glasses including sodium silicate glasses with high soda content have a positive IDFE value (summarized in Table 1.2, [22]). In

general, the negative IDFE glasses have cross-linked structures, whereas positive IDFE glasses have more non-bridging oxygens. One explanation for IDFE is that the structure of silicate glasses with relatively large fractions of non-bridging oxygens can reorganize or relax when stress is applied, perhaps in a manner similar to that which produces low-temperature internal friction peaks [57,58]. Given more time (slower v_{fp}), the structure can reorganize more before bonds fail and cracks are initiated, and thus failure occurs at a greater overall strain, countering the effects of weaker network bonds in the more depolymerized glass structures. The positive or negative of IDFE might result from a competition between this relaxation/deformation time and the inert fatigue factor.

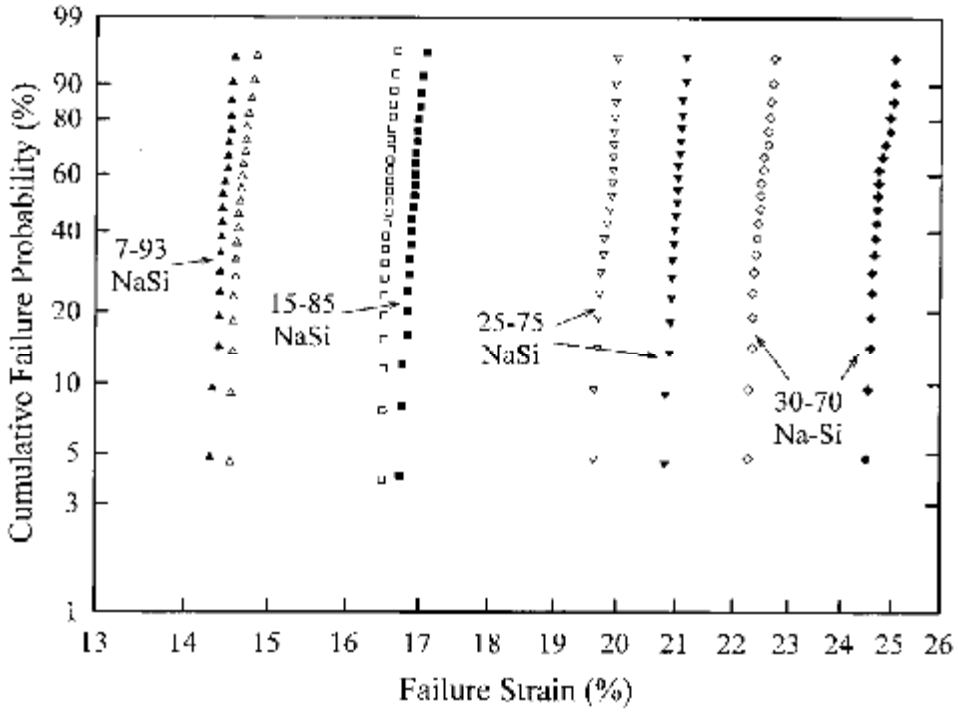

Figure 1.14. Weibull distributions of inert failure strains for sodium silicate glass fibers with compositions of xNa_2O-$ySiO_2$ (x+y=100, in mol%), using faceplate velocities (v_{fp}) of 4000 μm/s (open symbols) and 50 μm/s (closed symbols) [19].

Oxide glasses have been classified based on their elastic modulus derivatives, dM/dT and dM/dP (M: elastic modulus, T: temperature, P: pressure) [59,60,61]. 'Normal'

glasses have a negative dM/dT and a positive dM/dP, and 'anomalous' glasses have a positive dM/dT and a negative dM/dP.

Table 1.2. Collective IDFE data for several glass systems.

Zero or negative IDFE	Positive IDFE
Potassium Silicate (K_2O<25%)	Potassium Silicate (K_2O≥25%)
Sodium Silicate (Na_2O<15%)	Sodium Silicate (Na_2O≥15%)
Sodium Aluminosilicate (Na_2O=25%, Al_2O_3>25%)	Sodium Aluminosilicate (Na_2O=25%, Al_2O_3≤25%)
Silica	Soda-lime Silicate (Na_2O+CaO≥20%)
E-glass	

These elastic anomalies have been related to indentation behavior (shown in Figure 1.15, [62]). Normal glasses show shear lines upon indentation at room temperature, indicating the presence of shear flow, whereas anomalous glasses exhibit no shear lines upon indentation at room temperature. Instead of shear flow, they show deformation due to densification.

The two types of glasses are believed to have fundamental differences in the way they respond to stress. These differences coincide with the IDFE difference between silica and soda-lime silicate. Silica, classified as anomalous glass, has a zero or negative IDFE, while soda-lime silicate, classified as normal glass, has a positive IDFE. This coincidence is also valid for even more glass compositions. Table 1.3 shows the correlation between IDFE and elastic anomalies [59,60,61,62] for several glasses.

A possible explanation is that the ease of plastic flow for SLS glass can benefit from reorganization or relaxation under strains, therefore allowing higher failure strain if given more time.

1.6. SUMMARY

This dissertation is aimed at advancing the understanding of how glass fails. The two-point bending technique is used to measure the failure strain of freshly-drawn glass fibers. The failure behaviors for different glass systems under different conditions are

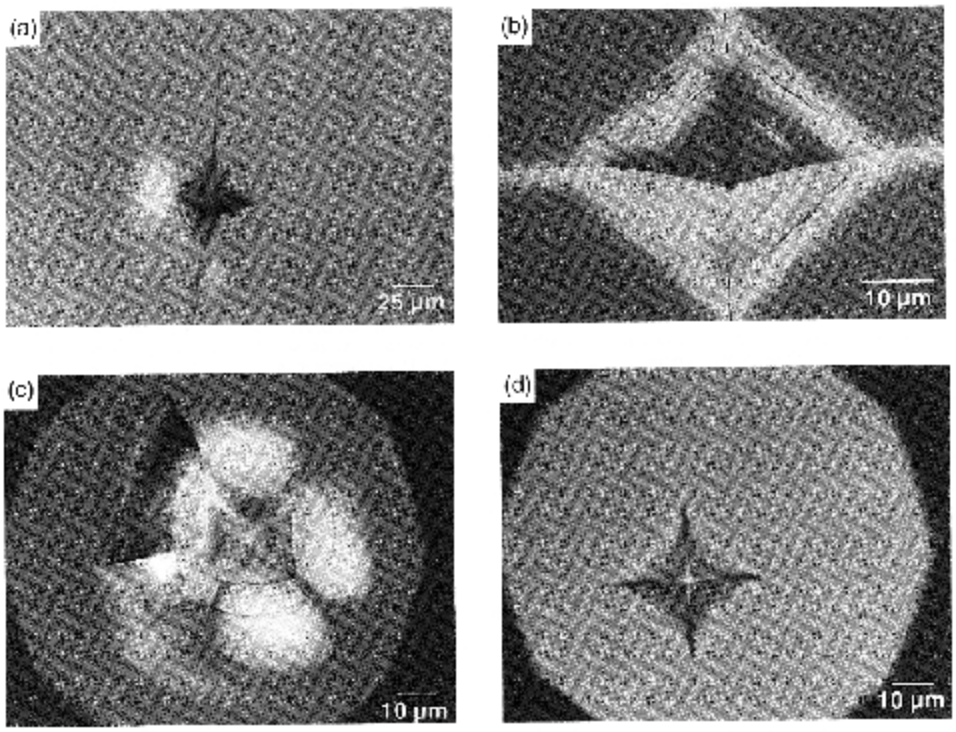

Figure 1.15. Room temperature indentation images for (a) soda-lime silica, optical; (b) soda-lime silica, HF etch, SEM; (c) fused silica, optical; (d) fused silica, under dry N_2, optical [62].

Table 1.3. IDFE and elastic anomalies for several glasses.

Glass	IDFE	Elastic anomaly
Silica (SiO_2)	≤0	anomalous
E-glass	≤0	anomalous
Soda-lime silicate (15%Na_2O, 5%CaO, 80%SiO_2)	>0	normal
Sodium silicate (Na_2O<15%)	≤0	anomalous
Sodium silicate (Na_2O≥15%)	>0	normal
Potassium silicate (K_2O<13%)	≤0	anomalous
Potassium silicate (13%<K_2O<25%)	≤0	normal
Potassium silicate (K_2O>25%)	>0	normal

studied. Paper 1 describes the calculation of failure stress from two-point bend failure strains and non-linear elastic modulus. Failure stresses were determined for silica, E-glass, a soda-lime silicate glass, a sodium aluminosilicate glass, a series of sodium silicate glasses and several potassium silicate glasses. In this chapter, the compositional dependence of inert intrinsic strength was studied. The inert delayed failure effect was discussed. Paper 1 is formatted following the requirement of Journal of the American Ceramic Society, and was submitted to this journal in August 2011. Paper 2 presents the measurements of inert failure strains for a series of sodium borate glasses. The vitreous B_2O_3 glass exhibits the greatest inert failure strains among all the glasses that had been tested. The compositional dependence of inert failure strain for sodium borate glasses was studied and related to the structure and bond strengths. The failure behaviors for sodium borate glasses were compared to those for silicate glasses. Paper 3 describes the dynamic fatigue behavior for several commercial silicate glasses and a series of lab-prepared sodium aluminosilicate glasses in distilled water. The dynamic fatigue parameter for these glasses will be determined by measuring the failure strains as a function of faceplate velocity. The temperature dependence of the failure strains in water was also determined. The activation energy for fatigue was related to the fatigue parameter. The fatigue mechanisms for the series of sodium aluminosilicate glasses were analyzed and related to their reactivity with water. Paper 4 describes the study of fatigue behaviors for silica, soda-lime silicate glass and E-glass in humid air. Failure strains were measured as a function of humidity, and the fatigue parameters were determined. The fatigue reaction order in the high humidity range was determined for all three glasses and was discussed. Papers 2, 3, and 4 were formatted following the requirement of Journal of Non-Crystalline Solids, and will be submitted to the journal in the near future.

REFERENCES

[1] A. K. Varshneya, *Fundamentals of Inorganic Glass,* Academic Press, San Diego, CA, 1994, p. 1.

[2] E. Orowan, 'The Mechanical Strength Properties and the Real Structure of Crystals,' ***Z. Krist.***, A89 327-43 (1934)

[3] C. E. Inglis, 'Stress in a Plate due to the Presence of Cracks and Sharp Corners,' *Trans. Inst. Naval Archit.*, 55, 219-30 (1913).

[4] A. A. Griffith, 'The Phenomena of Rupture and Flow in Solids' *Phil. Trans. Roy. Soc.*, 22 163-198 (1921).

[5] Y-M Chiang, D. P. Birnie III, W. D. Kingery, *Physical Ceramics: Principle for Ceramic Science and Engineering,* MIT Series, Wiley, 1996.

[6] C. R. Kurkjian, P. K. Gupta, R. K. Brow, 'The Strength of Silicate Glass: What Do We Know, What Do We Need to Know,' *Int. J. Appl. Glass Sci.*, 1 [1] 27-37 (2010).

[7] N. M. Cameron, 'Relation between Melt Treatment and Glass Fiber Strength,' *J. Am. Ceram. Soc.*, 49 [3] 144-8 (1966).

[8] M. D. Lund and Y. Yue, 'Impact of Drawing Stress on the Tensile Strength of Oxide Glass Fibers' *J. Am. Ceram. Soc.*, 93 [10] 3236-43 (2010).

[9] S. Feih, K. Manatpon, Z. Mathys, A. G. Gibson, and A. P. Mouritz, 'Strength Degradation of Glass Fibers at High Temperatures,' *J. Mater. Sci.*, 44 [2] 392-400 (2009).

[10] F. M. Ernsberger, 'Tensile and Compressive Strength of Pristine Glasses by an Oblate Bubble Technique,' *Phys. Chem. Glasses,* 10 [6] 240-5 (1969).

[11] V. P. Pukh, L. G. Baikova, M. F. Kireenko, L. V. Tikhonova, T. P. Kazannikova, and A. B. Sinani, 'Atomic Structue and Strength of Inorganic Glasses,' *Phys. Solid State,* 47 [5] 850-5 (2005).

[12] C. R. Kennedy, R. R. Bradt, and G. E. Rindone, 'The strength of binary alkali silicate glasses,' *Phys. Chem. Glasses,* 21 [3] 99-105 (1980).

[13] C. R. Kurkjian, P. K. Gupta, R. K. Brow, and N. P. Lower, 'The Intrinsic Strength and Fatigue of Oxide Glasses,' *J. Non-Cryst. Solids,* 316 [1] 114-24 (2003).

[14] J. B. Murgatoryd, 'The Strength of Glass Fibers,' *J. Soc. Glass Technol.*, 28 368-97 (1944).

[15] P. W. France, M. J. Paradine, M. H. Reeve, and G. R. Newns, 'Liquid Nitrogen Strengths of Coated Optical Glass Fibers,' *J. Mater. Sci.*, 15 [4] 825-830 (1980).

[16] M. J. Matthewson, C. R. Kurkjian, and S. T. Gulati, 'Strength Measurement of Optical Fibers by Bending,' *J. Am. Ceram. Soc.*, 69 [11] 815-21 (1986).

[17] R. K. Brow, N. P. Lower, and C. R. Kurkjian, 'TPB Test Provides New Insights to Fiber Strength and Quality,' *Ceram. Bull.*, 14 [4] 50-53 (2005).

[18] R. K. Brow, N. P. Lower, C. R. Kurkjian and H. Li, 'The Effects of Melt History on the Failure Characteristics of Pristine Glass Fibers,' *Phys. Chem. Glasses, Eur. J. Glass Sci. Tech.*, 50 [1] 31-33 (2009).

[19] N. P. Lower, R. K. Brow and C. R. Kurkjian, 'Inert Failure Strain Studies of Sodium Silicate Glass Fibers,' *J. Non-Cryst. Solids*, 349 168-172 (2004).

[20] N. P. Lower, R. K. Brow and C. R. Kurkjian, 'Inert Failure Strain Studies of Sodium Aluminosilicate Glass Fibers,' *J. Non-Cryst. Solids*, 344 [1-2] 17-21 (2004).

[21] R. K. Brow, N. P. Lower, A.J. Lang and C.R. Kurkjian 'Structure and the Intrinsic Strength of Glass,' *Glastech. Ber. Glass Sci. Technol.*, 75 C2 133-138 (2002).

[22] N. P. Lower, Ph D. Thesis, 'Failure Study of Glass Fibers,' Missouri University of Science and Technology, 2004.

[23] L. Grenet, 'Mechanical Strength of glass,' *Bull. Soc. Enc. Industr. Nat. Paris, (Ser. 5)*, 4 838-48 (1899).

[24] T. C. Baker and F. W. Preston, 'Wide Range Static Strength Testing Apparatus for Glass Rods,' *J. Appl. Phys.*, 17 [3] 162-9 (1946).

[25] T. C. Baker and F. W. Preston, 'Fatigue of Glass under Static Loads,' *J. Appl. Phys.*, 17 [3] 170-8 (1946).

[26] T. C. Baker and F. W. Preston, 'The Effect of Water on the Strength of Glass,' *J. Appl. Phys.*, 17 [3] 179-88 (1946).

[27] W. A. Wely, 'The Mechanical Strength of Glass,' *Glass Ind.*, 27 17-50 (1946)

[28] R. J. Charles, 'Static Fatigue of Glass. I', *J. Appl. Phys.*, 29 [11] 1549-53 (1958).

[29] R. J. Charles, 'Static Fatigue of Glass. II', *J. Appl. Phys.*, 29 [11] 1554-60 (1958).

[30] R. J. Charles, 'Dynamic Fatigue of Glass. II', *J. Appl. Phys.*, 29 [12] 1657-62 (1958).

[31] S. M. Wiederhorn, 'Influence of Water Vapor on Crack Propagation in Soda-Lime Glass,' *J. Am. Ceram. Soc.*, 50 [8] 407-14 (1967).

[32] B. R. Lawn, 'Physics of Fracture,' *J. Am. Ceram. Soc.*, 66 [2] 83-91 (1983).

[33] T. A. Michalske, S. W. Freiman, 'A Molecular Mechanism for Stress Corrosion in Vitreous Silica,' *J. Am. Ceram. Soc.*, 66 [4] 284-8 (1983).

[34] A. T. Taylor and M. J. Matthewson, 'Effect of pH on the Strength and Fatigue of Fused Silica Optical Fiber,' *Proc. Int. Wire & Cable Symp.*, 47th 874-80 (1998).

[35] R. H. Doremus, 'Interdiffusion of Hydrogen and Alkali Ions in A Glass Surface,' *J. Non-Cryst. Solids*, 19 137-44 (1975).

[36] T. Fett, J. P. Guin and S. M. Wiederhorn, 'Stress in Ion-Exchange Layers of Soda-Lime-Silicate Glass,' *Fatigue Fract. Engng. Mater. Struct.*, 28 [6] 507-14 (2005).

[37] W. J. Duncan, P. W. France and S. P. Graig, 'The Effect of Environment on the Strength of Optical Fiber,' in: C. R. Kurkjian (Ed.), *Strength of Inorganic Glass*, Plenum, 1985, p. 309-28.

[38] P. W. France, W. J. Duncan, D. J. Smith and K.J. Beales, 'Strength and Fatigue of Multicomponent Optical Glass Fibres,' *J. Mat. Sci*., 18 785-792 (1983).

[39] S. M. Wiederhorn, L. H. Bolz, 'Stress corrosion and Static Fatigue of Glass,' *J. Am. Ceram. Soc.*, 53 [10] 543-9 (1970).

[40] W. Griffeon, 'Evaluation of Optical Fiber Lifetime Models Based on the Power Law,' *Opt. Eng.*, 33 488-97 (1994).

[41] A. G. Evans, 'Slow Crack Growth in Brittle Materials under Dynamic Loading Conditions,' *Int. J. Fracture*, 10 251 (1974).

[42] R. J. Charles, 'Diffusion Controlled Stress Rupture of Polycrystalline Materials,' *Metall. Trans. A.*, 7 1081-9 (1976)

[43] J. C. Pollet and S. J. Burns, 'Thermally Activated Crack Propogation-Theory,' *Int. J. Fract.*, 13 667-79 (1977)

[44] B. R. Lawn, 'An atomistic Model of Kinetic Crack Growth in Brittle Solids,' *J. Mat. Sci.*, 10 469-80 (1975).

[45] Y. S. Shiue and M. J. Matthewson, 'Stress Dependent Activation Entropy for Dynamic Fatigue of Pristine Silica Optical Fibers,' *J. Appl. Phys.*, 89 [9] 4787-93 (2001).

[46] G. G. Trantina, 'Strength and Life Prediction for Hot-Pressed Silicon Nitride,' *J. Am. Ceram. Soc.*, 62 [7-8] 377-80 (1979).

[47] V. V. Rondinella and M. J. Matthewson, 'Effect of Loading Mode and Coating on Dynamic Fatigue of Optical Fiber in Two-Point Bending,' *J. Am. Ceram. Soc.*, 76 [1] 139-44 (1993).

[48] V. V. Rondinella, M. J. Matthewson and C. R. Kurkjian, 'Coating Additives for Improved Mechanical Reliability of Optical Fiber,' *J. Am. Ceram. Soc.*, 77 [1] 73-80 (1994).

[49] M. J. Matthewson and C. R. Kurkjian, 'Static Fatigue of Optical Fibers in Bending,' *J. Am. Ceram. Soc.*, 70 [9] 662-8 (1987).

[50] S. F. Cowap and S. D. Brown, 'Technique for the Static Fatigue Testing of Fibers,' *J. Am. Ceram. Soc.*, 70 [4] C-67-C-68 (1987).

[51] S. Bhaumik, 'Effect of Humidity of Drawing Environment on Dynamic Fatigue of Polymer Coated High Strength Silica Optical Fiber,' *Wire J. Int.*, 38 [3] 194-8 (2005).

[52] W. J. Duncan, P. W. France and S. P. Graig, 'The Effect of Environment on the Strength of Optical Fiber,' in: C. R. Kurkjian (Ed.), Strength of Inorganic Glass, Plenum, 1985, p. 309-28.

[53] B. A. Proctor, I. Whitney, and J. W. Johnson, 'Strength of Fused Silica,' *Proc. Roy Soc. A*, 297 [1451] 534-57 (1967).

[54] V. P. Pukh, L. G. Baikova, M. F. Kireenko, L. V. Tikhonova, T. P. Kazannikova, and A. B. Sinani, 'Atomic Structue and Strength of Inorganic Glasses,' *Phys. Solid State,* 47 [5] 850-5 (2005).

[55] W.A. Smith, T.M. Michalske, 'Inert Strength of Pristine Glass Fibers,' *Sandia Report,* SAND92-1107 (1993).

[56] M. J. Matthewson, C. R. Kurkjian, C. D. Haines and N. Venugopal, 'Temperature Dependence of Strength and Fatigue of Fused Silica Fiber in the Range 77 to 473 K,' *Proc. SPIE*, 4940 74-9 (2003).

[57] D. E. Day, and G. E. Rindone, 'Properties of soda aluminosilicate glasses. II. Internal Friction,' *J. Am. Ceram. Soc.*, 45 496-504 (1962).

[58] J. E. Shelby. Jr., and D. E. Day, 'Mechanical Relaxations in Mixed-Alkali Silicate Glasses: I, Results,' *J. Am. Ceram. Soc.*, 52 [4] 169-74 (1969).

[59] A. Arora, D.B. Marshall, B.R. Lawn and M.V. Swain, 'Indentation Deformation/ Fracture of Normal and Anomalous Glasses,' *J. Non-Cryst. Solids*, 31 415-428 (1979).

[60] J.T. Krause, C.R. Kurkjian, 'Vibrational Anomalies in Inorganic Glass Formers,' *J. Am. Ceram. Soc.*, 51 [4] 226-7 (1968).

[61] C.R. Kurkjian, J.T. Krause, H.J. McSkimmin, P. Andreatch and T.B. Bateman, 'Pressure Dependence of Elastic Constants and Gruneisen Parameters in Fused SiO_2, GeO_2, BeF_2 and B_2O_3,' p. 463-473 in *Amorphous Materials*, edited by R. W. Douglas and Bryan Ellis, Wiley, London, 1972.

[62] C.R. Kurkjian, G.W. Kammlott, M.M. Chaudhri, 'Indentation Behavior of Soda-Lime Silica Glass, Fused Silica, and Single-Crystal Quartz at Liquid Nitrogen Temperature,' *J. Am. Ceram. Soc.*, 78 737-744 (1995).

PAPER

1. TWO-POINT BEND MEASUREMENTS OF FAILURE STRESS OF PRISTINE GLASS FIBERS[*†]

Zhongzhi Tang[a], Nathan P. Lower[a,b], Prabhat K. Gupta[c], Charles R. Kurkjian[d], and Richard K. Brow[a,‡]

[a]Missouri University of Science & Technology, Department of Materials Science & Engineering, Rolla, MO 65409, USA

[b]Rockwell Collins, Inc., Advanced Technology Center, 400 Collins Road NE, MS 108-101, Cedar Rapids, IA 52498, USA

[c]The Ohio State University, Department of Materials Science & Engineering, 284 Watts Hall, 2041 College Rd., Columbus, OH 43210, USA

[d]University of Southern Maine, Department of Engineering, P.O. Box 9300, Gorham, ME 04038, USA

ABSTRACT

The two-point bend (TPB) technique was used to measure the failure strains of pristine glass fibers under liquid nitrogen and in ambient conditions and failure stresses were then calculated using values of the nonlinear elastic moduli reported in the literature. At a faceplate velocity of 4000 μm/s, for silica glass fibers, the failure stresses calculated from failure strains measured by TPB are 12.1±0.2 GPa in inert (liquid nitrogen) conditions and 7.0±0.1 GPa in ambient conditions (room temperature, 50% RH), compared to reports of 11-14 GPa for liquid nitrogen and 4-5 GPa ambient tensile

---

[*] Orally presented at the 2010 Glass & Optical Materials Division Meeting, Corning, NY, May 16, 2010 (Symposium III: Glass Technology), Abstract ID No. 768610
[†] Supported by the NSF Industry/University/Center for Glass Research (CGR)
[‡] Author to whom correspondence should be addressed: brow@mst.edu.

strength measurements, respectively. Failure stresses were also calculated for an E-glass, a soda-lime silicate glass, a nepheline sodium aluminosilicate glass, a series of sodium silicate glasses, and several potassium silicate glasses. These failure stresses were compared to the tensile strengths for similar glasses reported in the literature. Inert intrinsic strengths for alkali silicate glasses were related to the structure and corresponding bond strengths, and the dependence of the inert strengths on faceplate velocity (or strain rate) was discussed.

1.1. INTRODUCTION

Strength is one of the most important properties of glass, but also one of the most difficult to measure. Griffith [1] showed that practical strength is greatly reduced from its theoretical value due to strength-limiting flaws that form during processing or handling. Much effort has gone into preparing and testing "flaw free" or pristine samples to determine intrinsic strength [2]. The measurement of the intrinsic strength of glass is of significance because without the effect of surface flaws, strength is sensitive to glass composition and can be related to the nature of the glass structure. In addition, glass strength is reduced due to environmental fatigue effects [3,4,5], with water being the cause of this degradation [6]. The inert strength of glass is the strength measured under conditions where there is no environmental fatigue [7]. To avoid environmental fatigue effects, strength measurements have been carried out in high vacuum (~10^{-8} Torr) [8], or in liquid nitrogen, where the kinetics of the water degradation reactions are arrested [9]. Inert intrinsic strength should depend on the atomic level structure and corresponding bond strengths of a glass [7].

1.1.1. Conventional Glass Strength Measurement. Freshly drawn glass fibers are often used in studies of glass strength because they can be prepared and handled in such a way as to avoid damaging their pristine melt surfaces. Failure strengths of fibers have been measured by tensile tests [9,10-13], three-point bend tests [14] and four-point bend tests [15]. In a tensile test, the sample must be gripped on both ends and this may damage the sample surfaces causing a decrease in measured strength. Another disadvantage of the tensile test is that the test volume includes the entire length of the fiber between the grips, and this increases the probability of finding larger critical flaws and increases the scatter in measured values [2]. Three-point bend and four-point bend

tests, if performed on fibers, can significantly reduce the probability of encountering a critical surface defect, due to the smaller volume that is effectively under tension compared to typical tensile tests, but may create strength-limiting critical flaws where the testing fixtures touch the pristine surfaces.

1.1.2. Two-Point Bend Failure Strain Measurement. Although the two-point bending (TPB) technique was used as early as 1944 [16], its routine use in testing glass fibers began in 1980 [17]. In a TPB test, a pristine section of glass fiber, diameter *d*, is bent into a U-shape between two parallel faceplates, one of which travels towards the second at a constant faceplate velocity (v_{fp}), compressing the 'U' until failure (Figure 1.1). The gap distance at failure (*D*) is recorded, and the failure strain (e_f) is then calculated from [18]:

$$\varepsilon_f = \frac{1.198 \times d}{(D - d)} \tag{1}$$

The TPB test does not require the special grips needed for conventional tensile tests, and the relatively small gauge length (0.3-0.9 mm) in the region of highest tensile stress minimizes the probability of extrinsic flaws [17]. A more detailed gauge length calculation can be found in [18]. The application and possibilities of the TPB test are discussed in our previous publications [19-24]. For example, Lower et al. used TPB to determine the inert intrinsic failure strains for sodium silicate glass fibers [22], sodium aluminosilicate glass fibers [23] and E-glass fibers [24].

A TPB test has an advantage of not requiring any excessive handling of the glass samples. Moreover, the samples used in a TPB test can be freshly-drawn fibers with pristine surfaces. One disadvantage of TPB is that it measures failure strain, not failure stress.

1.1.3. Nonlinear Elastic Modulus of Glass. To convert the TPB failure strains to failure stresses, the elastic modulus must be known. For glass samples with failure strains less than about 1%, failure stress ($\sigma_f(0)$) can be calculated from Hooke's Law:

$$\sigma_f(0) = E_0 \times \varepsilon_f \tag{2}$$

where E_0 is the zero-strain (or linear) Young's modulus, and ε_f is failure strain. However, pristine glass fibers typically fail at significantly greater strains (5-25%), where the use of the zero-strain Young's modulus is no longer appropriate. For example, the Young's modulus of 10 μm E-glass fibers tested in tension drops from 74 to 60 GPa for a strain of 4% [25]. The nonlinear Young's elastic modulus may be approximated by the polynomial [26]:

$$E = E_0 + E_1\varepsilon + \frac{1}{2}E_2\varepsilon^2 \tag{3}$$

where E_1 is the third-order non-linear Young's modulus and E_2 is the fourth-order non-linear Young's modulus. These higher order elastic moduli can be measured using static techniques [27], ultrasonic techniques [28,29] or by Brillouin scattering [30,31]. Values of E_0 and E_1 for a variety of glasses have been reported, but very few values of E_2 for glasses are available in the literature, due to the difficulty of these measurements. Values of E_0, E_1 and E_2 for fused silica have been reported from studies in ambient conditions [32]. There are other reported values of E_0 and E_1 for silica in ambient conditions [29] and in liquid nitrogen [33], but these latter studies did not report values for E_2. Values of E_0, E_1 and E_2 for E-glass have been obtained under ambient conditions [25]. There are also reported values of E_0 and E_1 for soda-lime silicate glass [31] and a nepheline sodium aluminosilicate glass [34]. Manghnani [35] measured the pressure dependence of elastic modulus for Na-silicate and K-silicate glasses in air, and values of E_0 and E_1 were obtained using a method discussed by Gupta and Kurkjian [6]. Using equation (3), a stress-strain relation can be described as [6]:

$$\sigma = E_0\varepsilon + \frac{1}{2}E_1\varepsilon^2 + \frac{1}{6}E_2\varepsilon^3 \tag{4}$$

Assuming that the temperature dependence of these moduli are negligible, Gupta and Kurkjian noted that when pristine glasses fail under inert conditions (*), the stress is maximum with regard to strain and so the differential of stress to strain, the effective

Young's modulus, ds/de, goes to zero. Using this condition, a value for E_2 can be derived:

$$E_2 = -2\frac{E_0 + E_1\varepsilon_f^*}{\varepsilon_f^{*2}} \quad (5)$$

Substituting equation (5) into equation (4) provides an equation for failure stress that can be used when E_0, E_1 and ε_f* are known but E_2 is not:

$$\sigma_f = E_0\varepsilon_f + \frac{1}{2}E_1{\varepsilon_f}^2 - \frac{1}{3}\frac{E_0 + E_1\varepsilon_f^*}{\varepsilon_f^{*2}}{\varepsilon_f}^3 \quad (6)$$

Under inert conditions, when $\varepsilon_f = \varepsilon_f$*, equation (6) is simplified to:

$$\sigma_f^* = \frac{2}{3}E_0\varepsilon_f^* + \frac{1}{6}E_1\varepsilon_f^{*2} \quad (7)$$

In this paper, equation (6) is used to calculate failure stress under ambient conditions, and equation (7) is used to calculate the inert failure stress under liquid nitrogen. Values of E_0 and E_1 used to calculate failure stresses are gathered from the literature.

1.2. EXPERIMENTAL PROCEDURES

1.2.1. Sample Preparation. Materials used in this study include fused silica (AT&T, Amersil TO8 fused natural quartz), a commercial calcium aluminoborosilicate glass (PPG, E-glass), a commercial soda lime silicate glass (Owens-Illinois, flint container glass), a nepheline sodium aluminosilicate glass ($25Na_2O{\cdot}25Al_2O_3{\cdot}50\ SiO_2$, in mol%) from reference [22], a series of sodium silicate glasses, $x$$Na_2O{\cdot}(100\text{-}x)SiO_2$ ($10 \leq x \leq 35$), in mol%, described in references [21], and several potassium silicate glasses, y $K_2O{\cdot}(100\text{-}y)SiO_2$, y=15-25, in mol%, also described in reference [24].

Commercial E-glass has a nominal composition described by $(20\text{-}25)CaO{\cdot}(10\text{-}15)Al_2O_3{\cdot}(5\text{-}10)B_2O_3{\cdot}(50\text{-}55)SiO_2$, in wt%. E-glass marbles were remelted in platinum

crucibles in air at 1550°C for at least 4 hours prior to fiber pulling. The melts were then transferred to a second furnace set to a fiber pulling temperature of 1300°C. The second furnace was located below a custom fiber drawing system which pulled fiber from the surface of the melt. Fibers were drawn onto a rotating cage which was designed to prevent fiber overlap and damage. Fiber diameter was controlled by the fiber pulling temperature and the drawing speed. All fibers are drawn to a diameter of 125 ± 20 μm. The commercial soda-lime silicate (SLS) glass was remelted at 1220°C for 8 hours and fibers were pulled at 1175°C. The nepheline sodium aluminosilicate glass was melted at 1600°C for 19 hours and fibers were pulled at 1375°C [22]. For sodium silicate and potassium silicate glasses, the melting conditions depended on melt viscosities, with temperatures between 1200 and 1600°C and times between 6 and 20 hours. Alkali silicate glass fibers were pulled at a temperature between 1100°C and 1400°C [21,24].

The protective polymer coating was removed from the commercial silica glass fibers (125 μm in diameter) by immersing in acetone.

1.2.2. Two-Point Bend Test. TPB measurements were made using a home-built system, at a faceplate velocity of 50 or 4000 μm/sec, with fibers either immersed in liquid nitrogen or tested in room temperature (21±2°C) air at a relative humidity of 50±2%. The relative humidity was controlled by blowing a mixture of wet and dry air onto the surfaces of the fibers during the test, and was monitored using a digital psychrometer (Extech RH305). The fibers drawn from melts were tested within thirty minutes after they were formed. The commercial silica glass fibers were tested immediately after the removal of their polymer coatings. No aging effects were observed for any compositions over the course of their respective testing.

1.3. RESULTS AND DISCUSSION

1.3.1. TPB Failure Strain and Failure Stress Calculations. Figure 1.2 shows the TPB failure strain distributions, plotted using the Weibull formalism [36,37], for several glasses, measured in both inert and ambient conditions. The Weibull modulus (m) ranges from 50 to 200, equivalent to a relative standard deviation of ~2% to 0.5%, respectively. Duncan et al. [8] reported comparable values for failure strain for silica fibers under liquid nitrogen (17.6% vs. 17.2% on Figure 1.2) and in room temperature, ambient conditions (6.93% vs. 7.9%). The lower failure strains measured for fibers under

ambient conditions result from fatigue effects associated with water in the atmosphere. Due to the fatigue effect, failure strains are dependent on the measuring conditions, including temperature, humidity and strain rate (faceplate velocity, v_{fp}). Failure strains decrease systematically with increasing relative humidity [24], with increasing temperature [8], or with decreasing strain rate/stress rate [38]. The absolute values of failure strain (or stress) from TPB tests under ambient conditions are difficult to interpret unless these parameters are specified.

The TPB test in this study does not provide a measuring mode of constant stress rate or strain rate, but instead uses a mode of constant faceplate velocity (v_{fp}). This means that the applied strain rate increases with increasing strain (decreasing D, from equation (1)). With the diameter of the fiber known, the strain rate at failure can be calculated from failure strain and v_{fp}:

$$\left(\frac{d\varepsilon}{dt}\right)_{\varepsilon f} = \frac{{\varepsilon_f}^2 \times v_{fp}}{1.198 \times d} \tag{8}$$

E-glass fibers (d = 125 ± 20μm) have a failure strain of 5.6% in air at room temperature and 50% RH, measured at a v_{fp} of 4000μm/s (Figure 1.2). The calculated strain rate at failure is 0.076±0.007 s^{-1}. In liquid nitrogen, the failure strain of E-glass is 10.7%, measured at the same v_{fp} and this corresponds to a strain rate at failure of 0.27±0.03 s^{-1}. Strain rates (or stress rates) are not specified in most traditional strength measurements, except for dynamic fatigue tensile tests for which the strain rate can vary from 10^{-9} to 10^{2} s^{-1} [39]. The dependence of ambient failure strain on faceplate velocities is due to an environmental fatigue effect and will be discussed in another paper [40]. If not specified otherwise, the values of failure stress/strain reported here were obtained at a faceplate velocity of 4000 μm/s.

Table 1.1 summarizes the failure strain values for the glasses studied here, measured at a v_{fp} of 50 and 4000 μm/s and lists the respective strain rate. Table 1.2 lists the nonlinear elastic modulus parameters reported from the literature. Also listed are the calculated failure stresses from equation (6) (ambient data) and equation (7) (LN data), and the respective failure strengths reported from the literature. The failure stress under

inert conditions for fused silica fibers is 12.1±0.2 GPa, using the reported non-linear elastic modulus parameters [32]. Proctor, et al. [9] reported a tensile strength of 11.8±2.2 GPa for 20 μm diameter silica fibers in liquid nitrogen. Pukh, et al. [14] used a three-point bending technique to measure under liquid nitrogen the strength of a variety of compositions prepared as 100-150 μm fibers, and reported intrinsic strengths of 12.0 GPa for polymer coated silica glass. There are also reports of inert strength for silica of 11-14 GPa [41] and ~18% failure strain [2], not measured under liquid nitrogen but in room temperature high vacuum (~10^{-8} Torr). Thus, the value of the strength of silica calculated from the TPB failure strain measured in liquid nitrogen compares favorably with reported values of the inert strength for fused silica measured using conventional methods. Comparable values of strength for fibers with different diameters reported in the literature indicate that the strength is an intrinsic property.

Under ambient conditions, the failure stress for silica calculated from the TPB measurements falls to 7.0±0.1 GPa. Reported strength values include 5.1±1.0 GPa, from a tensile test in 25°C air [9], 4.8 GPa, from a tensile measurement in room temperature 45% RH air [42], 3.6-5.0 GPa in air at 23°C and 55% RH [43], and 4.1 GPa in air at room temperature and 100% RH [44]. The calculated strength from TPB data at 50 μm/s (5.5±0.1 GPa, Table 1.2) compares more favorably with these reported values. Failure strain is lower for slower values of v_{fp} because the longer experimental times allow for greater fatigue effects to reduce the measured glass strength.

For E-glass, the failure stresses calculated from failure strains under liquid nitrogen (5.1±0.1 GPa) and in air (3.8±0.1 GPa) are in good agreement with the respective values reported in the literature. Cameron measured the tensile strength of 75 μm diameter E-glass fibers and reported a value of 5.7±0.3 GPa in liquid nitrogen [45] and 3.8±0.1 GPa at a temperature of 23-28°C and a relative humidity of 32-44% [10]. Gupta [46] reported a tensile strength of 4.3-5.1 GPa for pristine E-glass fibers in room temperature and 50-60% humidity. Lund and Yue [11] reported a tensile strength of 3.0±0.3 GPa for E-glass measured at room temperature in ambient conditions (without specifying temperature and relative humidity). Feih et al. [12] reported a tensile strength of 2.5±0.5 GPa for E-glass in room temperature air.

The TPB failure stress values in Table 1.2 were obtained by estimating E_2 from e_f^* using equation (5). There are some reports for experimental values of E_2 for silica and E-glass and these values were used to calculate failure stresses using equation (4); the two sets of calculated TPB failure stresses are compared in Table 1.3. Using reported values of E_2 [32] and measured values of e_f^*, an inert stress of 14.4 GPa is calculated for silica, compared to values of 12.1-13.6 GPa using the estimate of E_2 from equation (5) and different reported values of E_0 and E_1 [27,29,32]. For E-glass, the inert failure stress calculated from e_f^* using reported [25] and calculated values of E_2 are similar, 5.2 GPa and 5.1 GPa, respectively. For both silica and E-glass, the values of failure stress calculated from the respective failure strains fall within the ranges reported for tensile tests, under liquid nitrogen and in air. The failure stress calculated using measured or estimated values of E_2 for silica differ by about 20%, and a similar variation exists when different values of E_0 and E_1 from the literature are used. Given the limitations in the precision of the higher order modulus terms, it appears that the estimation of E_2 by equation (5) still produces an adequate prediction of failure stress.

For the soda-lime silicate glass, the failure stresses calculated from failure strains are 8.4±0.1 GPa under liquid nitrogen and 4.0±0.1 in air, compared with a reported tensile strength of 7.4±0.6 GPa in liquid nitrogen and 3.4±0.4 GPa in 25°C air, determined by an oblate bubble technique [13]. Pukh, et al. [14] report an inert strength of 7.5 GPa for a soda-lime silicate glass.

The inert failure stress for the nepheline sodium aluminosilicate glass (25 mole% Na_2O, 25 mole% Al_2O_3, 50 mole% SiO_2) measured by the TPB technique (7.3±0.1 GPa) is about 15% lower than the tensile strength measured by a three-point bend technique (8.5 GPa) for a similar glass [14].

For the series of sodium silicate glasses, the inert failure stress increases systematically (after an initial drop from the value for silica), from 7.4±0.1 GPa for x=10 to 8.7±0.1 GPa for x=35 (Figure 1.3). These failure stresses are 2-3 times greater than the inert tensile strengths reported in three-point bend tests [15], four-point bend tests [14], and from theoretical ultimate strengths calculated from elastic constants [47]. The greater failure stresses from the present TPB measurements may be due to differences in sample quality or aging effects associated with the reported tensile tests, but are also

related to stress/strain rate effects in the TPB measurements, as discussed in more detail below. The increase in failure stress with increasing soda content, between 10 and 35 mole%, seems counterintuitive given the expectations that strength should decrease, as does the zero strain elastic modulus (E_0, Table 1.2), when alkali contents increase. Bridging oxygens in the silicate network are replaced by non-bridging oxygens with addition of Na_2O (or K_2O) and so the overall 'strength' of the network should decrease with the decrease in network connectivity. Bartenev reported an associated decrease in the theoretical strength of binary sodium silicate glasses with increasing soda contents [47]. However, the strength measurements reported by Kennedy et al. [15] and Pukh et al [14] have similar compositional trends, albeit lower absolute values, as our failure stress calculations (Figure 1.3). Kennedy argued that the increase in failure strength of Na-silicate glasses was a result of the development of nanoscale flaws associated with phase separation in glass with lower Na_2O-contents. In the present study, the probability of phase separation in thin, rapidly cooled fibers would be less than what Kennedy et al. encountered with their thicker samples.

For the series of potassium silicate glasses, the inert failure stress decreases from 6.4±0.1 for y=15 to 6.0±0.1 for y =25 (Table 1.2 and Figure 1.4). The absolute values are again about two times greater than the inert strengths calculated from indentation hardness measurements [47].

1.3.2. Inert Failure Strain Dependence on Faceplate Velocities. Figure 1.5 compares the failure strain measurements under liquid nitrogen at two different faceplate velocities, v_{fp} = 50 and 4000 μm/s, for several different glasses. There is a small, but reproducible, shift to greater values of ε_f^* at the greater value of v_{fp}, for both silica and E-glass, and a significant decrease in ε_f^* at the greater v_{fp} for the $25Na_2O{\cdot}75SiO_2$ glass, as well as for other binary sodium and potassium silicate glasses (Table 1.1).

'Inert fatigue' behavior has been reported before for silica [7,9,48]. Proctor et al. [9] attributed this to the finite activity of water in liquid nitrogen leading to normal environmental fatigue behavior. Kurkjian, et al. [7], however, explained the effect as a consequence of the normal probability of failure due to thermal fluctuations of bond strengths under high stress, with longer times (slower v_{fp}) allowing weaker bonds to rupture to initiate failure. Matthewson et al. [48] did not differentiate inert fatigue and

environmental fatigue and considered both processes as caused by stress-induced reactions leading to weaker bonds at longer times.

In contrast to the 'normal' inert fatigue behavior of silica, E-glass, and the nepheline glass (Table 1.1), the binary Na- and K-silicate glasses exhibit an opposite behavior for the dependence of inert failure strain on the faceplate velocity; that is, inert failure strains for these modified glasses are lower at greater values of v_{fp} (shown in Figure 1.5 and Table 1.1). This effect has been referred to as the Inert Delayed Failure Effect (IDFE), and has been seen in silicate glasses with depolymerized structures [21,24]. The SLS glass also exhibits IDFE behavior but to a much smaller degree than the binary alkali silicate glasses. One explanation for IDFE is that the structure of silicate glasses with relatively large fractions of non-bridging oxygens can reorganize or relax when stress is applied, perhaps in a manner similar to that which produces low-temperature internal friction peaks [49,50]. Given more time (slower v_{fp}), the structure can reorganize more before bonds fail and cracks are initiated, and thus failure occurs at a greater overall strain, countering the effects of weaker network bonds in the more depolymerized glass structures. The magnitude of the IDFE response is not as great for the K-silicate glasses as for the Na-silicate glasses. There is a small decrease in inert failure strength when the K_2O-content increases from 15 to 25 mole%. However, IDFE is significant for the $25K_2O{\cdot}75SiO_2$ glass (Table 1.1) and so at a slower faceplate velocity (50 μm/s), this glass has a greater failure stress than the $20K_2O{\cdot}80SiO_2$ glass.

The magnitude of IDFE for the Na-silicate glasses increases with increasing soda content [19], and this effect can possibly explain the counterintuitive compositional trend in failure stress shown in Figure 1.3. Figure 1.6 plots the inert failure stresses for the Na-silicate glasses as a function of the failure strain rate. Because the IDFE for the Na_2O-rich glasses are greater, failure stresses for these glasses will decrease more at higher values of strain rate (or faceplate velocity) than glasses with lower Na_2O-contents and a lower value of IDFE. If the extrapolation in Figure 1.6 is accurate, when the strain rate in a TPB experiment exceeds ~10^4 s^{-1}, the compositional dependence of the inert strength reverses so that glasses with lower Na_2O-contents are expected to have greater inert strengths, consistent with the compositional dependence of the silicate network structure.

An interesting concept, 'instantaneous strength' arises from this discussion. At what speed can a strength measurement be considered instantaneous and correlated to the ultimate strength or the theoretical strength of glass? In slow-crack growth studies, it has been suggested [51] that the crack speed corresponding to K_{IC}, ~0.1 m/s initiates 'spontaneous' crack growth. The theoretical maximum velocity of crack propagation is set by the Rayleigh wave speed limit [52,53,54]. For fused silica, V_R = 3420 m/s [55]. A crack propagating through a 100 μm sample at V_R that fails at 10% strain corresponds to a strain rate of ~10^6 s^{-1}, and this Rayleigh limit is indicated in Figure 1.6 (a). However, if instantaneous failure in a two-point bend test is controlled by crack nucleation instead of crack propagation, then the limit on strain rate may be related to the vibrational period of the bonds that constitute the glass structure [56]. The vibrational frequency of a Si-O is ~10^{14} s^{-1}. For a glass that fails at an inert strain of 10%, a corresponding strain rate limited by bond vibrations would be 10^{13} s^{-1}. If the strain rate limit is fixed either by the Rayleigh velocity or the bond vibrational frequencies, then one predicts that the "instantaneous strength" of the Na-silicate glasses should decrease with increasing Na_2O-content (Figure 1.6 (b)), as expected from the decreasing connectivity of the silicate network. For those glasses with no IDFE (viz., exhibit 'normal' inert fatigue behavior), like the $10Na_2O{\cdot}90SiO_2$ glass in Figure 1.6, the "instantaneous inert strength" will not differ significantly from the strengths measured in the TPB experiments.

1.3.3. Modified TPB Failure Strain Equation. The nonlinear elastic behavior of glass not only affects the strain-stress conversion but also generates a challenge to one of the assumptions in strain measurement by the two-point bend test. The original equation of TPB strain measurement (Equation (1)) is derived based on an assumption that the neutral (zero-strain) axis remains in the center of the fiber. Suhir [57] suggested that the neutral axis might shift due to the nonlinear elastic behavior of glass. Muraoka [58] expanded this analysis to include the effects of E_2 and predicted that the failure strain from a TPB test, calculated using equation (1), should be modified as according to:

$$\varepsilon_{f(M)} = \varepsilon_f \left\{ 1 - \frac{1}{8}\frac{E_1}{E_0}\varepsilon_f - \frac{1}{32}\frac{E_1}{E_0}\left[\frac{1}{2}\frac{E_2}{E_0} - \frac{1}{4}\left(\frac{E_1}{E_0}\right)^2\right]\varepsilon_f{}^3 \right\} \qquad (9)$$

Table 1.4 compares the failure strains calculated from Equations (1) and (9) for silica and E-glass, using reported values of E_0, E_1 and E_2. In general, the Muraoka equation predicts similar failure stains as those from equation (1), indicating that the non-linear modulus has little effect on the measured failure strain. Thus, equation (1) provides an adequate determination for failure strains, particularly for glasses for which information about the nonlinear modulus is lacking.

1.4. SUMMARY

The two-point bend technique is an effective and efficient way to measure failure strain of glass fibers in both inert and ambient conditions. With the knowledge of the higher order terms of elastic modulus, failure stress can be calculated from the failure strain data. The comparison with reported strength measurements is summarized as follows:

(1) The use of TPB failure strain measurements to predict the strength of glass has an advantage of experimental simplicity and minimizes the effects of extrinsic flaws when compared to traditional three- or four-point bending or tensile strength measurements. The test can be performed under a variety of conditions, including inert (liquid nitrogen) and ambient, and at different strain rates (faceplate velocities).

(2) Two-point bend failure strain data collected from glasses that exhibit normal ‘inert fatigue’ behavior, like silica, low soda-silicates, E-glass and a nepheline sodium aluminosilicate glass, yield values for failure strengths, based on reported values for nonlinear modulus parameters, that are in good agreement with the strengths reported from conventional tensile tests on the respective glasses.

(3) The calculated inert strengths for binary sodium silicate glasses increase with increasing Na_2O-contents. This is counterintuitive because the addition of modifying oxides is usually considered to weaken the glass structure. However, there is a dependence of failure strain on the strain rate, determined from the faceplate velocity. This inert delayed failure effect (IDFE) may account for the compositional dependence of the apparent failure strengths of these glasses. If the strain rates are extrapolated to limits defined by the Rayleigh wave speed limit or the vibrational limits of individual bonds, then the expected decrease in strength with increasing Na_2O-content could be realized.

ACKNOWLEDGMENT

The authors wish to thank colleagues at AT&T, PPG Industries, and Owens-Illinois for providing the commercial glass samples.

REFERENCES

[1] A. A. Griffith, 'The Phenomena of Rupture and Flow in Solids' *Phil. Trans. Roy. Soc.*, 22 163-198 (1921).

[2] C. R. Kurkjian, P. K. Gupta, R. K. Brow, 'The Strength of Silicate Glass: What Do We Know, What Do We Need to Know,' *Int. J. Appl. Glass Sci.*, 1[1] 27-37 (2010).

[3] R. J. Charles, 'Static Fatigue of Glass. I', *J. Appl. Phys.*, 29 [11] 1549-53 (1958).

[4] R. J. Charles, 'Static Fatigue of Glass. II', *J. Appl. Phys.*, 29 [11] 1554-60 (1958).

[5] R. J. Charles, 'Dynamic Fatigue of Glass. II', *J. Appl. Phys.*, 29 [12] 1657-62 (1958).

[6] P. K. Gupta and C. R. Kurkjian, 'Intrinsic failure and nonlinear elastic behavior of glass,' *J. Non-Cryst. Solids*, 351 2324-8 (2005).

[7] C. R. Kurkjian, P. K. Gupta, R. K. Brow, and N. P. Lower, 'The Intrinsic Strength and Fatigue of Oxide Glasses,' *J. Non-Cryst. Solids*, 316 [1] 114-24 (2003).

[8] W. J. Duncan, P. W. France, and S. P. Craig, 'The Effect of Environment on the Strength of Optical Fiber' in: C. R. Kurkjian (Ed.), *Strength of Inorganic Glass*, Plenum, 1985, p. 309.

[9] B. A. Proctor, I. Whitney, and J. W. Johnson, 'Strength of Fused Silica,' *Proc. Roy Soc. A*, 297 [1451] 534-57 (1967).

[10] N. M. Cameron, 'Relation between Melt Treatment and Glass Fiber Strength,' *J. Am. Ceram. Soc.*, 49 [3] 144-8 (1966).

[11] M. D. Lund and Y. Yue, 'Impact of Drawing Stress on the Tensile Strength of Oxide Glass Fibers' *J. Am. Ceram. Soc.*, 93 [10] 3236-43 (2010).

[12] S. Feih, K. Manatpon, Z. Mathys, A. G. Gibson, and A. P. Mouritz, 'Strength Degradation of Glass Fibers at High Temperatures,' *J. Mater. Sci.*, 44 [2] 392-400 (2009).

[13] F. M. Ernsberger, 'Tensile and Compressive Strength of Pristine Glasses by an Oblate Bubble Technique,' *Phys. Chem. Glasses,* 10 [6] 240-5 (1969).

[14] V. P. Pukh, L. G. Baikova, M. F. Kireenko, L. V. Tikhonova, T. P. Kazannikova, and A. B. Sinani, 'Atomic Structue and Strength of Inorganic Glasses,' *Phys. Solid State,* 47 [5] 850-5 (2005).

[15] C. R. Kennedy, R. R. Bradt, and G. E. Rindone, 'The strength of binary alkali silicate glasses,' *Phys. Chem. Glasses,* 21 [3] 99-105 (1980).

[16] J. B. Murgatoryd, 'The Strength of Glass Fibers,' *J. Soc. Glass Technol.*, 28 368-97 (1944).

[17] P. W. France, M. J. Paradine, M. H. Reeve, and G. R. Newns, 'Liquid Nitrogen Strengths of Coated Optical Glass Fibers,' *J. Mater. Sci.*, 15 [4] 825-830 (1980).

[18] M. J. Matthewson, C. R. Kurkjian, and S. T. Gulati, 'Strength Measurement of Optical Fibers by Bending,' *J. Am. Ceram. Soc.*, 69 [11] 815-21 (1986).

[19] R. K. Brow, N. P. Lower, and C. R. Kurkjian, 'TPB Test Provides New Insights to Fiber Strength and Quality,' Ceram. Bull., 14 [4] 50-53 (2005).

[20] R. K. Brow, N. P. Lower, C. R. Kurkjian and H. Li, 'The Effects of Melt History on the Failure Characteristics of Pristine Glass Fibers,' *Phys. Chem. Glasses, Eur. J. Glass Sci. Tech.*, 50 [1] 31-33 (2009).

[21] N. P. Lower, R. K. Brow and C. R. Kurkjian, 'Inert Failure Strain Studies of Sodium Silicate Glass Fibers,' *J. Non-Cryst. Solids*, 349 168-172 (2004).

[22] N. P. Lower, R. K. Brow and C. R. Kurkjian, 'Inert Failure Strain Studies of Sodium Aluminosilicate Glass Fibers,' *J. Non-Cryst. Solids*, 344 [1-2] 17-21 (2004).

[23] R. K. Brow, N. P. Lower, A.J. Lang and C.R. Kurkjian 'Structure and the Intrinsic Strength of Glass,' *Glastech. Ber. Glass Sci. Technol.,* 75 C2 133-138 (2002).

[24] N. P. Lower, Ph D. Thesis, 'Failure Study of Glass Fibers,' Missouri University of Science and Technology, 2004.

[25] R. Bruckner and G. Pahler, 'Strength and Elastic Constants of Multi Component Glass Fibers as a Function of Thermal and Mechanical Prehistory,' in C.R. Kurkjian (Ed.), *Strength of Inorganic Glass*, Plenum Press, New York, 1986, p. 329.

[26] A. L. Ruoff, 'On the Ultimate Yield Strength of Solids' *J. Appl. Phys.*, 49 [1] 197-200 (1978).

[27] A. K. Varshneya, *Fundamentals of Inorganic Glass*, Academic, New York, 1994, p. 164.

[28] Q. Wang, G. A. Saunders, H. B. Senin, and E. F. Lambson, 'Temperature Dependences of the Third-Order Elastic Constants and Acoustic Mode Vibrational Anharmonicity of Vitreous Silica,' *J. Non-Cryst. Solids*, 143 [1] 65-74 (1992).

[29] V. N. Sanin, B. G. Varshall, Y. L. Krenev, 'Third-Order Elastic Constants of Fused Silica and Silicate Glasses,' *Glass Phys. Chem.*, 21 [2] (1995) 111-14.

[30] C. Zha, R. J. Hemley, H. Mao, T. S. Duffy and C. Meade, 'Acoustic Velocities and Refractive Index of SiO_2 glass to 57.5 GPa by Brillouin Scattering' *Phy. Rev. B*, 50 [18] 13105-12 (1994).

[31] D. Cavaille, C. Levelut, R. Vialla, R. Vacher, E. L. Bourhis, 'Third-Order Elastic Constants Determination in Soda-Lime-Silica Glass by Brillouin Scattering,' *J. Non-Cryst. Solids,* 260 [3] 235-41 (1999).

[32] J. T. Krause, L. R. Testardi and R. R. Thurston, 'Deviations from Linearity in the Dependence of Elongation upon Force for Fibres of Simple Glass Formers and of Glass Optical Lightguides,' *Phys. Chem. Glasses,* 20 [6] 135-9 (1979).

[33] F. P. Mallinder and B. A. Proctor, 'Elastic Constants of Fused Silica as a Function of Large Tensile Strain,' *Phys. Chem. Glasses*, 5 91-103 (1964).

[34] P. M. Halleck, R. E. Pacalo and E. K. Graham, 'The Effects of Annealing and Aluminum Substitution on the Elastic Behavior of Alkali Silicate Glasses,' *J. Non-Cryst. Solids,* 86 [1-2] 190-203 (1986).

[35] M. H. Manghnani, 'Effects of Composition, Pressure, and Temperature on the Elastic, Thermal, and Ultrasonic Attenuation Properties of Sodium Silicate Glasses,' *Int. Congr. Glass,* 10th (1974) 11.104-14.

[36] W. Weibull, 'A Statistical Theory of the Strength of Materials,' *Eng. Res. Proc.* 151 1-45 (1939).

[37] W. Weibull, 'A Statistical Distribution of Wide Applicability,' *J. Appl. Mechan.*, 18 293-7 (1951)

[38] V. V. Rondinella and M. J. Matthewson, 'Effect of Loading Mode and Coating on Dynamic Fatigue of Optical Fiber in Two-Point Bending,' *J. Am. Ceram. Soc.*, 76 [1] 139-44 (1993).

[39] S. L. Semjonov, G. S. Glaesemann, D. A. Clark and M. M. Bubnov, 'Fatigue Behavior of Silica Fibers with Different Defects,' *Proc. SPIE*, 4215 28-35 (2001).

[40] Z. Tang, R. K. Brow, and C. R. Kurkjian, 'Two-Point Bend Studies of Fatigue Effects in Silicate Glasses,' to be submitted to *J. Non-Cryst. Solids,* (2011)

[41] W.A. Smith, T.M. Michalske, 'Inert Strength of Pristine Glass Fibers,' *Sandia Report*, SAND92-1107 (1993).

[42] H. H. Yuse, P. L. Key, and D. R. Biswas, 'Investigation of the Mechanical Behavior of Low Strength Fibers,' *Proc. SPIE,* 1174 272-8 (1989).

[43] J. E. Ritter, Jr, J. M. Sullivan, and K. Jakus, 'Application of Fracture Mechanics Theory to Fatigue Failure of Optical Glass Fibers,' *J. Appl. Phys.*, 49 [9] 4779-82 (1978).

[44] G. S. Glaesemann, 'The Mechanical Behavior of Large Flaws in Optical Fiber and Their Role in Reliability Predictions,' Corning, Inc. Available from internet:<http://www.new.corning.com/assets/0/433/573/625/631/F6439231-19C5-445B-947C-D5D5CB64951E.pdf>, sited: Jun 29, 2011

[45] N. M. Cameron, 'The Effect of Environment and Temperature on the Strength of E-glass Fibres. Part 1. High Vacuum and Low Temperature,' *Glass Tech.*, 9 [1] 14-21 (1968).

[46] P. K. Gupta, 'Effects of Testing Parameters on the Tensile Strength of Pristine E and S Glass Fibers,' in: C. R. Kurkjian (Ed.), *Strength of Inorganic Glass*, Plenum, 1985, p. 351.

[47] G. M. Bartenev and D. S. Sanditov, 'The Strength and Some Mechanical and Thermal Characteristics of High-Strength Glasses,' *J. Non-Cryst. Solids*, 48 [2-3] 405-21(1982).

[48] M. J. Matthewson, C. R. Kurkjian, C. D. Haines and N. Venugopal, 'Temperature Dependence of Strength and Fatigue of Fused Silica Fiber in the Range 77 to 473 K,' *Proc. SPIE*, 4940 74-9 (2003).

[49] D. E. Day, and G. E. Rindone, 'Properties of soda aluminosilicate glasses. II. Internal Friction,' *J. Am. Ceram. Soc.*, 45 496-504 (1962).

[50] J. E. Shelby. Jr., and D. E. Day, 'Mechanical Relaxations in Mixed-Alkali Silicate Glasses: I, Results,' *J. Am. Ceram. Soc.*, 52 [4] 169-74 (1969).

[51] A. K. Varshneya, *Fundamentals of Inorganic Glass*, Academic Press, San Diego, CA, 1994, p. 419.

[52] P. D. Washbaugh and W. G. Knauss, 'A Reconciliation of Dynamic Crack Velocity and Rayleigh Wave Speed in Isotropic Brittle Solids,' *Int. J. Fracture*, 65 97-114 (1994).

[53] N. Bourne, J. Millett, Z. Rosenberg, and N. Murray, 'On the shock induced failure of brittle solids,' *J. Mech. Phys. Solids*, 46 [10] (1998) 1887-1908.

[54] F. F. Abraham, R. Walkup, H. Gao, M. Duchaineau, T. D. D. L. Rubla, and M. Seager 'Simulating Materials Failure by Using up to One Billion Atoms and the World's Fastest Computer: Brittle Fracture' *Proc. Nat. Acad. Sci. USA*, 99 [9] 5777-82 (2002).'

[55] C. Comte and J. V. Stebut, 'Microprobe-Type Measurement of Young's modulus and Poisson Coefficient by Means of Depth Sensing Indentation and Acoustic Microscopy,' *Surf. Coat. Tech.*, 154 [1] 42-8 (2002).

[56] C. R. Kurkjian, and D. Inniss, 'Understanding Mechanical Properties of Lightguides: a Commentary,' *Optical Eng*., 30 [6] 681-9 (1991).

[57] E. Suhir, 'Effect of the Nonlinear Behavior of the Material on Two-Point Bending of Optical Glass Fibers,' *Trans. ASME, J. Electron. Packag.*, 114 [2] 246-50 (1992).

[58] M. Muraoka, 'The Maximum Stress in Optical Glass Fibers Under Two-Point Bending,' *Trans. ASME, J. Electron. Packag.*, 123 [1] 70-3 (2001).

Table 1.1. TPB failure strain (ε_f) and strain rate at failure ($\dot{\varepsilon}_f$) for glasses tested at faceplate velocities of 50 and 4000 μm/s, in liquid nitrogen and in air (20°C, 50% humidity).

Glass Composition	$\varepsilon_{f\cdot 4000}$ (%)	$\dot{\varepsilon}_{f\cdot 4000}$ (s^{-1})	$\varepsilon_{f\cdot 50}$ (%)	$\dot{\varepsilon}_{f\cdot 50}$ (s^{-1})
Silica (air)	7.9 ± 0.1	0.17 ± 0.01	6.4 ± 0.1	0.0014 ± 0.0001
Silica (LN)	17.2 ± 0.2	0.80 ± 0.02	16.9 ± 0.2	0.0099 ± 0.0002
E-glass (air)	5.6 ± 0.1	0.076 ± 0.007	4.4 ± 0.3	0.0006 ± 0.0001
E-glass (LN)	10.7 ± 0.2	0.27 ± 0.03	10.5 ± 0.2	0.0035 ± 0.0004
SLS (air)	5.6 ± 0.1	0.077 ± 0.006	4.3 ± 0.1	0.0006 ± 0.0001
SLS (LN)	16.4 ± 0.1	0.68 ± 0.05	16.5 ± 0.2	0.0083 ± 0.0007
Nepheline (LN)	14.8 ± 0.1 [20]	0.53 ± 0.05	14.8 ± 0.1 [20]	0.0069 ± 0.0008
$x$$Na_2O$·(100-$x$)$SiO_2$				
x = 10 (LN)	16.0 ± 0.1 [21]	0.52 ± 0.03	16.0 ± 0.1 [21]	0.007 ± 0.001
x = 15 (LN)	17.6 ± 0.1 [21]	0.81 ± 0.03	17.9 ± 0.1 [21]	0.011 ± 0.001
x = 20 (LN)	19.2 ± 0.1 [21]	0.99 ± 0.03	19.9 ± 0.1 [21]	0.012 ± 0.001
x = 25 (LN)	20.9 ± 0.1 [21]	1.08 ± 0.09	22.0 ± 0.1 [21]	0.015 ± 0.001
x = 30 (LN)	22.5 ± 0.1 [21]	1.15 ± 0.15	24.2 ± 0.1 [21]	0.018 ± 0.002
x = 35 (LN)	23.4 ± 0.2 [21]	1.37 ± 0.23		
$y$$K_2O$·(100-$y$)$SiO_2$				
y = 15 (LN)	18.0 ± 0.1 [24]	0.70 ± 0.03	18.0 ± 0.1 [24]	0.0089 ± 0.0004
y = 20 (LN)	18.9 ± 0.1 [24]	0.83 ± 0.04	18.9 ± 0.1 [24]	0.011 ± 0.001
y = 25 (LN)	19.5 ± 0.1 [24]	0.89 ± 0.12	20.1 ± 0.1 [24]	0.012 ± 0.001

Table 1.2. Nonlinear elastic moduli (E_0, E_1) reported in the literature and calculated from equation (5) (E_2), failure stresses (σ_f) calculated from TPB failure strains using equations (6) and (7), and measured failure strengths (σ_{fs}) reported in the literature, of available glasses tested at 50 and 4000 μm/s, in liquid nitrogen and in air (20°C, 50% humidity).

Glass Composition	E_0 (GPa)	E_1 (GPa)	E_2 (GPa)	$\sigma_{f\cdot 4000}$ (GPa)	$\sigma_{f\cdot 50}$ (GPa)	σ_{fs} (GPa)
Silica (air)	72 [32]	772.4 [32]	-12498	7.0 ± 0.1	5.5 ± 0.1	5.1 [53], 4.8 [42]
Silica (LN)	72 [a] [32]	772.4 [a] [32]	-12498	12.1 ± 0.2	11.5 ± 0.1	11.8 [53],12.0 [14], 11-14 [55]
E-glass (air)	74 [25]	-73.2 [25]	-7759	3.8 ± 0.1	3.1 ± 0.2	3.8 [10], 3.0 [11], 2.5 [12], 3.4 [45], 4.3-5.1 [46]
E-glass (LN)	74 [a] [25]	-73.2 [a] [25]	-7759	5.1 ± 0.1	5.0 ± 0.1	5.7 [45]
SLS (air)	72 [31]	121[31]	-6210	4.0 ± 0.1	3.1 ± 0.1	3.2 [14], 3.4 [13]
SLS (LN)	72 [a] [31]	121 [a] [31]	-6210	8.4 ± 0.1	8.5 ± 0.1	7.5 [14], 7.4 [13]
Nepheline (LN)	74.1[a] [34]	-0.9 [a] [34]	-6765	7.3 ± 0.1	7.3 ± 0.1	8.5 [14]
xNa$_2$O·(100-x)SiO$_2$						
x = 10 (LN)	65.3 [a] [35]	97.2 [a] [35]	-6317	7.4 ± 0.1	7.4 ± 0.1	
x = 15 (LN)	62.9 [a] [35]	47.7 [a] [35]	-4603	7.6 ± 0.1	7.8 ± 0.1	2.1[b] [15], 4.6 [b] [47], 2.7 [14]
x = 20 (LN)	61.1 [a] [35]	8.0 [a] [35]	-3396	7.9 ± 0.1	8.2 ± 0.1	2.3[b] [15], 4.0 [b] [47]
x = 25 (LN)	59.8 [a] [35]	-20.6 [a] [35]	-2539	8.2 ± 0.1	8.9 ± 0.1	2.7[b] [15]
x = 30 (LN)	59.3 [a] [35]	-36.9 [a] [35]	-2017	8.6 ± 0.1	9.2 ± 0.1	2.8[b] [15], 3.7 [b] [47]
x = 35 (LN)	58.2 [a] [35]	-47.6 [a] [35]	-1701	8.7 ± 0.1		2.9[b] [15], 3.7 [b] [47]
yK$_2$O·(100-y)SiO$_2$						
y = 15 (LN)	52.6 [a] [35]	22.8 [a] [35]	-3504	6.4 ± 0.1	6.4 ± 0.1	3.6[b] [47]
y = 20 (LN)	49.0 [a] [35]	-6.4 [a] [35]	-2679	6.1 ± 0.1	6.1 ± 0.1	3.4[b] [47]
y = 25 (LN)	46.4 [a] [35]	-8.3 [a] [35]	-2358	6.0 ± 0.1	6.2 ± 0.1	2.7[b] [47]

a. Nonlinear elastic moduli were measured at room temperature but used to calculate inert σ_f.

b. Reported values of strength are from Na-silicate glasses with slightly different compositions from those tested here.

Table 1.3. Calculated (equation (5) and reported fourth-order nonlinear elastic modulus (E_2), and corresponding calculated failure stress (σ_f) from TPB failure strains measured at a faceplate velocity of 4000 μm/s for silica and E-glass in liquid nitrogen and in air.

Glass Composition	$\varepsilon_f \cdot 4000$ (%)	E_0 (GPa)	E_1 (GPa)	E_2 from Eq. (5)		E_2 from literature	
				E_2(GPa)	σ_f (GPa)	E_2(GPa)	σ_f (GPa)
Silica (air)	7.9 ± 0.1	72 [32]	772.4 [32]	-12498	7.0 ± 0.1	-11084 [a] [32]	7.2 ± 0.1
Silica (LN)	17.2 ± 0.3	72 [a] [32]	772.4 [a] [32]	-12498	12.1 ± 0.2	-11084 [a] [32]	14.4 ± 0.3
Silica (air)	7.9 ± 0.1	72.4 [27]	906 [27]	-15429	7.3 ± 0.1		
Silica (LN)	17.2 ± 0.3	72.4 [a] [27]	906 [a] [27]	-15429	12.8 ± 0.2		
Silica (air)	7.9 ± 0.1	72 [32]	1074 [29]	-17383	7.6 ± 0.1		
Silica (LN)	17.2 ± 0.3	72 [a] [32]	1074 [a] [29]	-17383	13.6 ± 0.2		
E-glass (air)	5.6 ± 0.1	74 [25]	-73.2 [25]	-7759	3.8 ± 0.1	-11054 [25]	3.7 ± 0.1
E-glass (LN)	10.7 ± 0.2	74 [a] [25]	-73.2 [a] [25]	-7759	5.1 ± 0.1	-11054 [a] [25]	5.2 ± 0.1

a. Nonlinear elastic moduli were measured at room temperature but used to calculate inert σ_f.

Table 1.4. Failure strains (ε_f) measured at 4000 μm/s, in liquid nitrogen and in air (20°C, 50% humidity) calculated using equations (1) and (9).

Glass Composition	$\varepsilon_{f,\text{ Eq. (1)}}$ (%)	$\varepsilon_{f\text{ (M), Eq. (9)}}$ (%)
E-glass (air)	5.6 ± 0.1	5.7
E-glass (LN)	10.7 ± 0.2	10.8
Silica (air)	7.9 ± 0.1	7.3
Silica (LN)	17.2 ± 0.3	16.1

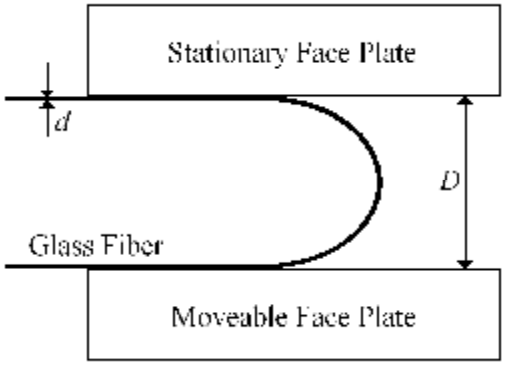

Figure 1.1. Schematic diagram of the TPB test.

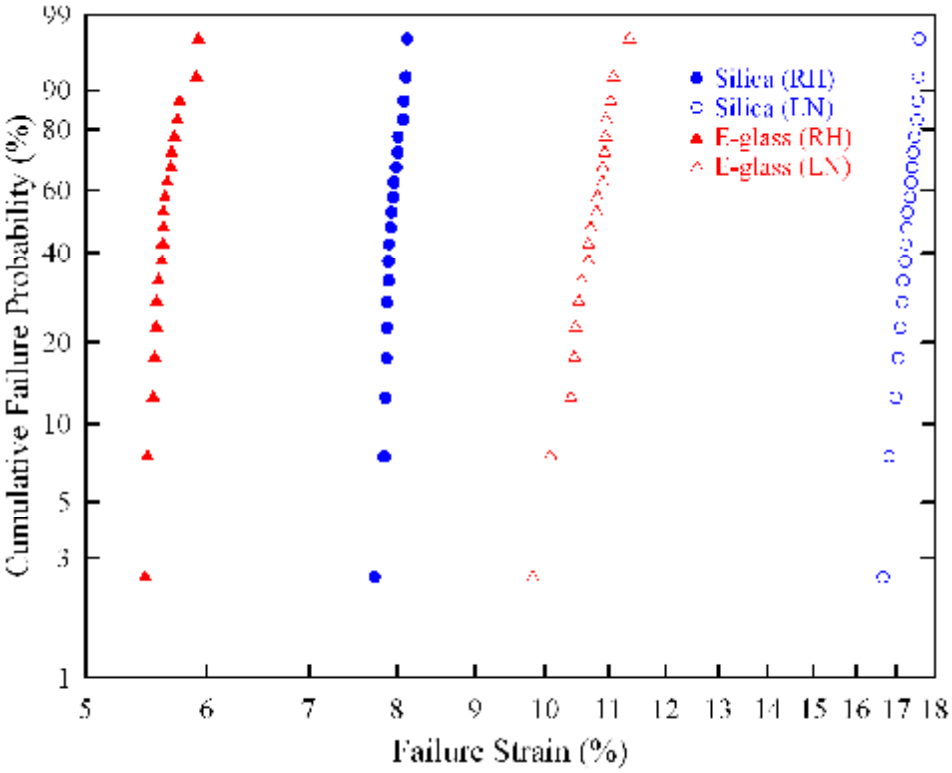

Figure 1.2. Weibull distributions of failure strains for silica and E-glass fibers measured using TPB (v_{fp} = 4000 μm/s) in inert (LN) and ambient (RH 50%) conditions.

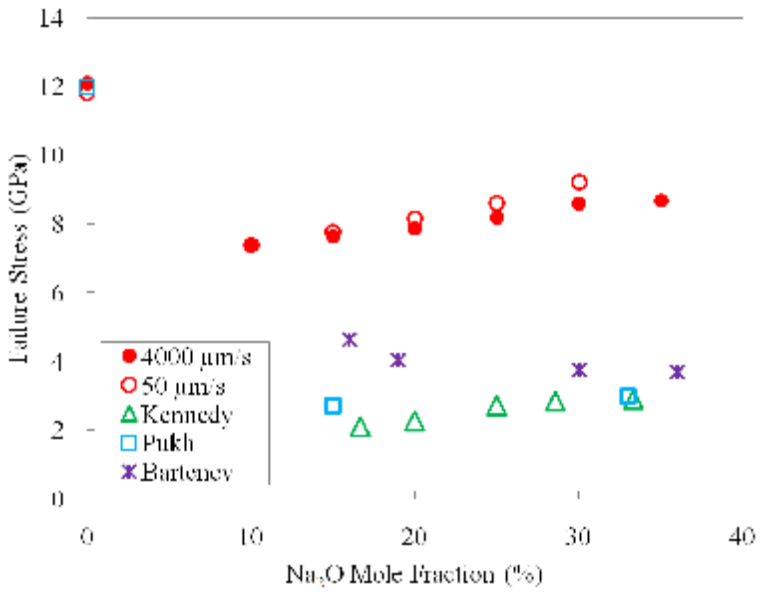

Figure 1.3. Inert failure stress for silica and xNa$_2$O·(100-x)SiO$_2$ glasses, calculated from TPB failure strains [19] (v_{fp} = 4000 μm/s and 50 μm/s), compared to inert strengths for similar glasses [14,15, 47].

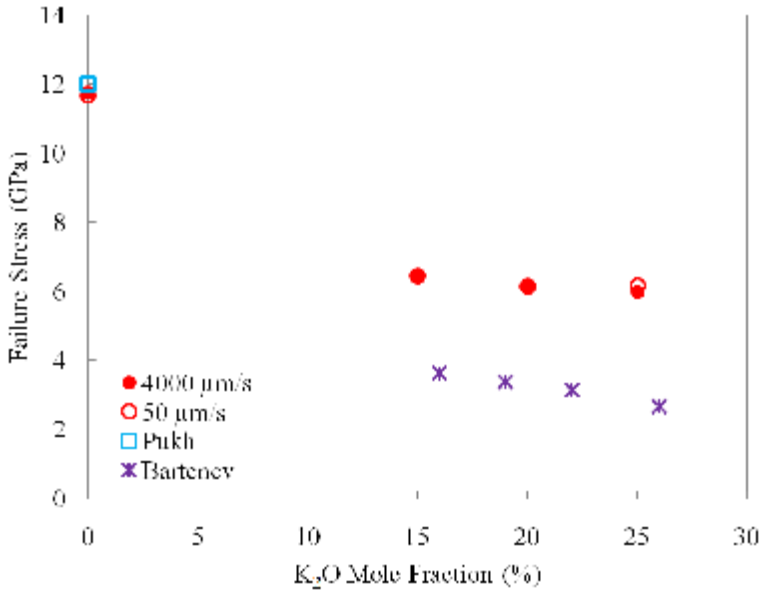

Figure 1.4. Inert failure stress for silica and yK$_2$O·(100-y)SiO$_2$ glasses, calculated from TPB failure strains [24] (v_{fp} = 4000 μm/s and 50 μm/s), compared to inert strengths for similar glasses [15,47].

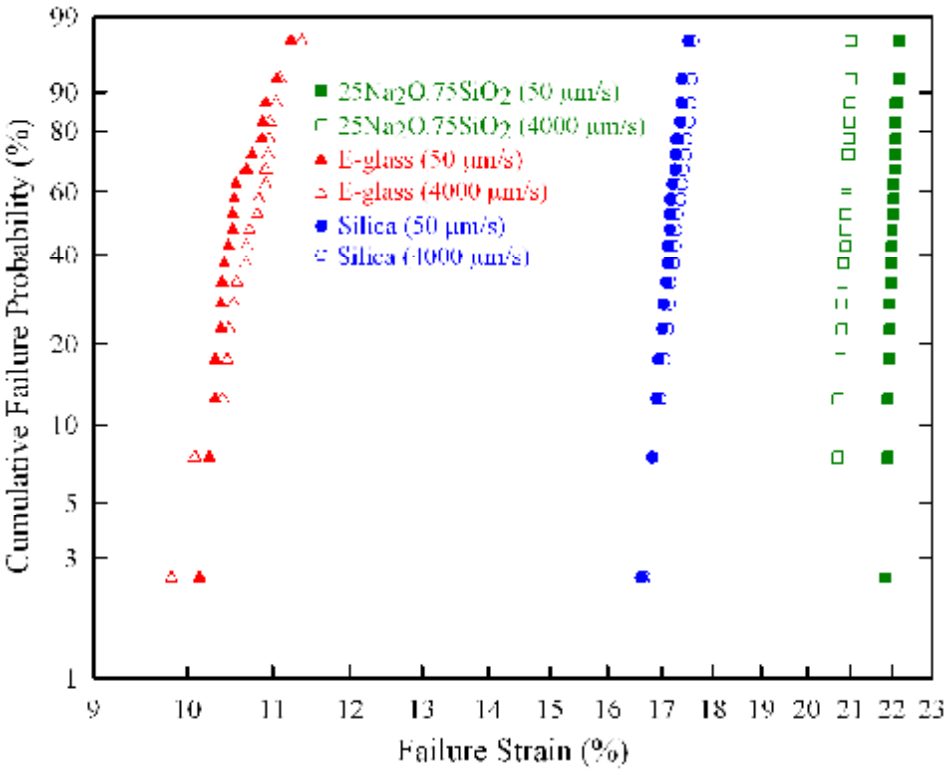

Figure 1.5. Weibull distributions of failure strains under inert conditions for several glasses measured using different faceplate velocities (v_{fp} = 50 μm/s, 4000 μm/s).

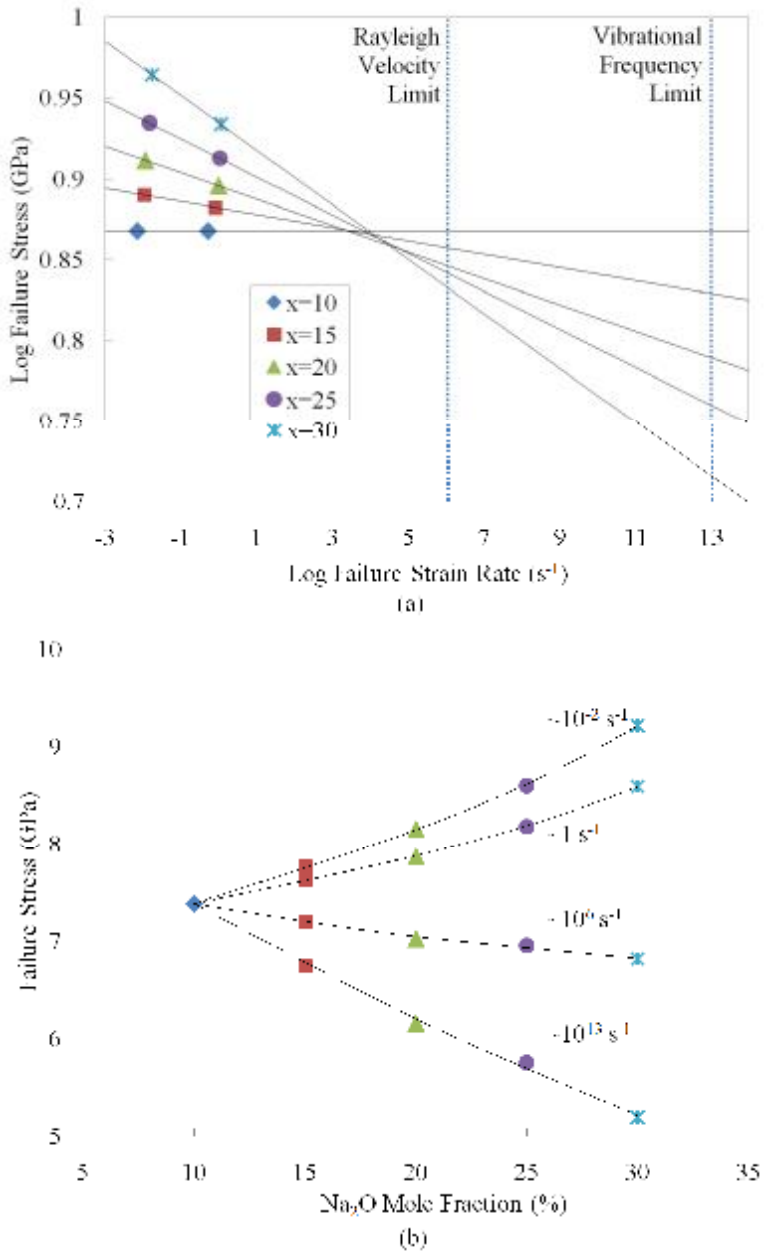

Figure 1.6. Inert failure stresses for xNa$_2$O·(100-x)SiO$_2$ glass, calculated from TPB failure strains [19] (v_{fp} = 4000 μm/s and 50 μm/s), (a) plotted against the failure strain rate, with extrapolations to the Rayleigh velocity limit and vibration frequency limit; (b) plotted as a function of Na$_2$O mole fraction.

2. INERT FAILURE STRAIN MEASUREMENTS OF SODIUM BORATE GLASS FIBERS

Zhongzhi Tang[a], Nathan P. Lower[a,b], Charles R. Kurkjian[c], and Richard K. Brow[a]

[a]Missouri University of Science & Technology, Department of Materials Science & Engineering, Rolla, MO 65409, USA

[b]Rockwell Collins, Inc., Advanced Technology Center, 400 Collins Road NE, MS 108-101, Cedar Rapids, IA 52498, USA

[c]University of Southern Maine, Department of Engineering, P.O. Box 9300, Gorham, ME 04038, USA

ABSTRACT

The two-point bend (TPB) technique was used to measure the failure strains of $x$$Na_2O$·(100-$x$)$B_2O_3$ glass fibers in inert conditions (under liquid nitrogen). In such experiments, the effects of extrinsic flaws and environmental fatigue are minimized so that intrinsic failure characteristics might be determined and related to glass composition and structure. The inert failure strain for pure B_2O_3 glass is 36±5%; to our knowledge this is the largest inert failure strain ever reported for an oxide glass in a TPB experiment. Failure strains decrease systematically as Na_2O contents of glasses increases. The addition of Na_2O increases the dimensionality and connectivity of the borate glass structure and hence increases its resistance to deformation before failure. Similar correlations between inert failure strain and network connectivity have been reported for silicate and aluminosilicate glasses.

2.1. INTRODUCTION

The experimental or practical strengths of glass are typically lower than the theoretical values, sometimes by several orders of magnitude, due to the existence of surface flaws [1] and to environmental fatigue [2,3,4]. Efforts have been made to determine intrinsic strength of glass by preparing and testing pristine glass samples in inert conditions, e.g. in high vacuum [5] or in liquid nitrogen [6]. It has been suggested

that these strengths are intrinsic, either because the glass has no 'flaws', or that the 'flaws' that limit strength are intrinsic to the structure of the glass [7]. The inert intrinsic strength can then be related to the atomic level structure and properties of the bonds that constitute the glass network, much like what has been done to explain the effects of glass composition on elastic modulus [8].

A number of studies have been performed to evaluate the inert strength of silica and silicate glasses [9,10,11], but few studies have been made on other oxide glass-formers. It is interesting to study the strength of borate glass since B_2O_3 melts form a glass as readily as do silica melts. The B-O single bond energy in vitreous B_2O_3 (498 kJ/mol) is comparable to that of Si-O in vitreous silica (444 kJ/mol) [12]. However, the structures of B_2O_3 and SiO_2 glasses are very different. Silica glass consists of corner-joined tetrahedra that form a three-dimension network, whereas in B_2O_3 glass the fundamental structural unit is the BO_3 triangle, and three of these triangles can form flat, relatively rigid boroxol rings [13]. Although there is some debate about what fraction of boron triangles and boroxol rings are found in B_2O_3 glass [14], the role that these boroxol rings play in determining glass properties is significant. Some mechanical properties for B_2O_3 glasses have been reported, e.g., Vickers hardness [15] (H ~ 1.7 GPa) and elastic constants [16,17,18,19] (Young's modulus, E ~ 17 GPa). These values are substantially lower than the corresponding values for fused silica [20,21] (H ~ 7 GPa and E ~ 70 GPa) and this suggests a much lower intrinsic strength for glassy B_2O_3 than that found for fused silica. On the other hand, the value of fracture toughness, K_{IC}, of B_2O_3 glasses [22], is almost twice that of silica [23] (1.44 vs. 0.8 $MPa{\cdot}m^{1/2}$). From Irwin's equation [24], therefore, one would predict that from the same 'critical flaw' size (c^*), B_2O_3 could be twice as strong as silica, assuming that K_{IC} is a constant with respect to stress and strain:

$$\sigma_f = \frac{K_{IC}}{\sqrt{\pi c^*}} \tag{1}$$

In view of the high value of fracture toughness, it is interesting to compare these two glasses on the basis of the 'brittleness parameter' (B) suggested by Marshall and Lawn [25]:

$$B = H / K_{IC} \quad (2)$$

Marshall and Lawn considered hardness (*H*) to be a measure of the resistance to deformation, and fracture toughness to be a measure of the resistance to cracking. Using the values for hardness and fracture toughness reported above, the *B*-value for silica glass is ~9 $\mu m^{-1/2}$ and for B_2O_3 glass is ~1.2 $\mu m^{-1/2}$. The relative difference in brittleness (~8×) is larger than the difference in elastic modulus (~4×). This suggests that the reason for the unexpectedly high value of fracture toughness found for B_2O_3 may be the existence of some 'inelasticity'. Stevels and co-workers [26,27] studied the flow behavior of B_2O_3 and sodium borate glasses near their glass transition temperature. B_2O_3 exhibited Newtonian flow, while the addition of sodium produced non-Newtonian behavior in simple shear. Hirao, et al. [28] determined the ratio of inelastic to elastic deformation in an experiment in which mode I stress was applied at room temperature. A maximum inelastic flow of ~10% was observed in glasses with 20 and 30 mole % sodium oxide, but lower amounts of inelastic flow were observed in glasses with 10 or 15 mole % sodium oxide. In addition it was found that the flow was independent of time and was thus plastic rather than viscoelastic. This suggests that plastic deformation is more pronounced in sodium borate glasses with higher soda content, and B_2O_3 glass may or may not exhibit plastic flow under stress.

Few measurements have been made of the mechanical strength of borate glass mainly because of its sensitivity to water. One group [12,29] studied the strength of fibers which were drawn in a dry atmosphere or in vacuum and tested (in tension) at room temperature in the same environment. Strengths of 0.8 to 1.2 GPa for B_2O_3 glass were reported. Another group [15,30] drew fibers under ambient conditions and tested them under liquid nitrogen in three point bending. Strengths of 1.2, 2.7 and 3.0 GPa were obtained for pure B_2O_3, $15Na_2O{\cdot}85B_2O_3$ and $33Na_2O{\cdot}67B_2O_3$ (in mole %) respectively. From equation (1), a critical flaw size on the order of 1 μm is obtained, assuming the flaw is an elliptical thorough crack in an infinite plate. A calculation of this sort for silica results in a critical flaw sized about 1 nm. The large flaw size for B_2O_3 seems unreasonable, and perhaps implies that the (brittle) fracture mechanics equation is not applicable.

The increase in 'inert strength', from 1.2 to 3.0 GPa noted above for the addition of 33 mole% Na_2O to B_2O_3 is consistent with reports of increasing elastic modulus for borate glasses with increasing modifier contents [18]. These trends reflect the well-known 'borate anomaly' for which the addition of modifying oxides strengthen the glass network by converting B-triangles into B-tetrahedra. The B-tetrahedra are linked at all four corners to other B-polyhedra, and so the network connectivity increases with increasing modifying oxide concentrations, at least up to about 30 mole% [18].

In this work we describe our inert failure strain measurements on pristine sodium borate glass fibers, with compositions of $x$$Na_2O$·(100-$x$)$B_2O_3$, $0 \leq x \leq 35$.

2.2. EXPERIMENTAL PROCEDURE

Glasses with molar compositions of $x$$Na_2O$·(100-$x$)$B_2O_3$, x=0, 5, 13, 20, 27 and 35 were prepared from mixtures of reagent grade sodium carbonate (Na_2CO_3) and boric acid (H_3BO_3) powders. All glasses were melted in platinum crucibles in air at 1000°C for 6 hours, except for B_2O_3 glass, which was prepared several different times from melts held at 1000°C for up to 30 hours. Weight loss measurements were taken after 1hour of melting and were found to be less than 0.05% per hour, thus the 'as batched' compositions are used in discussion. Fibers with diameters in the range of ~100 to 300 μm were drawn by hand and tested within 30 seconds of their creation to minimize the effects of aging.

Another independent set of B_2O_3 glass were prepared and the inert failure strains were measured by Kurkjian in 1995 and never published. Reagent grade boric acid powder was melted in a Pt crucible in an electric furnace at temperatures between 1000° and 1300°C. Melts were normally dried by bubbling with dry nitrogen, although no effect of water content was observed in the failure characteristics. Fibers of ~100 to 200 μm diameter were drawn from the melt by hand and then tested immediately by TPB at a faceplate velocity of 1000 μm/s. It was found that if the measurements were made within ~30 seconds, a reproducible value for the failure strain was obtained. After longer times, hydrates formed on the glass surface and degradation of the failure strain values was observed.

Failure strains of the B_2O_3 and Na-borate glass fibers were measured using the two-point bending (TPB) technique [31]. In a TPB test, a pristine section of glass fiber,

diameter *d*, is bent into a U-shape between two parallel face plates, one of which travels towards the second at a constant faceplate velocity (v_{fp}), compressing the 'U' until failure. The gap distance at failure (*D*) is recorded, and the failure strain (e_f) is then calculated from [32]:

$$\varepsilon_f = \frac{1.198 \times d}{(D - d)} \tag{3}$$

The diameters of the broken ends of each fiber tested were measured using a micrometer with a precision of 1 μm and these values were used to calculate e_f. Inert conditions are created by testing fibers immersed in liquid nitrogen. At the low temperature (77K, boiling point of liquid nitrogen at atmospheric pressure), the kinetics of fatigue reactions are arrested [7].

The TPB test in this study does not provide a measuring mode of constant stress rate or strain rate, but instead uses a mode of constant faceplate velocity (v_{fp}). This means that the applied strain rate increases with increasing strain (decreasing D, from equation (3)). With the diameter of the fiber known, the strain rate at failure ($\dot{\varepsilon}_f$) can be calculated from:

$$\dot{\varepsilon}_f = \frac{{\varepsilon_f}^2 \times v_{fp}}{1.198 \times d} \tag{4}$$

Faceplate velocities ranging from 50 to 4000 μm/sec were used in these experiments and are reported for each data set. The failure strain rate for each fiber was calculated and an average with one standard deviation is reported for each set of data.

2.3. RESULTS

The Weibull distributions [33,34] of the inert failure strains for B_2O_3 glass fibers prepared under various conditions are shown in Figure 2.1. The inert failure strains measured at v_{fp}=4000 μm/s decrease with increasing melting time, from 6 to 30 hours. An attempt to reproduce the 6h data results in a smaller failure strain. The inert failure strains measured at v_{fp}=50 μm/s are smaller than those measured at v_{fp}=4000 μm/s. The

'Kurkjian 1995' data has the widest inert failure strain distribution, ranging from 12% to 55%. Over all, there is a significant uncertainty associated with these measurements.

Figure 2.2 shows that the reproducibility of inert failure strains for $5Na_2O{\cdot}95B_2O_3$ glass (30±1% and 25±3%) is not as good as the reproducibility for $20Na_2O{\cdot}80B_2O_3$ glass (both 18±1%). Due to the fact that the failure strains for borate glass (especially for B_2O_3 rich glasses) are difficult to reproduce in air, to minimize the variability that affects the failure strains, fibers collected and tested under similar conditions were evaluated. Failure strains for all other glass fibers were collected from glass melted at 1000°C for 6 hours.

In room temperature air of ~40% humidity, a B_2O_3 glass fiber looks perfectly clear by eye when it is drawn. After 5 minutes in air, the fibers are less transparent. After 10 minutes, a white coating is visible. After 20 minutes, the entire fiber is covered by the white coating and attempts to load this fiber in the two-point bender will fail, indicating that its failure stain is less than 1%. A surface XRD study showed that the white substance on the surface of the B_2O_3 glass fibers is crystalline boric acid (Figure 2.3). This observation is consistent with the reported hydrated species of vitreous B_2O_3 glass [35].

Weibull distributions of the inert failure strains for $x Na_2O{\cdot}(100\text{-}x)B_2O_3$ fibers drawn by hand from the respective melts and tested at v_{fp} = of 4000 μm/s are shown in Figure 2.4. Much tighter failure strain distributions were obtained for the Na-containing glasses than for the B_2O_3 glass. The failure strain distributions shift to lower values with increasing Na_2O content.

Figure 2.5 compares the inert failure strains of Na-borate glass fibers drawn from melts by hand and drawn using the rotating cage method [36]. The compositional dependences of failure strains are similar, although the latter failure strains are somewhat lower than the former.

2.4. DISCUSSION

2.4.1. Compositional Dependence. It can be seen in Figure 2.5 that the inert failure strains for the sodium borate glasses decrease with increasing Na_2O content. B_2O_3 glass, in the short range order, has layered structure with strong chemical bonds (B-O) forming BO_3 triangles and B_3O_6 boroxol rings in the planes and weak van der Waals bonds between the planes [18,30]. Na_2O, when added into the B_2O_3 glass structure, can charge balance with boron with BO_3 units being converted into BO_4 units. So the addition of soda replaces some van der Waals bonds with B-O covalent bonds and turns the two dimensional (2D) structure into a 3D structure [15,30]. The decrease in inert failure strain with increasing soda should be related to the structure change.

To analyze the structural dependence of inert failure strains, it is important to look at some other mechanical properties that relate to the glass composition and structure. For sodium borate glasses, elastic properties, i.e., Young's modulus and bulk modulus increase with increasing Na_2O content [18,19]. A greater proportion of covalent bonds associated with higher amounts of Na_2O causes an increase in rigidity, or resistance to deformation [18]. Figure 2.6 shows that Young's modulus [19] increases systematically with increasing soda content, while inert failure strains decrease with increasing soda. Also shown in Figure 2.6 are the compositional dependence of Young's modulus and inert failure strains for sodium silicate glasses [9]. Different from the borate glasses, the addition of Na_2O weakens the structure of silicate glasses by replacing bridging oxygen with non-bridging oxygens, thus decreases the Young's modulus.

It is interesting that the failure strains and Young's moduli show opposite compositional dependence, for both sodium silicate glasses and sodium borate glasses. The correlations between failure strains and Young's moduli for sodium borate, sodium silicate [9] and sodium aluminosilicate glasses [9] are shown in Figure 2.7. It can be seen that for all three series of glasses, failure strains decrease with Young's moduli.

Young's modulus represents a material's resistance to elastic strain. A similar property is hardness, which measures a material's resistance to plastic deformation. For sodium borate glasses, hardness increases with increasing soda content ([15, 37], shown in Figure 2.8 (a)). A similar compositional trend in hardness was also observed in soda-lime borate glasses [38]. In the latter study, a model was proposed to predict the hardness

based on the numbers of ‘constraints’ for different types of bonds in the glass structure. The change in hardness was attributed to the number of constraints. The addition of soda in borate glasses increases the number of ‘constrains’ and thus increases hardness. But even if a structure has fewer constraints, that does not mean that failure is less easy in this structure.

A mechanical property that is related to the crack behavior is fracture toughness (K_{IC}). In fracture mechanics, fracture toughness is a property which describes the ability of a material containing a crack to resist fracture. The failure of a pristine fiber in inert conditions is a crack initiation controlled process. The inert intrinsic failure proceeds in the following steps, inspired by the idea of the indentation process described by Lawn and Marshall [25]: 1. The material deforms under stress; in this stage, the size of flaw nuclei does not change. 2. The material continues to deform; maybe some permanent deformation takes place, and the size of flaw nuclei increases to a size that is large enough to be called a crack. 3. The crack grows to a critical size and failure occurs. The mechanical response is on the verge of transforming from hardness-controlled to toughness-controlled, thus the idea of brittleness [25]. The brittleness parameter reflects the crack-initiation ability. The more brittle the material is, the easier a crack can initiate under stress. The brittleness for sodium borate glasses can be achieved by dividing hardness data [15] with fracture toughness [22] using equation (2). Figure 2.8 (b) shows that with increasing Na_2O, the brittleness increased systematically, whereas the failure strains decreased systematically. Apparently the transformation of structure not only increases the resistance to deformation but also increases the brittleness, and hence decreases failure strain.

2.4.2. Elastic Deformation or Plastic Deformation. Hirao et al. [28] showed that sodium borate glasses exhibit inelastic deformation during a crack growth study with loading-unloading cycles. Larger inelastic dissipation energy was observed for $x$$Na_2O$·(100-$x$)$B_2O_3$, x=10, 15, 25 and 30 glasses than soda-lime silicate glasses. They suggested that the fracture of borate glass is accompanied by plastic deformation. Since plastic deformation is observed in crack growth studies, it is possible that it also exists in the TPB inert failure strain studies. In TPB studies, it has been reported that for some glasses, inert failure strains increase with decreasing faceplate velocity, and this effect

has been referred to as the 'Inert Delayed Failure Effect' (IDFE) [10]. One explanation for IDFE is that the depolymerized structure of these glasses reorganize or relax under the applied stress [11], perhaps in processes similar to those that account for low-temperature internal friction [39,40]. Such internal inelasticity does not assure macroscopic plastic deformation like what is observed in indentation study, but it is also associated with time dependent energy dissipated relaxation [41]. Glasses that exhibit IDFE include $25Na_2O{\cdot}mAl_2O_3{\cdot}(75\text{-}m)SiO_2$, m<25 mol% [9], $yNa_2O{\cdot}(100\text{-}y)SiO_2$, y>15 mol% [10], $zK_2O{\cdot}(100\text{-}z)\ SiO_2$ z>25 mol% and soda-lime silicate glasses [36]. At lower faceplate velocities (or strain rates), the structure is given more time to reorganize and relax. However, for sodium borate glasses, the inert failure strains (listed in Table 2.1) are greater at a higher strain rate, except for $5Na_2O{\cdot}95B_2O_3$ glass. The 'IDFE' for $5Na_2O{\cdot}95B_2O_3$ glass might not be real considering the difficulty to reproduce the failure strain for B_2O_3-rich glasses. The lack of IDFE indicates that the low temperature inelastic flow mechanism does not exist in the TPB failure of borate glasses at 77K, and the plastic deformation observed at room temperature is a different mechanism.

It may be remembered that the Vickers hardness of silica and soda-lime-silica glasses increase by a factor of three as the temperature is decreased from room temperature to 77K [20]. So the mechanism which allows room temperature plastic flow of soda-lime silicate glass is 'frozen out' at such a low temperature. However, the IDFE of soda-lime silicate shows that the internal friction can exist at 77K. For sodium borate silicate glasses, the room temperature plastic flow is due to the shear of boroxol hexagonal planes in borate structure of the exchange of the coordination number of boron atoms [28]. If this mechanism is 'frozen out' at low temperature, it does not contribute to the strain in our TPB test.

Another possibility is that for some other reason, borate glasses tend to fail readily at lower strain rate. This phenomena of increasing inert strength with increasing strain rate/stress rate was referred to as 'inert fatigue' because it is similar to the environmental fatigue but in inert conditions [7]. 'Inert fatigue' behavior has been reported before for silica [6,7,42] and E-glass [11,36]. Matthewson et al. [42] did not differentiate inert fatigue and environmental fatigue and considered both processes as caused by stress-induced reactions leading to weaker bonds at longer times. Kurkjian, et al. [7], explained

the effect as a consequence of the normal probability of failure due to thermal fluctuations of bond strengths under high stress, with longer times (slower v_{fp}) allowing weaker bonds to rupture to initiate failure. Proctor et al. [6], however, attributed this to the finite activity of water in liquid nitrogen leading to normal environmental fatigue behavior. The higher sensitivity of borate glass to water might increase the effect of inert fatigue and overwhelm the IDFE. The mechanisms for IDFE and inert fatigue are not quite understood yet, and more research must be done.

2.5. SUMMARY

In summary, sodium borate glasses were prepared in the laboratory and inert failure strains were measured using the two-point bend technique in liquid nitrogen. A very large inert failure strain with a large variance was observed for B_2O_3 glass. The inert intrinsic failure strains decrease as Na_2O is added into the system. The addition of Na_2O increases the dimensionality and connectivity of the structure. From reported Young's modulus and hardness studies, the addition of soda increase the resistance to both elastic and plastic deformation of the glass. With increasing soda content, the decreasing failure strains correlate with increasing resistance to deformation and decreasing crack initiation ability, as was reported in literature the increasing brittleness. The inert failure strains for sodium borate glasses increase with increasing strain rate. The lack of IDFE might suggest that the reported plastic flow of sodium borate glass in room temperature might not exist in low temperature (77K), or the effect of plastic flow is overwhelmed by other effects accounting for inert fatigue.

ACKNOWLEDGMENT

We acknowledge the NSF/I/U CRC Center for Glass Research (CGR) for funding this research.

REFERENCES

[1] A. A. Griffith, 'The Phenomena of Rupture and Flow in Solids,' *Phil. Trans. Roy. Soc. A*, 221 163–98 (1921).

[2] R. J. Charles, 'Static Fatigue of Glass. I,' *J. Appl. Phys.*, 29 [11] 1549-53 (1958).

[3] R. J. Charles, 'Static Fatigue of Glass. II,' *J. Appl. Phys.*, 29 [11] 1554-60 (1958).

[4] R. J. Charles, 'Dynamic Fatigue of Glass. II,' *J. Appl. Phys.*, 29 [12] 1657-62 (1958).

[5] W. J. Duncan, P. W. France and S. P. Craig, 'The Effect of Environment on the Strength of Optical Fiber,' in: C. R. Kurkjian (Ed.), *Strength of Inorganic Glass*, Plenum, 1985, p. 309.

[6] B. A. Proctor, I. Whitney and J. W. Johnson, 'The Strength of Fused Silica,' *Proc. Roy Soc. A*, 297 534-557 (1967).

[7] C. R. Kurkjian, P. K. Gupta, R. K. Brow and N. P. Lower, 'The Intrinsic Strength and Fatigue of Oxide Glasses,' *J. Non-Cryst. Solids*, 316 [1] 114-124 (2003).

[8] A. Makishima and J. D. Mackenzie, 'Direct Calculation of Young's Modulus of Glass,' *J. Non-Cryst. Solids*, 12 35-45 (1973).

[9] N. P. Lower, R. K. Brow and C. R. Kurkjian, 'Inert Failure Strain Studies of Sodium Aluminosilicate Glass Fibers,' *J. Non-Cryst. Solids*, 344 [1-2] 17-21 (2004).

[10] N. P. Lower, R. K. Brow and C. R. Kurkjian, 'Inert Failure Strain Studies of Sodium Silicate Glass Fibers,' *J. Non-Cryst. Solids*, 349 168-172 (2004).

[11] Z. Tang, N. P. Lower, P. K. Gupta, C. R. Kurkjian, and R. K. Brow, 'Two-Point Bend Measurement of Failure Stress of Pristine Glass Fibers,' submitted to *J. Am. Ceram. Soc.*, August 2011.

[12] H. Hasegawa, M. Takaishi, I. Yasui and M. Imaoka, 'Tensile Strength of Boric Oxide Glass in Vacuum and at Very Low Humidities,' *J. Non-Cryst. Solids*, 69, 49-58 (1984).

[13] A. K. Varshneya, *Fundamentals of Inorganic Glass*, Academic, New York, 1994, p. 96.

[14] A. C. Wright, S. A. Feller, and A. C. Hannon, *Borate Glass, Crystals and Melts, Society of Glass Technology*, Sheffield, UK, 1997.

[15] T. I. Pesina, L. V. Romanenko, V. P. Pukh and I. I. Novak, 'Strength and structure of glasses in the Na2O-B2O3 system,' *Soviet J. Glass Phys. Chem.*, 7 [1] 68-72 (1981).

[16] J. T. Krause and C. R. Kurkjian, 'Acoustic Spectra of Glasses in the System Na_2O-B_2O_3,' in *Borate Glasses: Structure, Properties and Uses*, ed. L. D. Pye, V. D. Frechette and N. J. Kreidl, Plenum Press, NY 1978.

[17] A. A. El-Moneim, 'Quantitative Analysis of Elastic Moduli and Structure of B_2O_3-SiO_2 and Na_2O-B_2O_3-SiO_2 Glasses,' *Physica B*, 325 319-32 (2003).

[18] E. Latif, 'Ultrasonic Study on the Role of Na_2O on the Structure of Na_2O-B_2O_3 and Na_2O-B_2O_3-SiO_2 glasses,' ***J. Pure Appl. Ultrason.***, 27 80-91 (2005).

[19] M. Kodama, 'Ultrasonic Velocity in Sodium Borate Glasses,' ***J. Mater. Sci.***, 26 [15] 4048-53 (1991).

[20] C. R. Kurkjian, G. K. Kammlott, and M. M. Chaudhri, 'Indentation Behavior of Soda-Lime-Silica Glass, Fused Silica and Single Crystal Quartz at Liquid Nitrogen Temperature,' ***J. Am. Ceram. Soc.***, 78 [3] 737-44 (1995).

[21] J. T. Krause, L. R. Testardi and R. N. Thurston, 'Deviations from Linearity in the Dependence of Elongation on Force for Fibres of Simple Glass Formers and of Glass Optical Lightguides,' ***Phys.Chem. Glasses***, 20 [6] 135-9 (1979).

[22] E. Vernaz, F. Larche and J. Zarzycki, 'Fracture Toughness – Composition Relationship in Some Binary and Ternary Glass Systems,' ***J. Non-Cryst. Solids***, 37 [3] 359-65 (1980).

[23] S. M. Weiderhorn, 'Fracture surface energy of glass,' ***J. Am. Ceram. Soc.***, 52 [2] 99-105 (1969).

[24] G. R. Irwin, J. A. Kies, 'Fracturing and Fracture Dynamics,' ***Welding J.***, 31 55s-100s (1952).

[25] B. R. Lawn, D. B. Marshall, 'Hardness, Toughness, and Brittleness: an Indentation Analysis,' ***J. Am. Ceram. Soc.***, 62 [7] 347-50 (1979).

[26] Ch. W. Cornelisse, T. J. M. Visser, H. N. Stein, and J. M. Stevels, 'Deviation from Newtonian Rheological Behavior in Alkali Borate Glasses,' ***J. Non-Cryst. Solids***, 1 150-62 [1969].

[27] J. M. Stevels, 'Relaxation Phenomena in Glass,' ***J. Non-Cryst. Solids***, 73 [1] 165-78 (1985).

[28] K. Hirao, J. Matsuoka, and N. Soga, 'Inelastic Deformation and Structure of Borate Glasses", ***J. Non-Cryst. Solids***, 112 [1] 336-40 (1989).

[29] H. Hasegawa, K. Nishihama and M. Imaoka, 'Quick-Loading Strength of Na2O-B2O3-SiO2 Glass Fibers,' ***J. Non-Cryst. Solids***, 7 [1] 93-102 (1972).

[30] V. P. Pukh, L. G. Baikova, M. F. Kireenko, L. V. Tikhonova, T. P. Kazannikova and A. B. Sinani, 'Atomic Structure and Strength of Inorganic Glasses,' ***Phys. Solid State***, 47 [5] 850-5 (2005).

[31] P. W. France, M. J. Paradine, M. H. Reeve and G. R. Newns, 'Liquid Nitrogen Strengths of Coated Optical Glass Fibers,' ***J. Mater. Sci.***, 15 825-830 (1980).

[32] M. J. Matthewson, C. R. Kurkjian and S. T. Gulati, 'Strength Measurement of Optical Fibers by Bending,' ***J. Am. Ceram. Soc.***, 69 815-21 (1986).

[33] W. Weibull, 'A Statistical Theory of the Strength of Materials,' ***Eng. Res. Proc.*** 151 1-45 (1939).

[34] W. Weibull, 'A Statistical Distribution of Wide Applicability,' ***J. Appl. Mechan.***, 18 293-7 (1951).

[35] D. E. Clark and B. K. Zoitos, *Corrosion of Glasses, Ceramics and Ceramic Superconductors: Principles, Testing, Characterization and Applications*, Noyes Publications, New Jersey, 1992, p. 161.

[36] N. P. Lower, Ph D. Thesis, 'Failure Study of Glass Fibers,' Missouri University of Science and Technology, 2004.

[37] F. C. Eversteijn, J. M. Stevels and H. I. Waterman, 'The Diamond Pyramid Hardness of Sodium Borate Glasses as a Function of Their Composition and Heat Treatment,' *Phys. Chem. Glasses*, 1 [4] 134-6 (1960).

[38] M. M. Smedskjaer, J. C. Mauro, and Y. Yue, 'Predictions of Glass Hardness Using Temperature-Dependent Constraint Theory,' *Phys. Rev. Lett.*, 105 [11] 110503-1-4 (2010).

[39] D. E. Day, and G. E. Rindone, 'Properties of soda aluminosilicate glasses. II. Internal Friction,' *J. Am. Ceram. Soc.*, 45 496-504 (1962).

[40] J. E. Shelby. Jr., and D. E. Day, 'Mechanical Relaxations in Mixed-Alkali Silicate Glasses: I, Results,' *J. Am. Ceram. Soc.*, 52 [4] 169-74 (1969).

[41] L. Wondraczek, J. C. Mauro, J. Eckert, U. Kuhn, J. Horbach, J. Deubener, and T. Rouxel, 'Towards Ultrastrong Glasses,' *Adv. Mater.*, XX, 1-9 (2011).

[42] M. J. Matthewson, C. R. Kurkjian, C. D. Haines and N. Venugopal, 'Temperature Dependence of Strength and Fatigue of Fused Silica Fiber in the Range 77 to 473 K,' *Proc. SPIE*, 4940 74-9 (2003).

Table 2.1. Inert failure strain (ε_f) and failure strain rate ($\dot{\varepsilon}_f$) for sodium borate glass, measured at a faceplate velocity of 4000 and 50 μm/s.

$x$$Na_2O$·(100-$x$)$B_2O_3$	$\varepsilon_{f\cdot 4000}$ (%)	$\dot{\varepsilon}_{f\cdot 4000}$ (s^{-1})	$\varepsilon_{f\cdot 50}$ (%)	$\dot{\varepsilon}_{f\cdot 50}$ (s^{-1})
x=0	35.77 ± 4.55	1.95 ± 0.57		
x=0 (melted for 9h)	28.06 ± 5.00	1.48 ± 0.53	23.90 ± 3.96	0.013 ± 0.003
x=5	29.86 ± 1.09	1.68 ± 0.29	31.69 ± 0.57	0.023 ± 0.002
x=13	24.26 ± 1.70	1.45 ± 0.24	20.44 ± 1.97	0.013 ± 0.002
x=20	18.23 ± 0.68	0.78 ± 0.11	16.87 ± 0.69	0.010 ± 0.001
x=27	11.69 ± 0.59	0.40 ± 0.08	10.21 ± 0.92	0.0036 ± 0.0011
x=35	8.18 ± 0.52	0.19 ± 0.03		

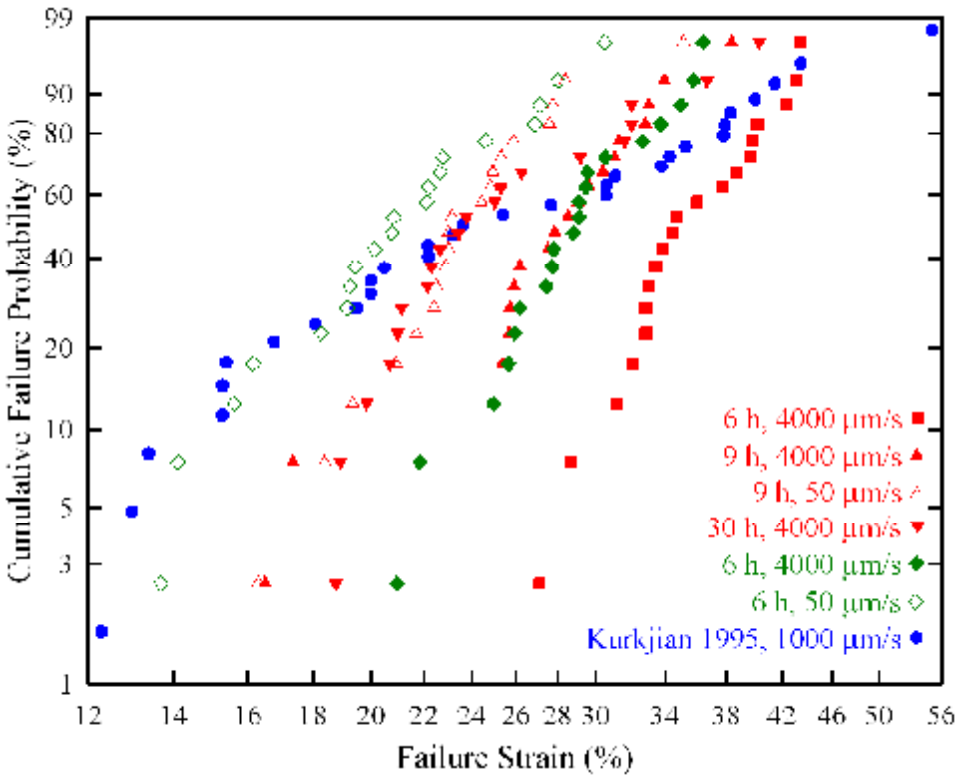

Figure 2.1. Weibull distributions of inert failure strains for B_2O_3 glass fibers, with legend indicating the melting time and faceplate velocity. Square and triangle data points were collected in May (lab humidity ~40%); diamond data points were collected in August (lab humidity ~60%); round data points were collected in January (lab humidity ~30%).

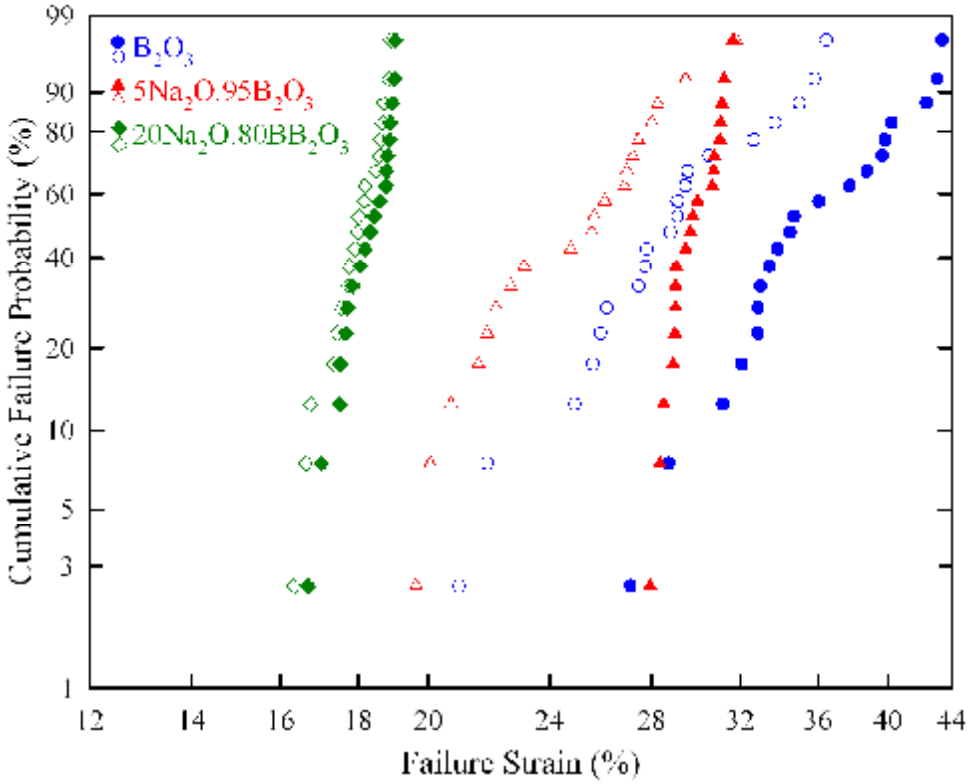

Figure 2.2. Weibull distributions of inert failure strains for xNa$_2$O·(100-x)B$_2$O$_3$ glass fibers, tested at v_{fp} = 4000 μm/s. Open symbols represent attempts to reproduce original data (solid symbols) in identical testing conditions.

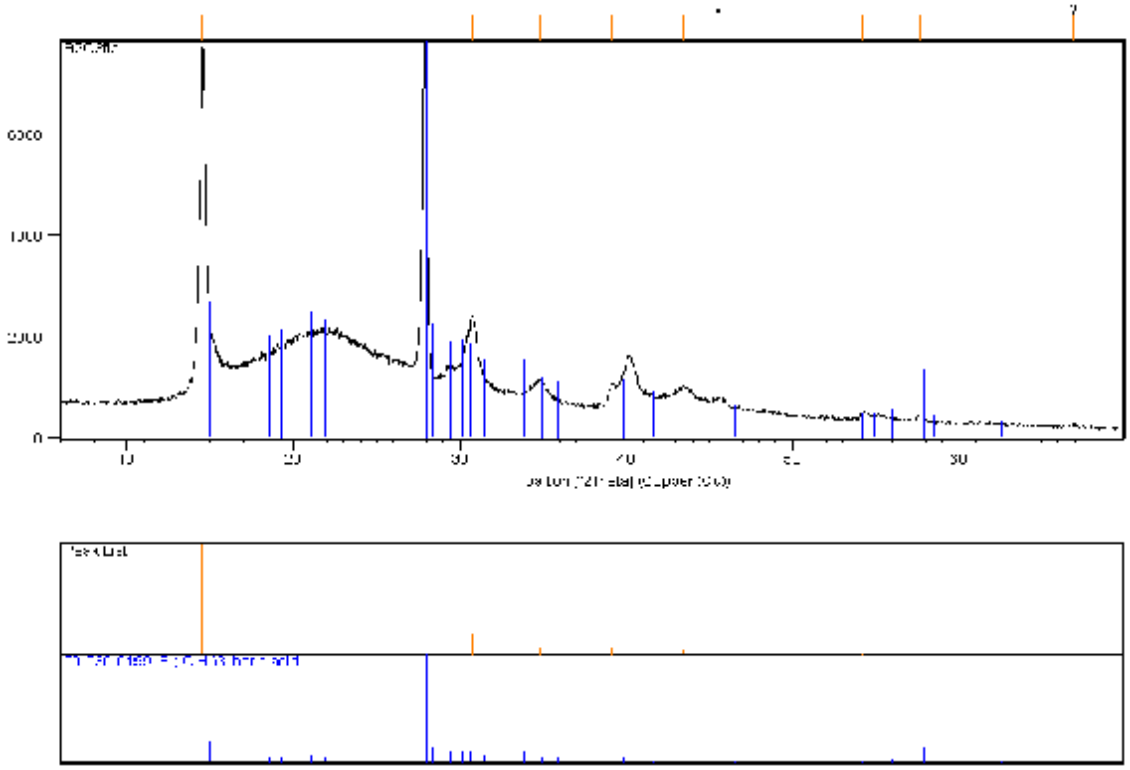

Figure 2.3. Surface XRD results from detection of B_2O_3 glass fibers aged 1 hour in 21°C and 60% RH air.

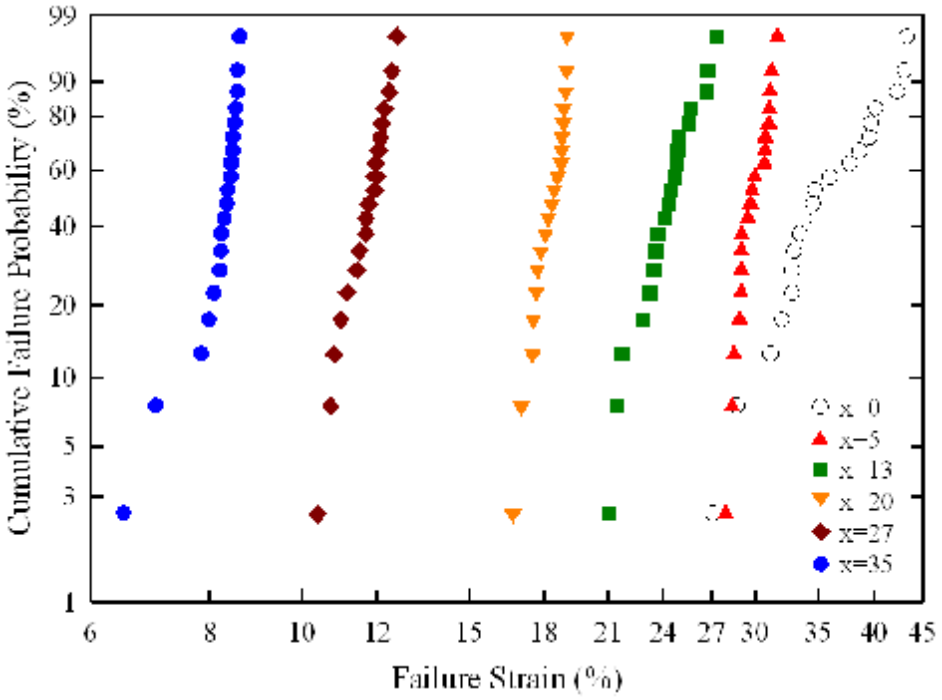

Figure 2.4. Weibull distributions of inert failure strains for xNa$_2$O·(100-x)B$_2$O$_3$ glass fibers, tested at v_{fp} = 4000 μm/s.

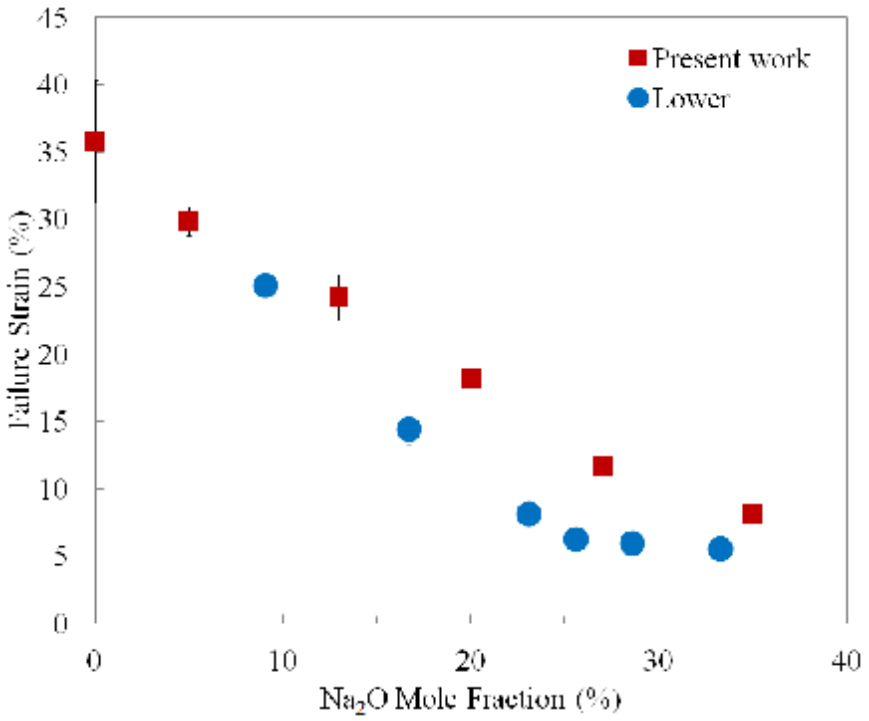

Figure 2.5. Inert failure strains for sodium borate glasses (v_{fp}=4000 μm/s), from present work and from Lower [36], decrease systematically with Na_2O content.

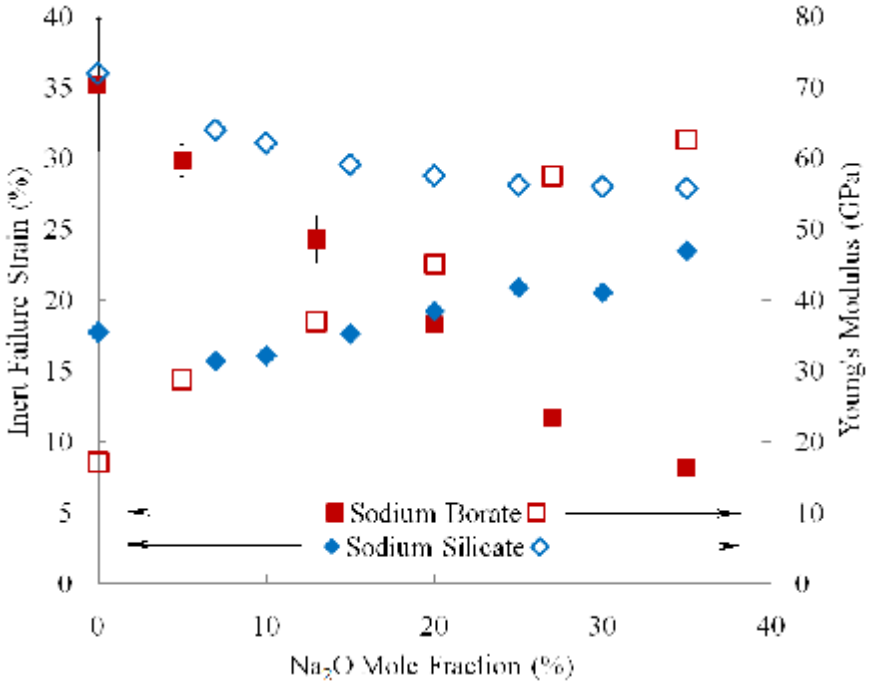

Figure 2.6. Compositional dependence of inert failure strains (closed symbols) (v_{fp}=4000 μm/s) and Young's moduli (open symbols) for sodium borate glasses and sodium silicate glasses.

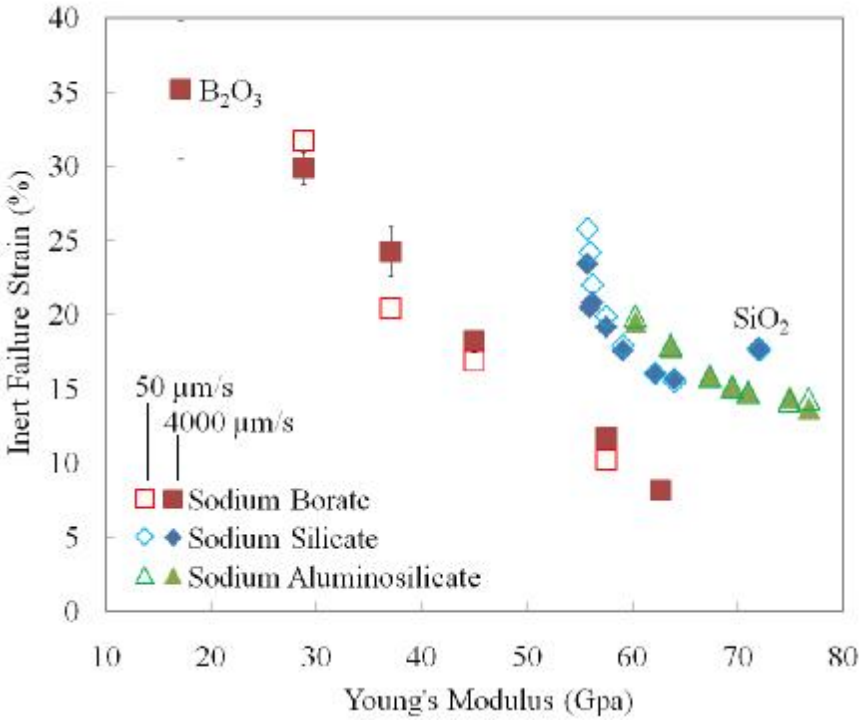

Figure 2.7. Inert failure strains measured at 50 and 4000 µm/s vs. Young's moduli for sodium borate, sodium silicate and sodium aluminosilicate glasses.

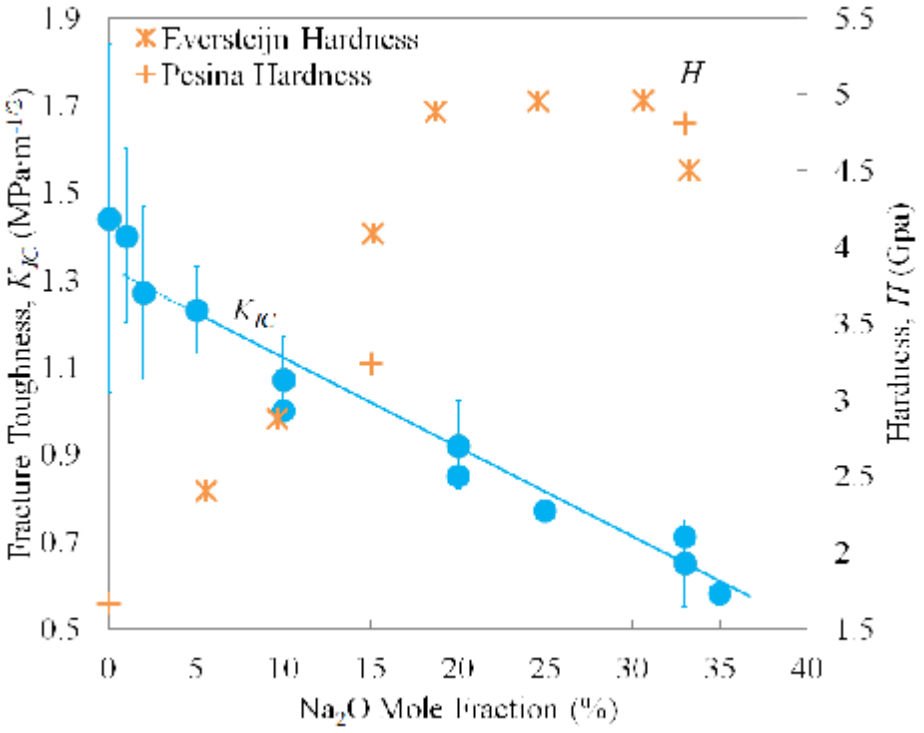

(a)

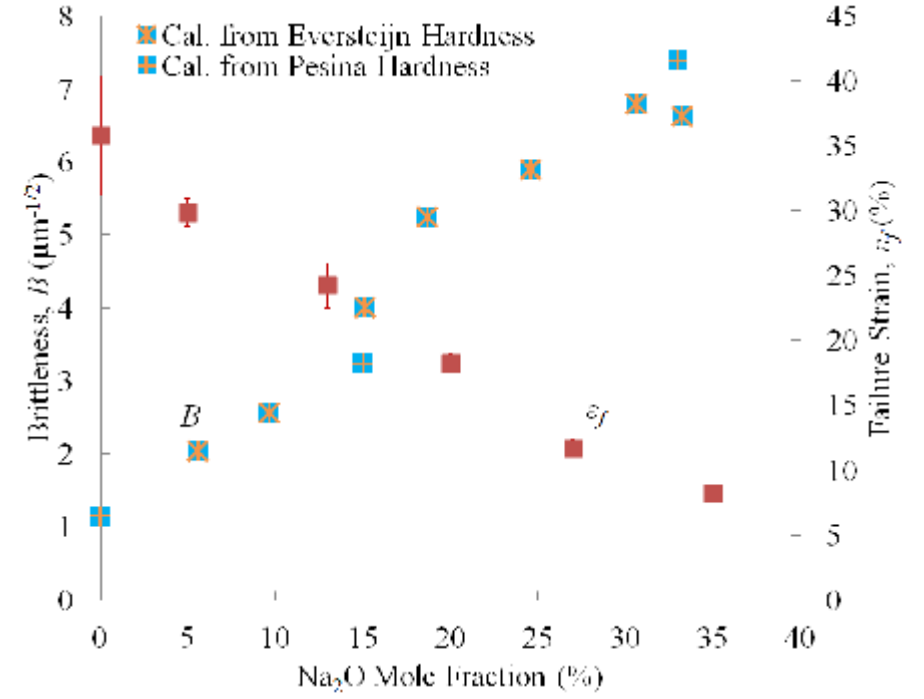

(b)

Figure 2.8. For sodium borate glasses, (a) Fracture toughness (●) [22] and Hardness reported by Eversteijn [37] and Pesina [15], (b) Brittleness calculated from equation (2) and failure strains.

3. TWO-POINT BEND STUDIES OF FATIGUE EFFECTS IN SILICATE GLASSES

Zhongzhi Tang[a], Charles R. Kurkjian[b], and Richard K. Brow[a]

[a]Missouri University of Science & Technology, Department of Materials Science & Engineering, Rolla, MO 65409, USA

[b]University of Southern Maine, Department of Engineering, P.O. Box 9300, Gorham, ME 04038, USA

ABSTRACT

The Two-Point Bend (TPB) method was used to measure fatigue effects on freshly-drawn silicate glass fibers, including several different commercial compositions and a series of $25Na_2O{\cdot}xAl_2O_3{\cdot}(75–x)SiO_2$ glasses ($0 \le x \le 25$). Fibers were tested in distilled water at different temperatures ranging from 3 to 93°C and failure strain was found to decrease with increasing temperature. The dynamic fatigue effect was characterized from TPB experiments in water at different faceplate velocities, ranging from 50 to 10,000 μm/s. The dynamic fatigue parameter (n) was found to be in good agreement with reported values measured using different methods for similar glasses. For the series of sodium aluminosilicate glasses, the susceptibility to fatigue decreases with increasing alumina content. A mechanism based on the exchange of sodium ions in the glass and protons or hydronium ions (H_3O^+) in solution is proposed to explain the effects of glass composition on fatigue behavior.

3.1. INTRODUCTION

3.1.1. Fatigue of Glass. The strength of glass measured in air is much lower than that measured in vacuum, liquid nitrogen or liquid helium [1]. It was found 100 years ago that in aqueous or humid environments, the strength of glass is dependent on the loading time and/or loading rate [2]. This phenomenon was probably first described as "fatigue" in 1946 [3]. Fatigue is important considering that many applications of glass involve some kind of applied force in the presence of ambient water.

It is widely accepted that failure of inorganic glasses in wet environments is controlled by stress corrosion due to the chemical reaction between water and strained bonds [4,5]. The glass-water reactions have been discussed by Bunker [6]. Generally, there are two categories of reactions between glass and water: (1) Hydrolysis, in which water reacts with metal-oxygen bonds and form hydroxyl groups; (2) Leaching, in which cations in glass (usually alkali modifiers) ion-exchange with protons or other cations in water. For silica glass, the hydrolysis process is described as:

$$\begin{array}{c} | \\ -Si-O- \\ | \end{array} \begin{array}{c} | \\ Si- \\ | \end{array} + H_2O \longrightarrow 2\left[\begin{array}{c} | \\ -Si-OH \\ | \end{array}\right] \quad (1)$$

Silica is often considered relatively inert to water at zero strain, but when the Si-O-Si bond is strained, it can react with water much faster than in dry conditions [7,8]. Silica is more susceptible to fatigue in the presence of basic solutions because hydroxyl ions further attack the glass network [6,9]:

$$\begin{array}{c} | \\ -Si-O- \\ | \end{array} \begin{array}{c} | \\ Si- \\ | \end{array} + OH^- \longrightarrow \begin{array}{c} | \\ -Si-O^- \\ | \end{array} + \begin{array}{c} | \\ -Si-OH \\ | \end{array} \quad (2)$$

For alkali silicate glasses, the initial attack by water progresses by an ion-exchange process that selectively leaches the alkali ions from the glass [6]:

$$\begin{array}{c} | \\ -Si-O^-Na^+ \\ | \end{array} + H^+ \longrightarrow \begin{array}{c} | \\ -Si-OH \\ | \end{array} + Na^+ \quad (3)$$

Doremus [10] suggested the possibility that hydronium ions (H_3O^+) are involved in this ion-exchange process. Depth profile studies of hydrated soda-lime silicate glass have shown that three H-atoms replace each Na atom leached from a hydrated glass surface, consistent with a Na^+-H_3O^+ exchange mechanism [11, 12]:

$$\begin{array}{c} | \\ -Si- \\ | \end{array} O^{-}Na^{+} + H_3O^{+} \longrightarrow \begin{array}{c} | \\ -Si- \\ | \end{array} OH + H_2O + Na^{+} \quad (4)$$

Charles [13,14,15] attributed the fatigue of sodium silicate glass to the extension of surface flaws by the leaching of Na^+ ions from the glass in the vicinity of the flaw tip. Duncan and France et al [16] studied the fatigue of silica and sodium borosilicate glass in air and discovered that the sodium borosilicate glass is more susceptible to fatigue than silica. They also studied the fatigue of sodium borosilicate glasses with different soda contents and recognized that reducing soda increased resistance of the glass to fatigue [17]. Wiederhorn and Bolz [18] studied stress corrosion behavior (another form of fatigue) for several different silicate glasses. Among those compositions, silica glass had the greatest stress corrosion resistance, followed by low-alkali aluminosilicate and borosilicate glass. Soda-lime silicate glass however, was sensitive to stress corrosion, indicating that the alkali component is playing a detrimental role in fatigue. Fatigue studies have also been performed on soda-lime silicate (SLS) glasses [12,19,20], but no compositional dependence was reported. Less is known about fatigue effects for sodium aluminosilicate glasses. These glasses are finding increasing applications, particularly in flat panel displays and touch-screen applications [21].

3.1.2. Fatigue of Glass in Fracture Mechanics. Fatigue processes in glass have been studied using several different methods [22]. The most conventional way is the measurement of slow crack growth velocities (a.k.a. subcritical crack growth) using fracture mechanics analyses [18,23]. The theory behind this is that a defect (assuming an elliptical thorough crack in an infinite plate) can serve as a stress concentrator [24]:

$$K_I = \sigma\sqrt{\pi c} \quad (5)$$

where K_I is stress intensity factor ($MPa \cdot m^{1/2}$), σ is the remotely applied stress (MPa) and c is the crack length (m). When K_I reaches its critical value, K_{IC}, the crack will propagate at its 'spontaneous' crack growth speed ≥0.1 m/s [25]. At this stage, the failure occurs essentially instantaneously. Before this stage, when $K_I < K_{IC}$, the crack grows at a much slower velocity, called subcritical crack growth velocity. The slow crack velocity data is

usually shown in a '*K*-*V*' curve, where crack velocity (V or $\dot{c}$) is recorded as a function of K_I. The most widely used model is based on an empirical power law: [26,27]

$$\dot{c} = A(K_I/K_{IC})^n \tag{6}$$

Here, $\dot{c}$ is the crack growth velocity, n is termed the fatigue parameter or the stress corrosion susceptibility parameter, and A is the environmental parameter which has an Arrhenius temperature dependence. In addition to this model, an activation volume model [18] based on exponential law has been proposed:

$$\dot{c} = A' \exp(n' K_I/K_{IC}) \tag{7}$$

Other models based on exponential laws have also been used [28,29,30], but their formulations are similar to equation (7). Shiue and Matthewson [31] compared several different models for fatigue and suggested that the power law fits the fatigue data the best, while the exponential law has a better physical meaning.

The effects of fatigue on the failure strength (σ_f) of glass has been analytically derived [32]:

$$\sigma_f = D\dot{\sigma}^{(1/n+1)} \tag{8}$$

where D is a constant, and $\dot{\sigma}$ is the applied stress rate. This equation allows direct comparison between slow-crack growth results and those obtained in dynamic fatigue studies. Most researchers prefer the power law model.

Fatigue can also be examined from strength measurements, including tensile test [33,34], three-point bending [35], and four-point bending [36,37], etc. These studies are usually categorized in two forms: static fatigue and dynamic fatigue. Static fatigue is usually measured by determining the time-to-failure under a constant applied stress or at a constant strain. Dynamic fatigue is usually measured by determining the failure stress or failure strain under different loading rates. According to the type of strength

measurement, loading modes include constant stress rate, constant strain rate, and constant faceplate velocity (in two-point bending tests).

3.1.3. Two-Point Bending (TPB) Dynamic Fatigue. The two-point bending (TPB) technique was first described in detail in 1980 [38]. In a TPB test, a pristine section of glass fiber, diameter *d*, is bent into a U-shape between two parallel face plates, one of which travels towards the second, compressing the 'U' until failure. The gap distance at failure (*D*) is recorded, and the failure strain (ε_f) is then calculated from: [39]

$$\varepsilon_f = \frac{1.198 \times d}{(D - d)} \tag{9}$$

TPB does not require the special grips needed for conventional tensile tests, and the relatively small gauge length of 0.3-0.9 mm in the region of highest stress minimizes the probability of large extrinsic flaws lowering failure strains [38]. More details about the TPB technique can be found in our previous publications [40,41]. Lower et al. used TPB to determine the inert failure strains for sodium silicate glass fibers [42], sodium aluminosilicate glass fibers [43] and E-glass fibers [44].

In TPB studies, the environmental fatigue effect has been characterized in different ways: Failure strains decrease systematically with increasing relative humidity [40], with increasing temperature [37], or with decreasing strain rate/stress rate [45]. In this research, the TPB test uses a measuring mode of constant faceplate velocity (v_{fp}). Rondinella and Matthewson [45] compared three different loading modes: constant strain rate, constant stress rate and constant faceplate velocity (v_{fp}), and calculated the dynamic fatigue parameter, *n*, for each mode. For the constant faceplate velocity, *n* can be calculated by:

$$n = 1 + 1/\frac{d\log(\varepsilon_f)}{d\log(v_{fp})} \tag{10}$$

This *n* is equivalent to the *n* in equations (6) and (8). However, the value of *n* for the same glass can vary considerably when testing samples with different dimensions and

surface conditions. This will be discussed later. There have been reports on the use of TPB to measure the fatigue for silica glass fibers [45,46,47,48,49] and sodium borosilicate glass fibers [38] .

In the present study, the temperature dependence of failure strain and the dynamic fatigue characteristics will be determined for several different silicate glasses. The fatigue behaviors will be related to the composition and structure. The fatigue mechanism will be discussed, especially for a series of sodium aluminosilicate glasses.

3.2. EXPERIMENTAL PRECEDURE

3.2.1. Sample Preparation. Silica glass fibers (Amersil TO8 fused natural quartz, 125 μm in diameter) were provided by AT&T. The protective polymer coatings on the fibers were removed by immersing the fiber in acetone immediately before testing.

Fibers of other glass compositions were drawn from melts. A commercially available soda-lime silicate flint container glass, a calcium aluminoborosilicate fiber glass (nominal composition in the ranges [20-25]CaO, [10-15]Al_2O_3, [5-10]B_2O_3, and [50-55]SiO_2, wt%), a sodium borosilicate glass similar to Pyrex, and a commercial sodium aluminosilicate display glass were each remelted in a platinum crucible in air, for the times and temperatures indicated in Table 3.1, to produce bubble-free, homogeneous melts. Laboratory melts of glasses from the series of $25Na_2O{\cdot}xAl_2O_3{\cdot}(75–x)SiO_2$, where x = 0, 5, 9, 12.5, 18.75, and 25 in mole %, termed the NaAlSi series, were prepared from batches of reagent grade Na_2CO_3, Al_2O_3 and SiO_2. The batches, sufficient to produce 25 grams of glass, were thoroughly mixed with a mortar and a pestle and melted in platinum crucibles in air for the times and temperatures shown in Table 3.1 to produce bubble-free, homogeneous melts. The weight of glass melts were measured after one hour of melting and before fibers were pulled. The weight losses were found to be less than 0.1%, thus the ‘as batched’ compositions are used in discussion.

3.2.2. Fiber Pulling. Glass fibers are produced using a method described in [40]. When the glass melt reaches a bubble-free and homogeneous state, the crucible is transferred into a box furnace located below a custom built fiber drawing system. The box furnace is set at a pulling temperature (Table 3.1) at which the viscosity of the glass is appropriate for fiber drawing, that is, above the liquidus temperature and up to the 100 Pa-s isokom temperature of the melt. A water cooled copper coil is carefully positioned

above the melt surface through a hole in the furnace lid. The fiber drawing is initiated by dipping a silica rod through the cooling coil into the center of the melt surface, drawing a fiber up and attaching it to an arm of rotating cage (diameter ~45 cm), with 12 arms separated by a distance of 12 cm. Once it is attached, the fiber is drawn continuously as the rotating cage spins. The cage spins and translates along the rotation axis, preventing the fiber from overlapping itself as it is collected. The fiber diameter is controlled by adjusting the rotation speed of the cage, furnace temperature and the height of the cooling coil. The preferred diameter of fibers for the TPB test is 125±20 microns.

3.2.3. TPB Test. Failure strains of freshly drawn fibers were measured using a homebuilt two-point bending system [40]. Inert failure strains were measured by testing in liquid nitrogen at a faceplate velocity (v_{fp}) of 4000 μm/s. At this low temperature (77 K), the kinetics of the fatigue reactions are considered arrested [50], thus environmental fatigue is minimized. Temperature-dependent fatigue experiments were carried out by testing fibers immersed in distilled water at four different temperatures, using TPB at a constant faceplate velocity (v_{fp} = 4000 μm/s). Each fiber was tested immediately after immersion in water (within 5 seconds) to avoid aging effects. Five measurements were made at each temperature and then repeated until a total of 20 measurements were made at each temperature. The water temperature was controlled by a hot plate and monitored by thermometers with 1°C precision. Dynamic fatigue was determined by measuring the failure strains of fibers immersed in room temperature (21 ± 2°C) distilled water using faceplate velocities (v_{fp}) of 50, 500, 4000 and 10000 μm/s. Again, each fiber was tested immediately after immersion in water (within 5 seconds) to avoid aging effects; five measurements were made at each v_{fp} and then repeated until a total of 20 measurements were made under each condition. The fibers drawn from melts were tested immediately after they were first formed. The failure strains for each testing condition are independent of testing sequence, so there was no aging effect. The commercial silica glass fibers were tested immediately after removal of their polymer coatings.

3.3. RESULTS

3.3.1. Failure Strains. Figure 3.1 shows the Weibull distributions [51,52] of failure strain for commercial glasses measured in liquid nitrogen and in distilled water at room temperature, each at a faceplate velocity of 4000 μm/s. The inert (liquid nitrogen) failure strains are greater than the failure strains measured in water for all glasses. Broad failure strain distributions for the commercial Na-borosilicate and Na-aluminosilicate glasses were obtained for fibers drawn from several different melts. The high viscosities of these two glasses made it difficult to produce fibers with tighter distributions noted in Figure 3.1 for the commercial soda-lime and Ca-aluminoborosilicate glasses.

3.3.2. Temperature Dependence. Figure 3.2 shows the Weibull distribution of failure strains for the NaAlSi (x=5) glass fibers measured in distilled water at different temperatures. The failure strains shift to lower values with increasing temperature. Similar results were obtained for the commercial glasses and the other NaAlSi glasses, and they are summarized in Table 3.2 and illustrated in Figure 3.3 and Figure 3.4. The average failure strains for each glass at the different temperatures are reported with one standard deviation. The relatively large standard deviation for the commercial Na-borosilicate and Na-aluminosilicate glasses reflect the broad distributions noted in Figure 3.1 for these compositions.

The temperature dependence of failure strain from a TPB test has been described using an Arrhenius equation [16]:

$$\varepsilon = \varepsilon_0 \exp \frac{E_a}{RT} \tag{11}$$

where E_a is the apparent activation energy, R is the gas constant and T is the temperature. Thus E_a can be obtained by plotting the log of failure strain vs $1/T$. The Arrhenius plots of failure strains for silica from this study and two studies reported in the literature are shown in Figure 3.2. The apparent activation energy for failure strains for silica in water is 1.7±0.1 kJ/mol, compared to the value of 1.3 kJ/mol, derived from failure strain measured in various water saturated conditions (for example water bath at room temperature and subliming CO_2 in acetone at 195K) by Matthewson et al [53]. Duncan et

al. [16], also measured failure strain for silica glass in 100% humidity and report a value of 2.4 kJ/mol for coated silica fibers.

Table 3.2 shows that the values of E_a for the commercial Na-borosilicate and Na-aluminosilicate glasses are lower than that measured for silica, and the values measured for the commercial Ca-aluminoborosilicate and Na-Ca-silicate are greater. The values of E_a for the NaAlSi glasses decrease systematically from 8.3±0.3 to 2.3±0.3 kJ/mole with increasing alumina content.

3.3.3. Dynamic Fatigue. Figure 3.6 shows an example of the Weibull distributions of failure strains for NaAlSi (x=5) glass fibers measured at different faceplate velocities in room temperature distilled water. The failure strains increase with increasing faceplate velocity. Table 3.3 lists the average failure strains (± 1 s.d.) of various glass fibers measured using TPB at the different values of v_{fp}. Generally, failure strain increases with increasing v_{fp} for every composition. Dynamic fatigue parameters (n) were calculated from equation (10) from the slopes of the plots, like those shown in Figure 3.7 and Figure 3.8; the values for n for all glasses studied are also given in Table 3.3.

The value for n for silica in 21°C distilled water is 23.7±1.5. Similar TPB dynamic fatigue studies have been reported for silica in 30°C distilled water (n=22±0.5 [54]), and in 90°C pH 7 buffer solution (n=20.0±1.7 [48,55]).

The value of n for the commercial Na-Ca-silicate glass in this study was 14.9±2.1. This compares favorably to a reported value of 16.6 [18] from a bulk crack propagation study in distilled water at 25°C, a value of 16.1 [56] from a slow crack growth study, and a value of 16.0 [36] using abraded rods in a 4-point bend study. Baikova et al. [20] measured the dynamic fatigue parameter for soda-lime silicate glasses in water, using several different methods. The values of n for abraded sheet glass samples were 13.6 by central symmetrical bending and 14.7 by four-point bending. The values of n for abraded soda-lime silicate glass rod samples were 15.5-16.8 by three-point bending.

The value of n for the commercial Ca-aluminoborosilicate glass is 16.6±2.8, compared to a value of 16.1 reported for E-glass at 20°C and 100% relative humidity from a static fatigue study [57].

The *n* value of the commercial Na-borosilicate glass fibers is 21.6±11.7, compared to values of 27.4 [36] and 27.8-47.4 [37] in dynamic fatigue studies of Pyrex glass rods, which were abraded, aged in distilled water, then immersed in distilled water immediately before measured using 4-point bend technique. Another value, 34.1, was reported by Wiederhorn and Bolz [18] in a slow-crack growth study of bulk Pyrex glass, tested in distilled water at 25°C. The *n* value for our commercial Na-aluminosilicate glass is 27.2±18.5. The great uncertainties in this value and that for the Na-borosilicate glasses are due to the broad distributions of failure strains (Figure 3.1) rather than the quality of the fit of the data to equation.

The dynamic fatigue parameter, *n*, of the sodium aluminosilcate glasses increases from 6.9±0.2 for NaAlSi (*x*=0) to 19.6±2.4 for NaAlSi (*x*=25) (shown in Figure 3.9). Gehrke [58] measured the crack growth velocity of a series of sodium aluminosilicate glasses, including a glass with the composition: 26%Na_2O, 11%Al_2O_3, 63%SiO_2. The value of *n* for this glass was approximately 25, compared to the value of 16.1±1.7 for our sample NaAlSi (x=12.5). The value of *n* for Gehrke's 24% Na_2O, 76%SiO_2 glass was 17, compared to the value of 8.1±0.2 for our NaAlSi (x=0) glass.

3.4. DISCUSSION

3.4.1. Slow Crack Growth vs. Fatigue of Pristine Fibers. A comprehensive summary of fatigue data for silica reported by Glaesemann [59] shows that the fatigue parameter derived for different types of samples or from different types of measurement will not necessarily be the same. Such differences were also reported by Maurer [60] and Kurkjian et al. [61]. As-drawn silica fibers generally have lower fatigue parameters with most values ranging between 20-26 [34,54,55]. Abraded silica fibers or rods seem to be more resistant to fatigue, with reported values of *n* ranging from 22.1 to 42.6. Abraded bulk samples of silica have the greatest values of *n*, ranging from 30.7 to 45 [18,36]. Direct comparisons between indented and pristine silica fibers [33] and among silica fibers with different indentation flaw sizes [62] showed that the fatigue parameter increases with increasing indentation flaw size.

Kurkjian et al. [61] suggested that the failure of pristine glass fibers is controlled by crack initiation, whereas the failure of abraded or precracked samples is controlled by crack propagation, thus modeling fatigue of high strength fibers by means of slow crack

growth may not be appropriate. Dabbs et al. [62] suggested that there is a threshold of flaw size (~10μm) indicating a transition from crack propagation-controlled failure to a crack initiation-controlled failure mechanism. Most likely, the kinetics of the fatigue process for pristine glass fibers is quite different from that for slow crack growth. In slow crack growth studies, crack propagation behavior dominates, whereas in fatigue studies for pristine glass fibers, crack initiation must be considered. On pristine fiber surfaces, there is no crack tip for stress to concentrate. In the case of pristine glass fibers in TPB study, all reactive Si-O bonds in the gauge length are in contact with water, whereas in a slow crack growth experiment, the most reactive Si-O bonds are at the crack tip where water supply is limited and there might be some diffusion limit associated with it to slow down the fatigue. In a word, the fatigue reaction on a strained pristine surface might be different from that at a crack tip. It would be interesting if one could examine the in-situ structural change of a strained fiber until failure. It might give us some information about the difference between the fatigue mechanism before and after a crack is initiated.

From another point of view, the fatigue parameter n appears to decrease with increasing failure strain, since failure strain for pristine fibers are several orders of magnitude greater than for pre-cracked samples [61]. This is contrary to France and Duncan's observation of increased fatigue parameter with increasing failure strain [38]. However, their correlation was based on failure strains in different environments (i.e. in water, air, vacuum, liquid nitrogen), which involved different temperatures and water activities.

3.4.2. Activation Energy vs. Fatigue Parameter. It is noteworthy that the Arrhenius equation is usually used to describe the temperature dependence of a reaction rate (X), which increases with increasing temperature:

$$X = X_0 \exp \frac{-H}{RT} \tag{12}$$

where H is the activation energy. In the TPB test, the failure strain decreases with increasing temperature, so the apparent activation energy E_a in equation (11) does not have the negative sign. The value of E_a is used for the convenience of comparing the

temperature dependence of failure strain, for different glass compositions, since failure strains are controlled by the fatigue reaction rate, thus justifies the use of an Arrhenius relationship.

For the glasses tested in this study, the commercial silica, Na-borosilicate, and Na-aluminoslicate glasses, and the laboratory NaAlSi (25%) glass each have greater values for the fatigue parameter (>19, Table 3) and lower apparent activation energies for failure strains in water (<2.5 kJ/mol, Table 2). The low-alumina (≤9 mol %) NaAlSi glasses have low values for the fatigue parameter (<10) and greater values for E_a (>5 kJ/mole). Figure 3.10 compares n and E_a for each glass, and it is clear that there is an inverse relationship between the two parameters. This implies that if a material is susceptible to fatigue (has a low value of n), the temperature dependence of the associated fatigue reactions is large (great value of E_a).

Although it is suggested that the failure of pristine glass fibers is controlled by crack initiation, whereas slow crack growth is controlled by crack propagation. Both processes depend on the activated fatigue reaction, and so the slow crack growth models can help us understand the relationship between apparent activation energy (temperature dependence of fatigue) and the fatigue parameter (stress dependence of fatigue). The difference in the two tests is that failure strains from TPB are inversely correlated with the fatigue reaction rate, and thus failure strains decrease with increasing temperature, whereas crack growth rates are positively correlated with the fatigue reaction rate and thus increase with increasing temperature. So in Arrhenius equations, there is a negative sign in front of the activation energy term for slow crack growth, but no negative sign in front of the activation energy term for failure strains.

According to the activation volume model [18], the activation energy required for stress corrosion of a Si-O bond is dependent on the stress intensity:

$$\dot{c} = \dot{c}_0 \exp(-E^* + bK_I)/RT \tag{13}$$

where $\dot{c}$ is the crack velocity, K_I is the stress intensity factor, R is the gas constant, T is the temperature, E^* is the stress-free activation energy, b is a parameter related to the

activation volume, and $\dot{c}_0$ is a constant. A rough relationship between the fatigue parameter n' and b can be deduced by substituting equation (13) into (7):

$$n' \propto b + a \tag{14}$$

where a is a constant. In other words, the effective activation energy (E^*-bK_I) decreases with increasing n'. Although the activation energy here is different from the apparent activation energy E_a in equation (11), both energy terms provide a measure of the temperature dependence of the stress-corrosion reaction rate (greater activation energy means steeper Arrhenius slope). Similarly, the fatigue parameter n' is different from n in equation (10), but they both provide a measure of the inverse fatigue susceptibility. Thus this analysis qualitatively explains the trend in Figure 3.10.

3.4.3. Fatigue Mechanism for NaAlSi Glasses. The chemical reaction for fatigue in sodium silicate glasses is widely discussed [32,6]. It is well accepted that ion-exchange contributes to the extension of cracks in alkali silicate glass:

$$\begin{array}{c} | \quad | \\ -Si-O-Si-O^-Na^+ + H_2O \end{array} \longrightarrow \begin{array}{c} | \quad | \\ -Si-O-Si-OH + Na^+ + OH^- \end{array} \tag{15}$$

This ion-exchange reaction is greatly influenced by the stress applied on the glass structure. Celarie et al [63] studied ion diffusion at the vicinity of a crack tip in soda-lime silicate glass in humid air. They claim a two-step process in slow crack growth: 1. a fast migration of sodium ions to the fracture surface; 2. a slower inter-diffusion between alkali ions and protons (or hydronium ions) enhanced by the relaxation of the glass network changing the bond angles and lengths under stress. An explanation of this phenomenon is that sodium ions near NBO sites form a modifier channel [64,65] which works as a path for sodium diffusion [66]. Such diffusion channels are opened through the glass structure by the tensile stress near the crack tip. The sodium flow is balanced by interchange with hydrogen or hydronium ions to preserve charge neutrality [35].

It has been shown that the conductivity of a bent soda-lime silicate glass sheet is higher on the tension surface than on the compression surface [67,68]. The differences in

conductivity were attributed to higher sodium ion density in the tension regions because of sodium ion migration from the compression regions. The channel opening theory also provides an explanation of this phenomenon; viz., the conductivity increased as the alkali ion mobility increased as the structure was opened by the tensile stress. This suggests that the ability of a structure to reorganize, or the potential of 'channel opening' of the glass, has an influence on the stress-enhanced diffusion of alkali ions, and thus will affect the fatigue characteristics.

The fatigue mechanisms for sodium aluminosilicate glasses should be similar to those for other modified silicate glasses. Ion-exchange of sodium ions and hydrogen-bearing species (protons or hydronium ions) in sodium calcium aluminosilicate glass has been observed under atomic force microscope [69]. When an alumina ion is added to sodium silicate structure, an alumina tetrahedron (AlO_4^-) forms and one sodium ion is attracted to charge balance the site [70]. The addition of alumina eliminates non-bridging oxygens from the glass structure. The bond strength of sodium ions with alumina tetrahedra is weaker than the bond strength between sodium ions and NBO [70,71], thus alumina is added in alkali silicate glasses to enhance the sodium diffusivity. For example, Ag-Na interdiffusion rate was increased by adding alumina to sodium silicate glasses [72]. However, the ion-exchange between sodium and water species does not increase with the addition of alumina. Wassick et al. [73] studied the hydration of soda-lime silicate glass and found that the hydrogen penetration was ten times slower, and the diffusion coefficients of sodium and hydrogen were 50 times smaller, after 5 mole % of calcium oxide was replaced by alumina. A similar study showed that adding alumina to alkali silicate glasses resulted in an improvement in resistance to hydration [74]. A recent study showed that the sodium ion-exchange rate with protons (or hydronium ions) decreased by three orders of magnitude as alumina mole fraction increased from 0 to 15% in sodium aluminosilicate glasses [75]. Bunker [6] showed that alkali ions on NBO sites fully exchange with water species in a pH~8 basic solution, whereas alumina tetrahedral anionic sites resist exchange down to almost pH 5, indicating a much lower leachability for sodium cations from AlO_4^- sites than those from NBO sites. Bunker suggested that the $H^+AlO_4^-$ tetrahedra are not a stable structure.

The difference in the ion-exchange rate is usually attributed to the increased fraction of bridging oxygen bonds cross-linking the sodium filled channels [76], and this might be related to the compositional dependence of the fatigue behavior shown in Figure 3.9. Consider the fatigue process proposed by Celarie et al [63], where sodium channels in sodium silicate glasses can be opened by the tensile stress, thus enhancing cation diffusion and ion-exchange. When alumina is added to the glass, the ion-exchange rate decreases. In the meantime, the sodium channel is more and more cross-linked, thus the stress-enhanced diffusion also decreases as well. Thus the fatigue effect is less pronounced (greater n) with increasing alumina content.

Schematic representations of the fatigue processes for a sodium silicate glass and a fully cross-linked sodium aluminosilicate glass are shown in Figure 3.11 and Figure 3.12 respectively. For the sodium silicate glasses, the ion-exchange between sodium cations and hydrogen bearing species takes place in the sodium-rich channels [64,65] (Figure 3.11 (a)). The inter-diffusion between alkali ions and protons (or hydronium ions) is enhanced by the opening of the channel due to the remotely applied tensile stress (Figure 3.11 (b)). Finally the hydration of the nonbridging oxygens leads to the bonds breaking and crack initiation (Figure 3.11 (c)). For the sodium aluminosilicate glass (Figure 3.12), the ion-exchange rate is decreased when alumina is added to the glass. In these glasses, crack initiation requires the hydrolysis of more chemically-stable bridging oxygen bonds, consistent with the increases in n with increasing alumina content.

It is interesting to compare the failure strains measured in ambient conditions with those measured in inert conditions for the same glass (Figure 3.1). This enables us to differentiate the two mechanisms that lead glasses to fail in a TPB experiment. In inert conditions, the environmental fatigue effect is minimized, and the failure of glass solely depends on the types and properties of bonds that constitute the structure of the glass. In ambient conditions, fatigue plays an important role in determining the failure strain. France et al. [77] compared the failure strains in liquid nitrogen and in 20°C air (humidity not specified) for silica and several sodium borosilicate glasses which had been stored in a variety of environments for different lengths of time. They suggested that despite the differences in glass composition and aging conditions, the ratio (γ) between the inert failure strain and failure strain measured in air appeared to be constant at a value of about

2.8. This suggestion was probably the result of a coincidence that their compositions happened to have similar fatigue behaviors. Figure 3.13 compares the inert failure strains [43] and failure strains measured in water for the series of sodium aluminosilicate glasses studied here. It can be seen that for low alumina content glasses, the decrease in failure strain from inert conditions to ambient conditions is greater, compared to high alumina content glasses. The γ parameter introduced by France et al. [77] thus decreases, from 3.2 to 2.4 as the alumina content increases from 0 to 25 mole % (for data collected at 4000 μm/s). Similar phenomena can be found in commercial glasses. Figure 3.1 shows that silica and soda-lime silicate glasses have almost identical inert failure strain, whereas silica has a greater failure strain in water. Thus, γ for silica is 2.4 and that for soda-lime silicate glass is 3.3. The γ parameter is difficult to predict because it not only depends on the environmental fatigue parameter n, but also depends on the inert fatigue effect [22] or inert delayed failure effect [43], both of which describe the time dependent inert failure strains of glass.

3.5. CONCLUSION

The two-point bend (TPB) technique has been used to measure failure strains of glass fibers in water. Temperature dependence and strain rate dependence have been studied for several commercial glasses and a series of sodium aluminosilicate glasses. Failure strains decrease with increasing temperature, showing that fatigue effect depends on an activated chemical reaction. The dynamic fatigue parameters determined using TPB are comparable with reported values obtained using different methods but under similar conditions. It is found that glasses with cross-linked structures exhibit lower apparent activation energies and have a greater fatigue parameter.

For laboratory melts of sodium aluminosilicate glasses, the apparent activation energy decreases and the fatigue parameter increases with increasing alumina contents. The mechanism of fatigue in sodium aluminosilicate glass is similar to that of other modified silicate glass. Sodium ion exchanges with hydrogen ion or hydronium ion (H_3O^+), then the crack grows under the loading force with an assist from further chemical reactions, which depend on the further diffusion of sodium from the glass bulk. When alumina is added to sodium silicate glass, sodium ions charge balance with the aluminum to form alumina tetrahedra, so the non-bridging oxygens are replaced by bridging

oxygens. The sodium channel opening mechanism is reduced by the cross-link structure, leading to decreasing susceptibility to fatigue.

ACKNOWLEDGMENT

We gratefully acknowledge the NSF/I/U CRC Center for Glass Research (CGR) for funding this research. We also wish to thank PPG, Inc., Owens-Illinois Inc. and Sandia National Laboratories for providing glass samples. Thanks are also due to Nate Lower for building the two-point bender and the fiber drawing system used in this research.

REFERENCES

[1] B. A. Proctor, I. Whitney and J. W. Johnson, 'The Strength of Fused Silica,' *Proc. Roy. Soc. London, Series A, Math. Phys. Sci.*, 297 [1451] 534-57 (1967).

[2] L. Grenet, 'Mechanical Strength of glass,' *Bull. Soc. Enc. Industr. Nat. Paris,* (Ser. 5), 4 838-48 (1899).

[3] T. C. Baker and F. W. Preston, 'Fatigue of Glass under Static Loads,' *J. Appl. Phys.*, 17 [3] 170-8 (1946).

[4] M. Ciccotti, 'Stress-Corrosion Mechanisms in Silicate Glasses,' *J. Phys. D: Appl. Phys.*, 42 [21] 214006/1-18 (2009).

[5] S. W. Freiman, S. M Wiederhorn, and J. J. Mecholsky, Jr., 'Environmentally Enhanced Fracture of Glass: A Historical Perspective,' *J. Am. Ceram. Soc.*, 92 [7] 1371-82 (2009)

[6] B. C. Bunker, 'Molecular Mechanisms for Corrosion of Silica and Silicate Glasses,' *J. Non-Cryst. Solids*, 179 300-8 (1994).

[7] B. R. Lawn, 'Physics of Fracture,' *J. Am. Ceram. Soc.*, 66 [2] 83-91 (1983).

[8] T. A. Michalske, S. W. Freiman, 'A Molecular Mechanism for Stress Corrosion in Vitreous Silica,' *J. Am. Ceram. Soc.*, 66 [4] 284-8 (1983).

[9] A. T. Taylor and M. J. Matthewson, 'Effect of pH on the Strength and Fatigue of Fused Silica Optical Fiber,' *Proc. Int. Wire & Cable Symp.*, 47th 874-80 (1998).

[10] R. H. Doremus, 'Interdiffusion of Hydrogen and Alkali Ions in A Glass Surface,' *J. Non-Cryst. Solids*, 19 137-44 (1975).

[11] W. A. Lanford, K. Davis, P. Lamarche, T. Laursen, and R. Groleau, 'Hydration of Soda-Lime Glass,' *J. Non-Cryst. Solids*, 33 249-66 (1979).

[12] T. Fett, J. P. Guin and S. M. Wiederhorn, 'Stress in Ion-Exchange Layers of Soda-Lime-Silicate Glass,' *Fatigue Fract. Engng. Mater. Struct.*, 28 [6] 507-14 (2005).

[13] R. J. Charles, 'Static Fatigue of Glass. I,' *J. Appl. Phys.*, 29 [11] 1549-53 (1958).

[14] R. J. Charles, 'Static Fatigue of Glass. II,' *J. Appl. Phys.*, 29 [11] 1554-60 (1958).

[15] R. J. Charles, 'Dynamic Fatigue of Glass,' *J. Appl. Phys.*, 29 [12] 1657-62 (1958).

[16] W. J. Duncan, P. W. France and S. P. Graig, 'The Effect of Environment on the Strength of Optical Fiber,' in: C. R. Kurkjian (Ed.), *Strength of Inorganic Glass*, Plenum, 1985, p. 309-28.

[17] P. W. France, W. J. Duncan, D. J. Smith and K.J. Beales, 'Strength and Fatigue of Multicomponent Optical Glass Fibres,' *J. Mat. Sci*., 18 785-792 (1983).

[18] S. M. Wiederhorn, L. H. Bolz, 'Stress corrosion and Static Fatigue of Glass,' *J. Am. Ceram. Soc.*, 53 [10] 543-9 (1970).

[19] M. H. Krohn, J. R. Hellmann, D. L. Shelleman, C. G. Pantano and G. E. Sakoske, 'Biaxial Flexure Strength and Dynamic Fatigue of Soda-Lime-Silica Float Glass,' *J. Am. Ceram. Soc.*, 85 [7] 1777-82 (2002).

[20] L. G. Baikova, Kh. Ullner, V. P. Pukh, and T. I. Pensina, 'Determination of the Fatigue Parameters of Soda-Lime-Silicate Glass in Measurement of Strength by Different Methods,' *Sov. J. Glass Phys. Chem. (Eng. Trans.),* 17 [5] 418-24 (1991).

[21] S.Yoshida, A. Hidaka, and J. Matsuoka, 'Crack Initiation Behavior of Sodium Aluminosilicate Glasses,' *J. Non-Cryst. Solids*, 344 [1-2] 37-43 (2004).

[22] C. R. Kurkjian, P. K. Gupta, R. K. Brow, and N. Lower, 'The Intrinsic Strength and Fatigue of Oxide Glasses,' *J. Non-Cryst. Solids*, 316 114-24 (2003).

[23] T. C. Baker and F. W. Preston, 'Fatigue of Glass under Static Loads,' *J. Appl. Phys.*, 17 170-8 (1946).

[24] G. R. Irwin, J. A. Kies, 'Fracturing and Fracture Dynamics,' *Welding J.*, 31 (1952) 55s-100s.

[25] A. K. Varshneya, *Fundamentals of Inorganic Glass*, Academic Press, San Diego, CA, 1994, p. 419.

[26] W. Griffioen, 'Evaluation of Optical Fiber Lifetime Models Based on the Power Law,' *Opt. Eng.*, 33 488-97 (1994).

[27] A. G. Evans, 'Slow Crack Growth in Brittle Materials under Dynamic Loading Conditions,' *Int. J. Fracture*, 10 251 (1974).

[28] R. J. Charles, 'Diffusion Controlled Stress Rupture of Polycrystalline Materials,' *Metall. Trans. A.*, 7 1081-9 (1976)

[29] J. C. Pollet and S. J. Burns, 'Thermally Activated Crack Propogation-Theory,' *Int. J. Fract.*, 13 667-79 (1977)

[30] B. R. Lawn, 'An atomistic Model of Kinetic Crack Growth in Brittle Solids,' *J. Mat. Sci.*, 10 469-80 (1975).

[31] Y. S. Shiue and M. J. Matthewson, 'Stress Dependent Activation Entropy for Dynamic Fatigue of Pristine Silica Optical Fibers,' *J. Appl. Phys.*, 89 [9] 4787-93 (2001).

[32] G. G. Trantina, 'Strength and Life Prediction for Hot-Pressed Silicon Nitride,' *J. Am. Ceram. Soc.*, 62 [7-8] 377-80 (1979).

[33] S. L. Semjonov, G. S. Glaesemann, D. A. Clark and M. M. Bubnov, 'Fatigue Behavior of Silica Fibers with Different Defects,' *Proc. SPIE*, 4215 28-35 (2001).

[34] J. E. Ritter, Jr., J. M. Sullivan, Jr., and K. Jakus, 'Application of Fracture-Mechanics Theory to Fatigue Failure of Optical Glass Fibers,' *J. Appl. Phys.*, 49 [9] 4779-82 (1978).

[35] R. E. Mould and R. D. Southwick, 'Strength and Static Fatigue of Abraded Glass Under Controlled Ambient Conditions: I, General Concepts and Apparatus,' *J. Am. Ceram. Soc.*, 42 [11] 542-7 (1959).

[36] J. E. Ritter, Jr. and C. L. Sherburne, 'Dynamic and Static Fatigue of Silicate Glasses,' *J. Am. Ceram. Soc.*, 54 [12] 601-5 (1986).

[37] J. E. Ritter, Jr. and R. P. LaPorte, 'Effect of Test Environment on Stress-Corrosion Susceptibility of Glass,' *J. Am. Ceram. Soc.*, 58 [7-8] 265-7 (1975).

[38] P. W. France, M. J. Paradine, M. H. Reeve and G. R. Newns, 'Liquid Nitrogen Strengths of Coated Optical Glass Fibers,' *J. Mater. Sci.*, 15 825-830 (1980).

[39] M. J. Matthewson, C. R. Kurkjian and S. T. Gulati, 'Strength Measurement of Optical Fibers by Bending' *J. Am. Ceram. Soc.*, 69 [11] 815-821 (1986).

[40] R. K. Brow, N. P. Lower and C. R. Kurkjian, 'TPB Test Provides New Insights to Fiber Strength and Quality,' *Ceram. Bull.*, 84 [10] 50-53 (2005).

[41] R. K. Brow, N. P. Lower, C. R. Kurkjian and H. Li, 'The Effects of Melt History on the Failure Characteristics of Pristine Glass Fibers,' *Phys. Chem. Glasses, Eur. J. Glass Sci. Tech.*, 50 [1] 31-33 (2009).

[42] N. P. Lower, R. K. Brow and C. R. Kurkjian, 'Inert Failure Strain Studies of Sodium Silicate Glass Fibers,' *J. Non-Cryst. Solids*, 349 168-172 (2004).

[43] N. P. Lower, R. K. Brow and C. R. Kurkjian, 'Inert Failure Strain Studies of Sodium Aluminosilicate Glass Fibers,' *J. Non-Cryst. Solids*, 344 17-21 (2004).

[44] R. K. Brow, N. P. Lower, A. J. Lang and C. R. Kurkjian, 'Structure and the Intrinsic Strength of Glass,' *Glastech. Ber. Glass Sci. Technol.*, 75 C2 133-138 (2002).

[45] V. V. Rondinella and M. J. Matthewson, 'Effect of Loading Mode and Coating on Dynamic Fatigue of Optical Fiber in Two-Point Bending,' *J. Am. Ceram. Soc.*, 76 [1] 139-44 (1993).

[46] V. V. Rondinella, M. J. Matthewson and C. R. Kurkjian, 'Coating Additives for Improved Mechanical Reliability of Optical Fiber,' *J. Am. Ceram. Soc.*, 77 [1] 73-80 (1994).

[47] M. J. Matthewson and C. R. Kurkjian, 'Static Fatigue of Optical Fibers in Bending,' *J. Am. Ceram. Soc.*, 70 [9] 662-8 (1987).

[48] S. F. Cowap and S. D. Brown, 'Technique for the Static Fatigue Testing of Fibers,' *J. Am. Ceram. Soc.*, 70 [4] C-67-C-68 (1987).

[49] S. Bhaumik, 'Effect of Humidity of Drawing Environment on Dynamic Fatigue of Polymer Coated High Strength Silica Optical Fiber,' *Wire J. Int.*, 38 [3] 194-8 (2005).

[50] B. A. Proctor, I. Whitney, and J. W. Johnson, 'Strength of Fused Silica,' *Proc. Roy Soc. A*, 297 [1451] 534-57 (1967).

[51] W. Weibull, 'A Statistical Theory of the Strength of Materials,' *Eng. Res. Proc.* 151 (1939) 1-45.

[52] W. Weibull, 'A Statistical Distribution of Wide Applicability,' *J. Appl. Mechan.*, 18 (1951) 293-7

[53] M. J. Matthewson, C. R. Kurkjian, C. D. Haines and N. Venugopal, 'Temperature Dependence of Strength and Fatigue of Fused Silica Fiber in the Range 77 to 473 K,' *Proc. SPIE* 4940 74-9 (2003).

[54] Y. S. Shiue and M. J. Matthewson, 'Stress Dependent Activation Entropy for Dynamic Fatigue of Pristine Silica Optical Fibers,' *J. Appl. Phys.*, 89 [9] 4787-93 (2001).

[55] V. V. Rondinella, M. J. Matthewson and C. R. Kurkjian, 'Coating Additives for Improved Mechanical Reliability of Optical Fiber,' *J. Am. Ceram. Soc.*, 77 [1] 73-80 (1994).

[56] V. P. Pukh, L. G. Baikova, M. F. Kireenko and L.V. Tikhonova, 'On the Kinetics of Crack Growth in Glass,' *Glass Phys. Chem.*, 35 [6] 560-6 (2009).

[57] A. G. Metcalfe and G. K. Schmitz, 'Mechanism of Stress Corrosion in E-glass Filaments,' *Glass Tech.*, 13 [1] 5-16 (1972).

[58] E. Gehrke, Ch. Ullner, and M. Hahnert, 'Fatigue Limit and Crack Arrest in Alkali-Containing Silicate Glasses,' *J. Mater. Sci.*, 26 5445-55 (1991).

[59] G. S. Glaesemann, 'The Mechanical Behavior of Large Flaws in Optical Fiber and Their Role in Reliability Predictions,' Corning, Inc. Available from internet:<http://www.new.corning.com/assets/0/433/573/625/631/F6439231-19C5-445B-947C-D5D5CB64951E.pdf>, sited: Jun 29, 2011

[60] R. D. Maurer, 'Behavior of Flaws in Fused Silica Fibers,' in: C. R. Kurkjian (Ed.), *Strength of Inorganic Glass*, Plenum, 1985, p. 291-308.

[61] C. R. Kurkjian, J. T. Krause and U. C. Paek, 'Tensile Strength Characteristics of "Perfect" Silica Fibers,' *J. de. Physque*, C9-585-586 (1982).

[62] T. P. Dabbs and B. R. Lawn, 'Strength and Fatigue Properties of Optical Glass Fibers Containing Microindentation Flaws,' *J. Am. Ceram. Soc.*, 68 [11] 563-9 (1985).

[63] F. Celarie, M. Ciccotti and C. Marliere, 'Stress-Enhanced Ion Diffusion at the Vicinity of a Crack Tip as Evidenced by Atomic Force Microscopy in Silicate Glasses,' *J. Non-Cryst. Solids*, 353 51-68 (2007).

[64] G. N. Greaves, 'EXAFS and the structure of glass,' *J. Non-Cryst. Solids*, 71 203-17 (1985).

[65] A. Meyer, J. Horbach, W. Kob, F. Kargl and H. Schober, 'Channel Formation and Intermediate Range Order in Sodium Silicate Melts and Glasses,' *Phys. Rev. Lett.*, 93 [2] 027801-1 (2004).

[66] P. Jund, W. Kob, and R. Jullien, 'Channel Diffusion of Sodium in a Silicate Glass,' *Phys. Rev. B.*, 64 134303-1-5 (2001).

[67] W. S. Gorsky, 'Theory of Elastic Aftereffect in Unordered Mixed Crystals,' Phys. Zeit, Sowjet., 8 457-71 (1935).

[68] N. Weber and M. Goldstein, 'Stress-Induced Migration and Partial Molar Volume of Sodium Ions in Glass,' *J. Chem. Phys.*, 41[9] 2898-2901 (1964).

[69] A. Gob, E. Radlein and G. H. Frischat, "Atomic Force Microscope Study of Silicate Glass Fracture Surfaces in Air and in Water Environment," ***Glass Sci. Tech.***, 76 [5] 244-51 (2003).

[70] A. K. Varshneya, Fundermentals of Inorganic Glasses, pp 113-114,CA 1994.

[71] S. N. Houde-Walter, J. M. Inman, A. J. Dent and G. N. Greaves, 'Sodium and Silver Environments and Ion-Exchange Processes in Silicate and Aluminosilicate Glasses,' ***J. Phys. Chem.***, 97 9330-6 (1993).

[72] A. J. Burggraaf and J. Cornelissen, 'Strengthening of Glass by Ion Exchange, Part I,' ***Phys. Chem. Glasses***, 5 [5] 123-9 (1964).

[73] T. A. Wassick, R. H. Doremus, W. A. Lanford, and C. Burman, 'Hydration of Soda-Lime Silicate Glass, Effect of Alumina,' ***J. Non-Cryst. Solids***, 54 139-51 (1983).

[74] R. H. Doremus, Y. Mehrotra, W. A. Lanford, and C. Burman, 'Reaction of Water with Glass: Influence of a Transformed Surface Layer,' ***J. Mater. Sci.***, 18 612-22 (1983).

[75] B. P. McGrail, J. P. Icenhower, D. K. Shuh, P. Liu, J. G. Darab, D. R. Baer, S. Thevuthasen, V. Shutthanandan, M. H. Engelhard, C. H. Booth and P. Nachimuthu, 'The Structure of Na_2O-Al_2O_3-SiO_2 Glass: Impact on Sodium Ion Exchange in H_2O and D_2O,' ***J. Non-Cryst. Solids***, 296 10-26 (2001).

[76] D. M. Zirl and S. H. Garofalini, 'Structrue of Sodium Aluminosilicate Glasses Surfaces,' ***J. Am. Ceram. Soc.***, 75 [9] 2353-62 (1992).

[77] P. W. France, M. J. Paradine, M. H. Reeve, and G. R. Newns, 'Liquid Nitrogen Strengths of Coated Optical Glass Fibres,' ***J. Mat. Sci.***, 15 825-30 (1980).

Table 3.1. Melting temperature (T_{melt}), melting time (t_{melt}) and pulling temperature (T_{pull}) for the commercial glasses and the series of $25Na_2O{\cdot}xAl_2O_3{\cdot}(75–x)SiO_2$ glasses prepared in the laboratory.

Source	Composition	T_{melt} (°C)	t_{melt} (hour)	T_{pull}(°C)
Commercial	Ca-aluminoborosilicate	1550	4	1300
Commercial	Na-Ca-silicate	1220	4	1150
Commercial	Na-borosilicate	1600	16	1375
Commercial	Na-aluminosilicate	1600	10	1375
Laboratory	NaAlSi (x = 0)	1300	5	1150
Laboratory	NaAlSi (x = 5)	1350	5	1150
Laboratory	NaAlSi (x = 9)	1400	6	1200
Laboratory	NaAlSi (x = 12.5)	1450	8	1200
Laboratory	NaAlSi (x = 18.75)	1550	16	1300
Laboratory	NaAlSi (x = 25)	1600	16	1375

Table 3.2. TPB average failure strain (ε_f) measured in distilled water at different temperatures with a faceplate velocity (v_{fp}) of 4000 μm/s and apparent activation energy (E_a) calculated from equation (7).

	Average Failure Strain, ε_f (%)				E_a (kJ/mol)
Temperature (°C)	3±2	21±2	55±2	94±2	
Fused silica	7.42±0.09	7.22±0.08	6.63±0.07	6.22±0.04	1.7±0.1
Ca-aluminoborosilicate	5.86±0.18	5.36±0.22	4.76±0.25	3.87±0.23	3.6±0.5
Na-Ca-silicate	5.36±0.14	5.06±0.20	4.45±0.13	3.95±0.08	2.8±0.3
Na-borosilicate	5.30±0.28	5.24±0.52	4.75±0.39	4.52±0.36	1.5±0.8[a]
Na-aluminosilicate	3.75±0.35	3.45±0.34	3.43±0.29	3.25±0.28	1.1±1.1[a]
NaAlSi (x = 0)	7.83±0.12	6.55±0.14	4.55±0.10	3.12±0.10	8.3±0.3
NaAlSi (x = 5)	7.78±0.25	7.01±0.12	5.45±0.12	4.35±0.13	5.6±0.3
NaAlSi (x = 9)	8.03±0.35	6.89±0.36	5.70±0.21	5.05±0.18	4.2±0.5
NaAlSi (x = 12.5)	7.29±0.22	6.48±0.14	5.70±0.14	5.52±0.11	2.4±0.3
NaAlSi (x = 18.75)	6.92±0.13	6.41±0.08	5.58±0.13	5.61±0.14	2.2±0.3
NaAlSi (x = 25)	6.84±0.17	6.12±0.16	5.52±0.09	5.30±0.12	2.3±0.3

a. Broad distributions of failure strains lead to great uncertainty of activation energy calculation, as the errors of failure strains were weighed in linear fit.

Table 3.3. Failure strain (ε_f) measured at different faceplate velocities (v_{fp}) in distilled water at 21°C and the fatigue parameter (n) calculated from equation (6).

	ε_f (%) in 21˚C distilled water				n
v_{fp} (μm/s) =	50	500	4000	10000	
Fused silica	5.92±0.07	6.60±0.07	7.22±0.08	7.49±0.08	23.7±1.5
Ca-aluminoborosilicate	4.14±0.24	4.68±0.24	5.36±0.22	5.77±0.17	16.6±2.8
Na-Ca-silicate	3.71±0.15	4.37±0.19	5.06±0.20	5.47±0.28	14.9±2.1
Na-borosilicate	4.31±0.42	4.71±0.44	5.23±0.51	5.56±0.39	21.6±11.7[b]
Na-aluminosilicate	2.97±0.22	3.27±0.25	3.45±0.34	3.68±0.30	27.2±18.5[b]
NaAlSi (x=0)	3.10±0.06	4.67±0.10	6.55±0.14	7.62±0.15	6.9±0.2
NaAlSi (x=5)	3.70±0.07	5.18±0.16	7.01±0.12	7.69±0.16	8.1±0.2
NaAlSi (x=9)	4.21±0.14	5.39±0.18	6.89±0.36	7.53±0.43	10.0±0.9
NaAlSi (x=12.5)	4.91±0.16	5.64±0.22	6.48±0.14	7.01±0.19	16.1±1.7
NaAlSi (x=18.75)	4.85±0.13	5.63±0.25	6.41±0.08	6.71±0.08	17.4±1.4
NaAlSi (x=25)	4.90±0.17	5.49±0.19	6.12±0.16	6.50±0.11	19.6±2.4

b. Great uncertainties are due to broad distributions of failure strains rather than the quality of the fit, as the errors of failure strains were weighed in linear fit.

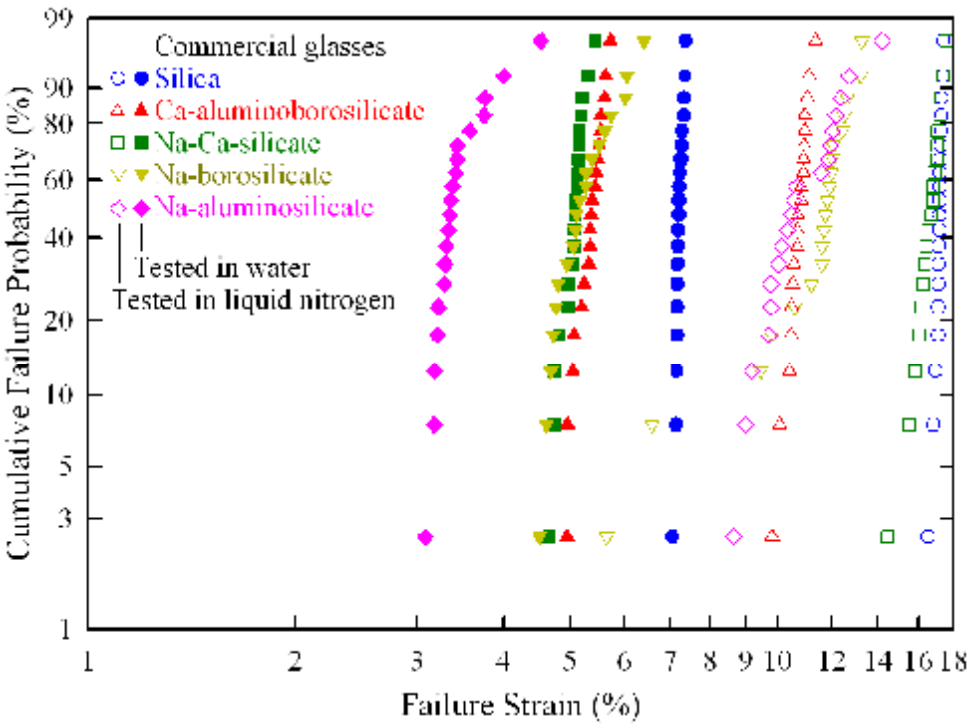

Figure 3.1. Weibull distributions of failure strains for commercial glass measured using two-point bend technique (v_{fp}=4000 μm/s) in liquid nitrogen (open symbols) and in room temperature distilled water (solid symbols).

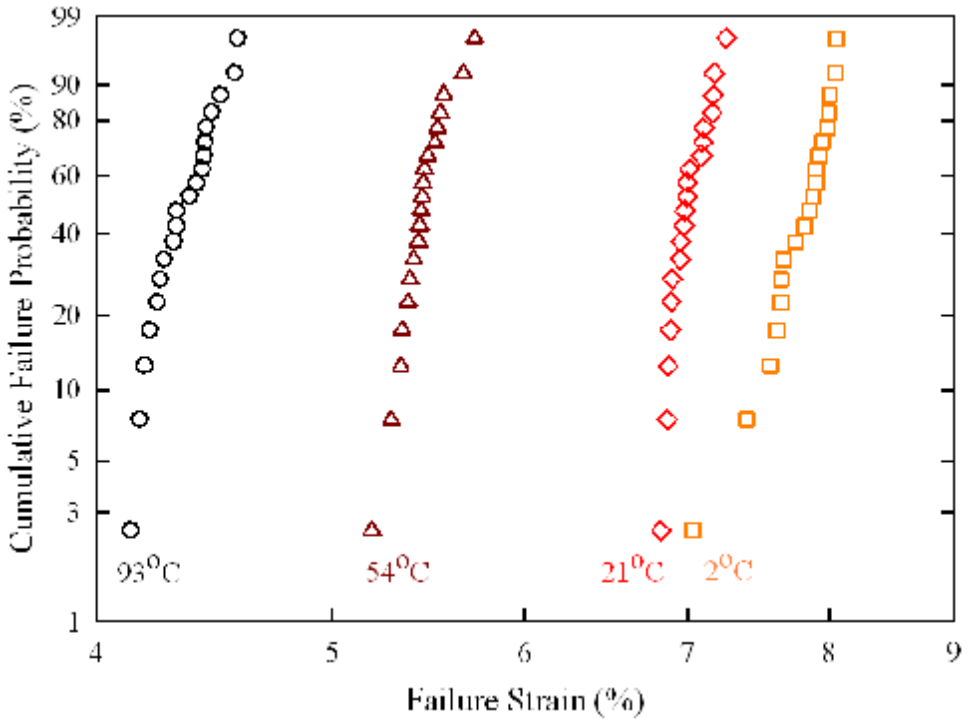

Figure 3.2. Weibull distributions of failure strains of NaAlSi (x=5) glass fibers measured in distilled water at different temperatures (v_{fp}=4000 μm/s).

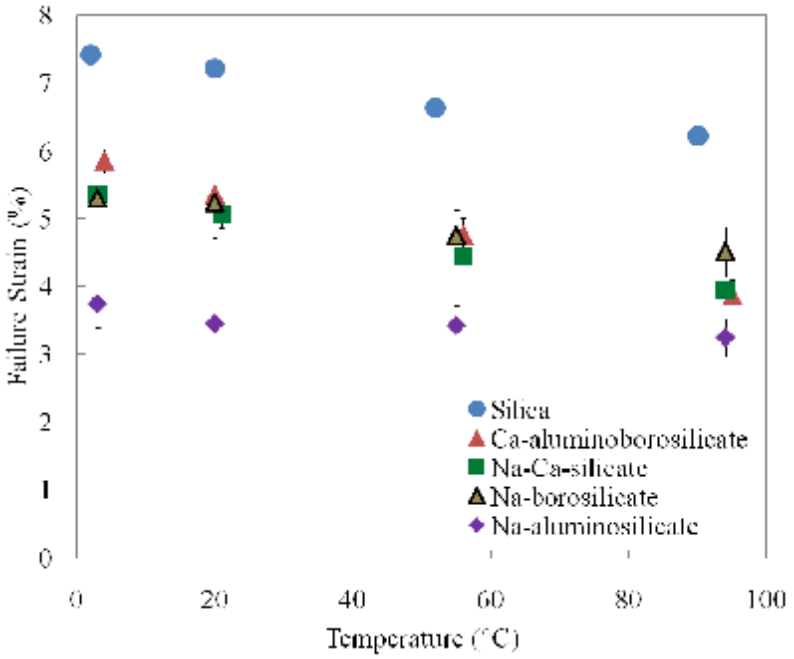

Figure 3.3. Temperature dependence of failure strains for commercial silicate glasses measured in distilled water (v_{fp}=4000 μm/s).

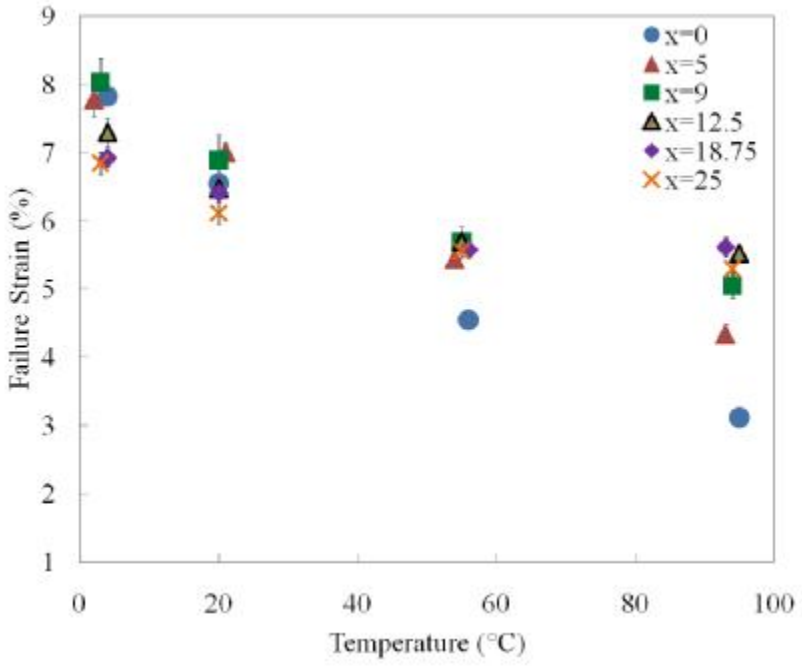

Figure 3.4. Temperature dependence of failure strains for the $25Na_2O{\cdot}xAl_2O_3{\cdot}(75–x)SiO_2$ glasses measured in distilled water (v_{fp}=4000 μm/s).

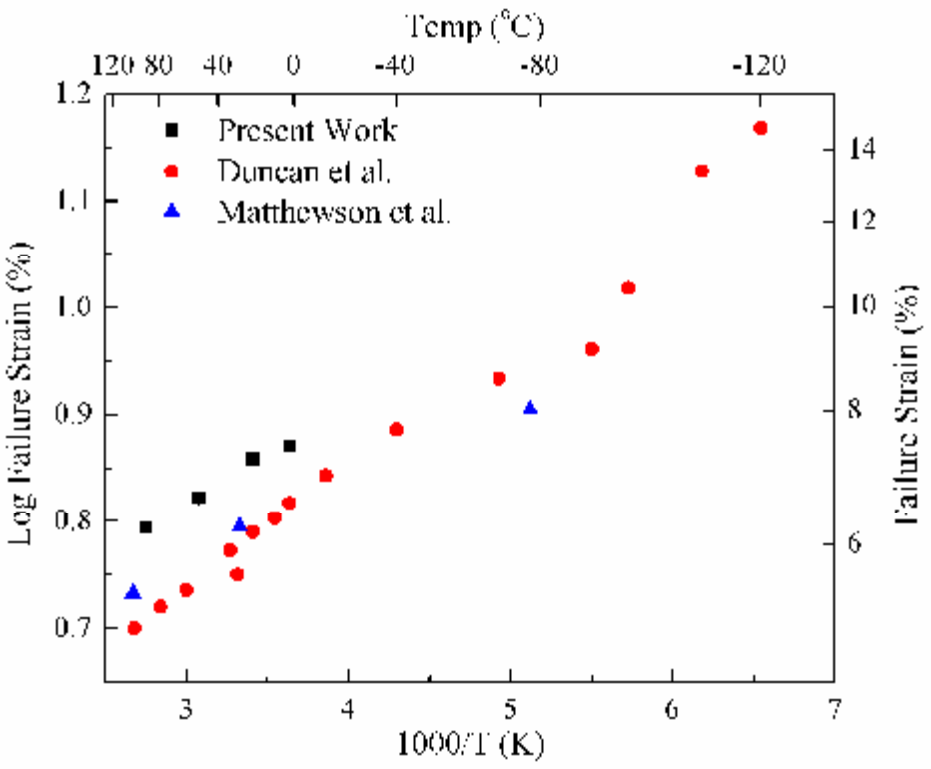

Figure 3.5. Temperature dependence of failure strains of silica from present work (measured in distilled water), Duncan et al. (measured in 100% humidity) [16] and Matthewson et al. (measured in water and moisture saturated acetone at lower temp) [53].

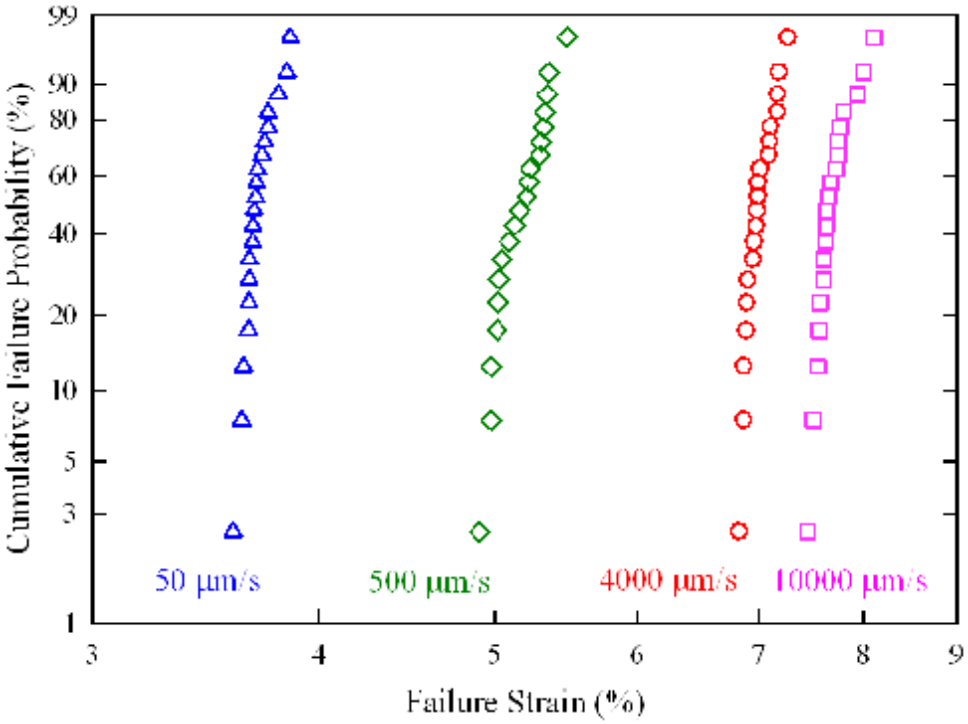

Figure 3.6. Weibull distributions of failure strains for NaAlSi (x=5) glass in 21˚C distilled water measured at different faceplate velocities.

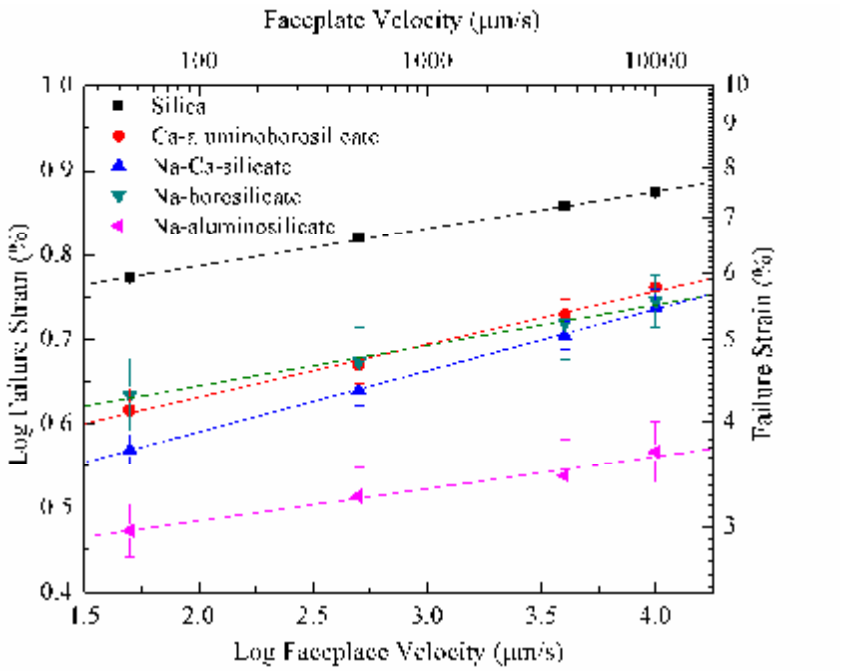

Figure 3.7. Failure strains (measured in 21°C distilled water) as a function of faceplate velocity for commercial silicate glasses.

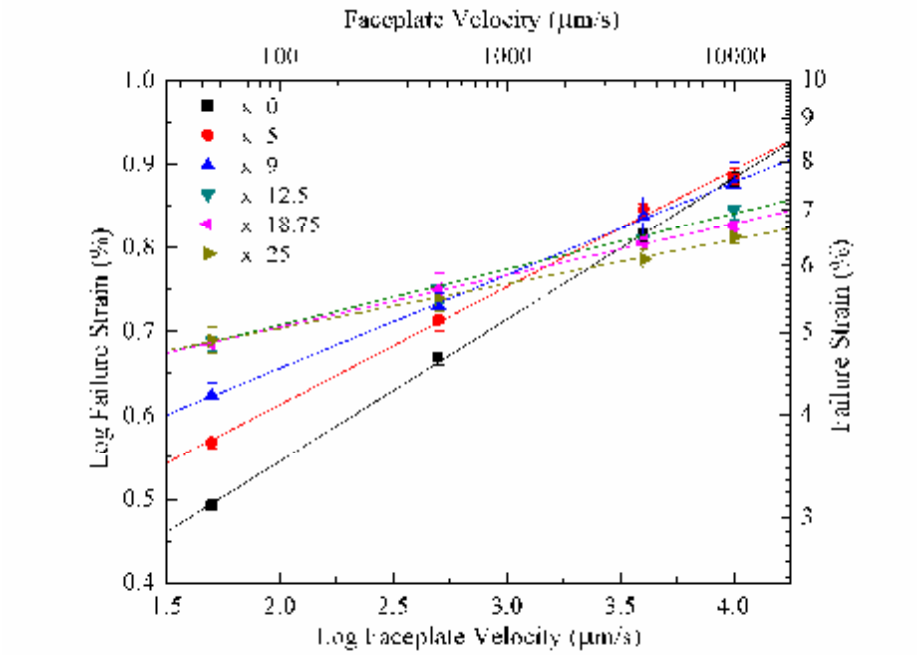

Figure 3.8. Failure strains (measured in 21°C distilled water) as a function of faceplate velocity for $25Na_2O{\cdot}xAl_2O_3{\cdot}(75–x)SiO_2$ glasses.

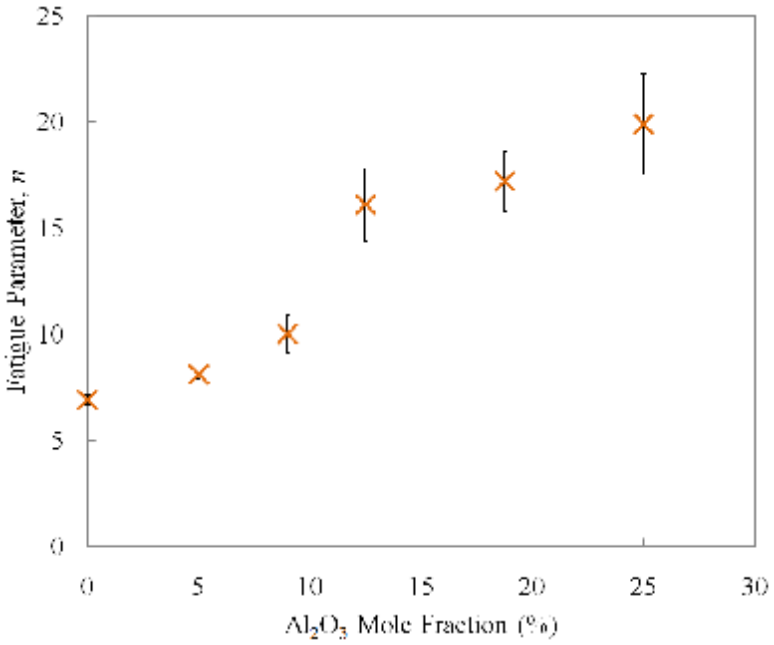

Figure 3.9. Dynamic fatigue parameters for lab made sodium aluminosilicate glasses measured by TPB in 21˚C distilled water.

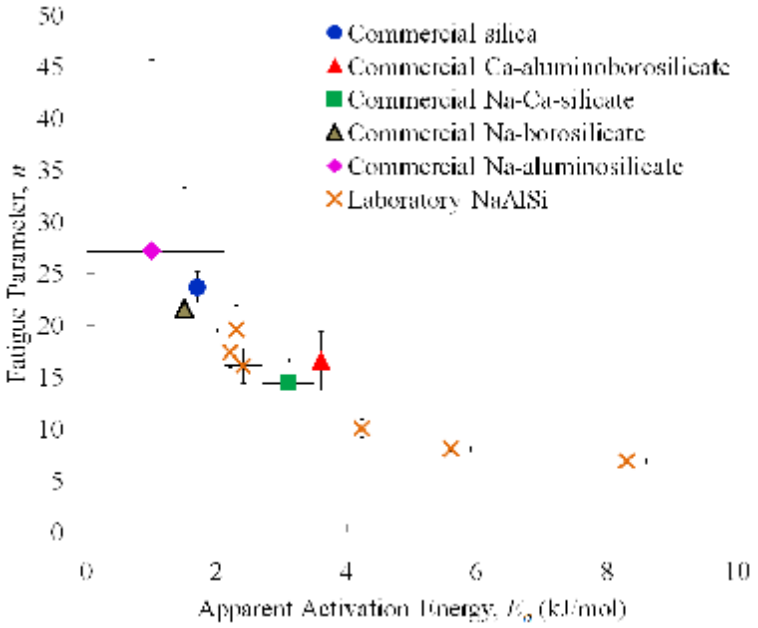

Figure 3.10. Fatigue parameter and apparent activation energy of selected glasses.

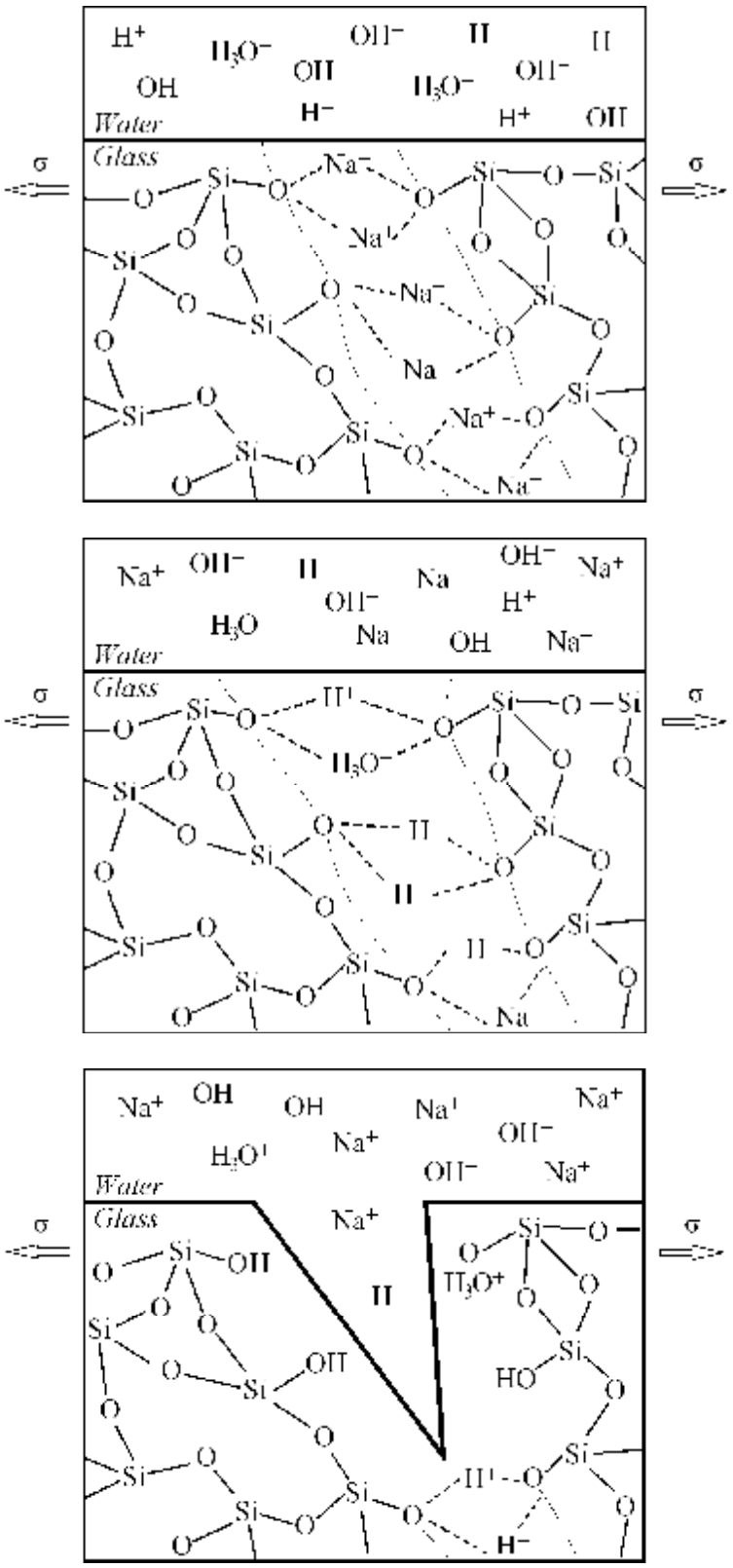

Figure 3.11. Schematic drawings for fatigue process for a sodium silicate glass in water.

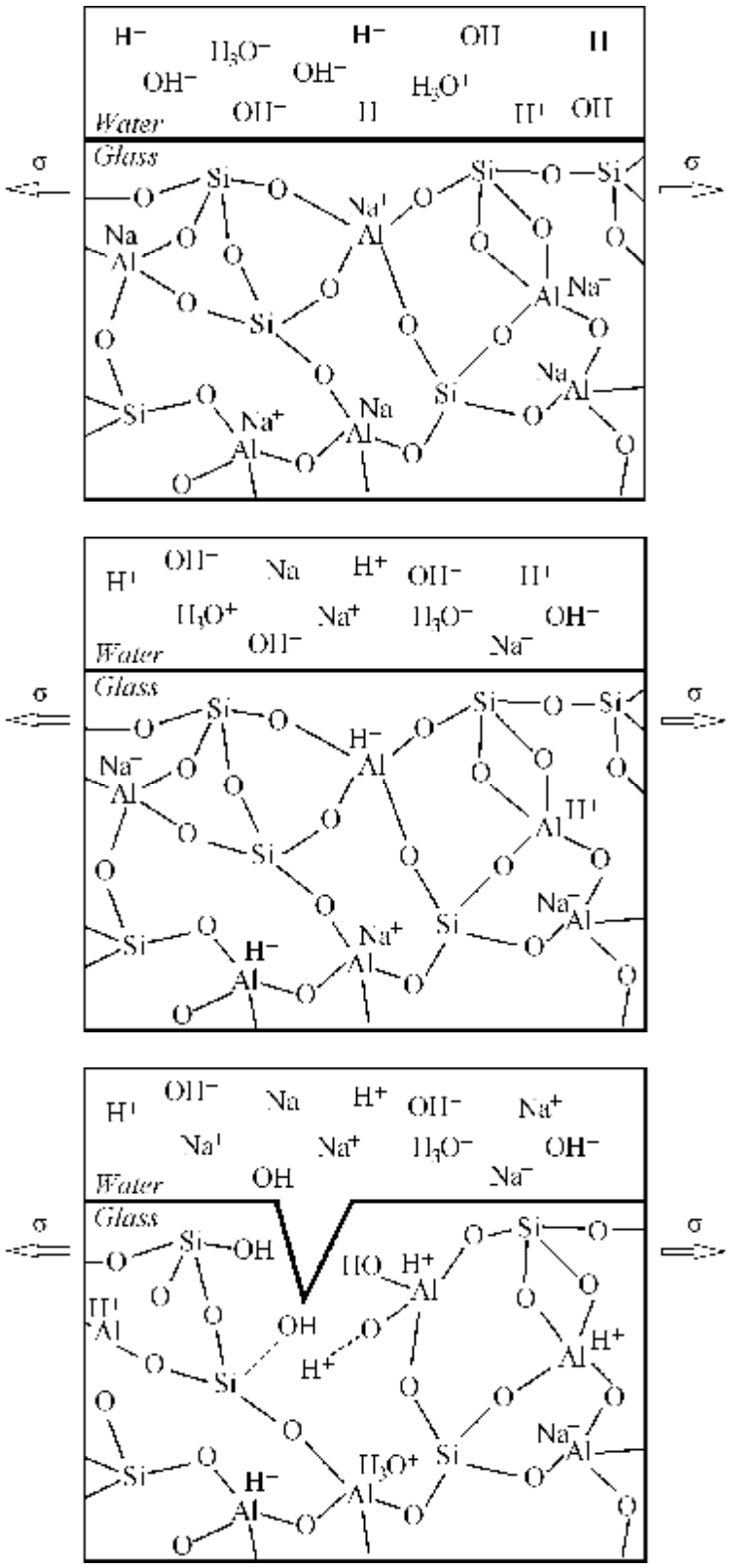

Figure 3.12. Schematic drawings for fatigue process for a fully cross-linked sodium aluminosilicate glass in water.

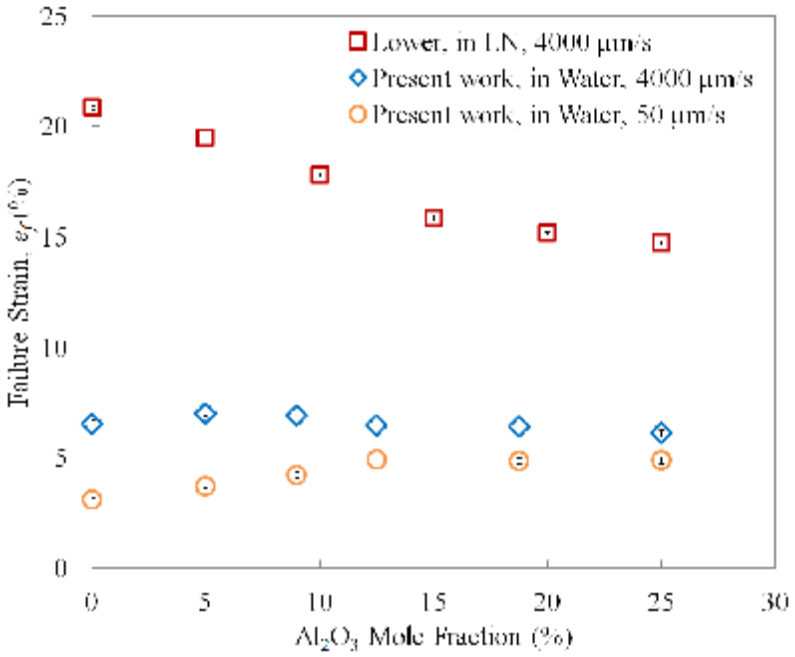

Figure 3.13. Inert failure strains measured in liquid nitrogen at v_{fp} = 4000 µm/s from Lower [43] and failure strains measured in 21°C distilled water at v_{fp} = 4000 and 10000 µm/s (present work) as a function of Al_2O_3 mole fraction for $25Na_2O{\cdot}xAl_2O_3{\cdot}(75\text{-}x)SiO_2$ (mole %) glasses.

4. ENVIRONMENTAL FATIGUE OF SILICATE GLASSES IN HUMID CONDITIONS

Zhongzhi Tang and Richard K. Brow

[a]Missouri University of Science & Technology, Department of Materials Science & Engineering, Rolla, MO 65409, USA

ABSTRACT

Failure strains of commercial silica, soda-lime silicate and E-glass fibers were measured using two-point bending in room temperature humid air. Humidity dependence and dynamic fatigue behavior were studied and the fatigue reaction orders in terms of humidity were determined. In the humidity range tested (~0.1% to ~100%), the dynamic fatigue parameters for silica and E-glass are found to be greater in lower humidity (~0.1% to ~10%), whereas the fatigue parameter for soda-lime silicate is independent of humidity. The humidity dependence of failure strains for all three glasses was more pronounced in high humidity (~10% to ~100%) than in low humidity (~0.1% to ~10%), indicating that the reaction order decreases with decreasing humidity. These observations were correlated to the different structures of the glasses and their corresponding fatigue mechanisms.

4.1. INTRODUCTION

About 100 years ago, Grenet [1] observed that the strength of glass is dependent on the loading time and/or loading rate in aqueous or humid environments. Even though a glass might withstand a certain load for a short period of time, it might fail later. This phenomenon was probably first describes as ‘fatigue’ by Baker and Preston in 1946 [2,3,4]. The static fatigue (loading time dependence) and the dynamic fatigue (loading rate dependence) for silica and soda-lime silicate glasses were studied by Charles [5,6,7]. It is well accepted that the fatigue effect is due to some stress-induced chemical reaction between glass and water [8,9]. The general fatigue reactions for silica and alkali silicate glasses were summarized in our other paper [10].

4.1.1. Fatigue Measurements. A popular way to study the fatigue effect is to study the slow-crack growth behavior (a.k.a. subcritical crack growth). A typical experiment is a double cantilever beam test, in which a constant force is applied to a predetermined length of crack on a glass sample, and the crack propagation velocity is measured as a function of the force [11,12]. The most widely used model to describe the slow crack growth is based on an empirical power law [13,14]:

$$V = A(K_I/K_{IC})^n \quad (1)$$

where V is the crack growth velocity, n is termed the stress corrosion susceptibility parameter, or the fatigue parameter, K_I is stress intensity factor, K_{IC} is the critical value of K_I, or fracture toughness, and A is the environmental parameter which has a Arrhenius temperature dependence.

Fatigue has also been studied by measuring the time or rate dependent strength of glass. For example, dynamic fatigue can be described as [15]:

$$\sigma_f = D\dot{\sigma}^{(1/n+1)} \quad (2)$$

where σ_f is the strength, or failure stress, $\dot{\sigma}$ is the applied stress rate, D is a constant, and n is the fatigue parameter equivalent to the n in equation (1). This equation allows direct comparison between slow-crack growth studies and dynamic fatigue studies. The fatigue of glass has been studied using different strength measurements, including tensile tests [16,17,18,19,20], two-point bending tests [10,21,22,23,24], three-point bending tests [3,25], four-point bending tests [26,27], and ring-on-ring tests [28].

Even though the fatigue parameters for slow crack growth and strength measurements are equivalent, differences in the value of n for the same materials (silica glass) have been reported [29,30,31]. As-drawn silica fibers generally have smaller fatigue parameters, abraded silica fibers or rods exhibit an intermediate value for n, and abraded or pre-cracked bulk samples of silica have the greatest values of n. Kurkjian et al. [31] suggested that the failure of pristine glass fibers is controlled by crack initiation while the failure of abraded or pre-cracked samples is controlled by crack propagation;

thus, modeling fatigue of high strength fibers by means of slow crack growth may not be appropriate. It was suggested that the transition from crack propagation-controlled failure to a crack initiation-controlled failure mechanism occurs at a threshold flaw size of ~10 μm [32]. Duncan et al. [23] suggested that the fatigue reaction is the same for slow crack growth and fiber strength measurements, but the kinetics might be slightly different.

4.1.2. Water vs Humidity. Fatigue has been studied in both liquid water and in moist air. There is no substantial difference in mechanism considering that fatigue in both environments is essentially a stress-enhanced reaction between water molecules and glass bonds; however, differences exist in the kinetics of the reaction. Celarie et al. [33] studied stress-enhanced ion-diffusion at the crack tip of soda-lime silicate glass in ~50% RH using atomic force microscopy, and observed a condensation from the gaseous atmosphere to continuous aqueous liquid phase. It is likely that the liquid water is enriched with ions which allow same ion-exchange mechanism that was observed in soda-lime silicate glass in water [8].

As was stated by Glasstone et al. [34], generally, a reaction occurring between a gas/liquid and a solid can be separated into five consecutive steps: (1) Transport of the gas reactants to the surface (2) Absorption of the gas/liquid reactants by the surface, (3) Reaction between the gas/liquid reactants and the surface, (4) Desorption of the products, and (5) Transport of the liberated products away from the surface. The overall reaction rate is limited by the slowest steps of the five. In the case of fatigue reactions, step (4) and (5) can be neglected because fracture produces new surface (fresh reaction sites) and the reaction products (broken bonds) are left behind and have no effect on the subsequent reactions. It was suggested that the early stage (region I crack growth) of crack propagation is controlled by step (3), the glass-water reaction rate [12]. However, when the humidity is low enough, the water concentration and mobility are greatly reduced, it is possible that step (1) and (2), water transportation and absorption become the limiting factors [35]. Mrotek et al. [22] suggested that a complete monolayer of water is formed on the silica surface in above ~18% RH so below this the water condensation observed by Celarie et al. [33] may not occur at lower RH and, if present, may not act in the same

manner. This might result in completely different fatigue mechanisms at different humidities and, in turn, vary from that seen in liquid water.

The study of fatigue in humidity brings important information because if there is only one simple fatigue reaction, the rate constant A in equation (1) should depend on the relative humidity, RH, according to [12]:

$$A \propto (\mathrm{RH})^{m} \tag{3}$$

in which, m is the reaction order, defined as the number of molecules of water that are involved in the bond-breaking reactions. Wiederhorn [12] reported that the reaction order for fatigue in soda-lime silicate glasses, measured in a slow crack growth study, decreased from ~1.3 in the range of 10-100% RH to ~0.5 in the range of 0.017%-1% RH (It was reported that m~1 in the high RH range, but the data reported in Figure 5 from Wiederhorn's paper indicates that m~1.3). Wiederhorn suggested that the change in m near RH ~1-10% indicates that there is more than one reaction occurring between water and glass.

In two-point bend tests, the empirical dependence of failure strain (ε_f) on relative humidity (RH) can be obtained by [23]:

$$\varepsilon_f \propto (\mathrm{RH})^{a}, \tag{4}$$

and the reaction order (m) can be determined by [23]:

$$m = a \times (1 - n) \tag{5}$$

The reasoning behind this can be seen from the relationship between the failure strain (ε_f) and the environmental constant (A) for two-point bending at a constant faceplate velocity (v_{fp}) [36]:

$$(E\varepsilon_f)^{n-1} = \frac{n-1}{(n-2)AEY^2 \times 1.198\, r} \left(\frac{\sigma_i}{K_{IC}}\right)^{n-2} v_{fp} \tag{6}$$

where E is the Young's modulus, Y is the crack shape parameter, r is the radius of the fiber, and σ_i is the inert strength. Taking the log of ε_f from equation (6), and assuming that the fatigue parameter (n) does not depend on humidity [23], it can be shown that:

$$\log \varepsilon_f \times (n-1) = -\log A + B \tag{7}$$

where B is a constant with regards to RH. Substituting equation (3) and (4) into (7) gives (5). Using this approach, Duncan et al. [23] reported that m for silica decreased from ~2.3 in the range of 15-100% RH to ~1.1 in the range of 10^{-4}-10^{-8} RH, and that m for a sodium borosilicate glass decreased from ~1.7 in the range of 15-100% RH to ~0.9 in the range of 10^{-5}-10^{-8} RH. As pointed out by Mrotek et al. [22], if Duncan's data were plotted in a single log RH axis, the trend in high and low humidity do not intersect at an intermediate humidity. Mrotek et al. [22] measured failure strains for silica in a 25°C glove box and reported that the fatigue parameter (n) gradually decreased from ~31 in 0.025% RH to ~22 in 95% RH, which violates Duncan's assumption of n being independent of RH. Mrotek et al. also reported that the reaction order droped from 2.1 in the range of 20-95% RH to 0.9 in the range of 0.025-13% RH.

The study of fatigue behaviors for several different silicate glass fibers in distilled water is presented in another paper [10]. In this paper we will focus on the fatigue behaviors for commercial silica, soda-lime silicate glass and E-glass compositions in humid air. From this we hope to obtain some information on the kinetics of the chemical reaction occurring on the strained surface of glass. We also expect to see some compositional dependence of the fatigue behavior as was seen in the studies of fatigue in water [10].

4.2. EXPERIMENTAL PROCEDURE

Materials used in this study included polymer coated fused silica fibers (AT&T, Amersil TO8 fused natural quartz, 125 μm), a commercial soda lime silicate (SLS) glass (Owens-Illinois, flint container glass) and a commercial calcium aluminoborosilicate glass (PPG, E-glass). The polymer coatings on the silica fibers were removed by immersing the fibers in a mixture of acetone and methanol (lacquer thinner). Fibers were immediately tested after removal of the coating. The soda-lime silicate glass was

remelted in a platinum crucible in air at 1220°C for at least 8 hours prior to fiber drawing. The E-glass was remelted in a platinum crucible in air at 1550°C for at least 8 hours prior to fiber drawing.

The homogeneous melts were transferred to a second furnace set to a fiber pulling temperature (1150°C for the soda-lime silicate glass and 1275°C for the E-glass). Fibers were drawn from the glass melts using a custom-built fiber drawing system. Fibers were drawn onto a rotating cage which was designed to prevent fiber overlap and damage. Fiber diameter was controlled by the fiber pulling temperature and the drawing speed. All fibers were drawn to a diameter of 125 ± 20 μm.

Failure strains of fiber samples were measured using a two-point bending (TPB) technique [37]. In a TPB test, a pristine section of glass fiber, diameter d, is bent into a U-shape between two parallel faceplates, one of which travels towards the second at a constant faceplate velocity (v_{fp}), compressing the 'U' until failure. The gap distance at failure (D) is recorded, and the failure strain (e_f) is then calculated from [38]:

$$\varepsilon_f = \frac{1.198 \times d}{(D - d)} \tag{8}$$

The dynamic fatigue was studied at room temperature (21±2°C) by measuring the failure strains at different faceplate velocities (50, 500, 4000 and 10000 μm/s) and in different relative humdities. The relative humidity was controlled by blowing a mixture of wet and dry air onto the surfaces of the fibers, and was monitored. Dry air was obtained by flowing air through a desiccant column. Wet air was obtained by bubbling air through room temperature distilled water. The temperature and relative humidity was measured using a digital psychrometer (Extech RH305). Twenty fibers were tested at each combination of faceplate velocity and relative humidity. The dynamic fatigue parameter n, which is equivalent to n in equations (1) and (2), was determined from [39]:

$$n = 1 + \frac{1}{d \log \varepsilon_f / d \log v_{fp}} \tag{9}$$

Some fibers were also tested after up to 10 minutes of equilibrium time and no time dependence of failure strain was observed. This is consistent with the observation by Mrotek et al. [22] that no equilibration time is needed because glass samples are in direct contact with moisture.

4.3. RESULTS AND DISCUSSION

The Weibull distributions [40,41] of failure strains for silica, soda-lime silicate glass and E-glass measured at different humidities are shown in Figure 4.1, Figure 4.2 and Figure 4.3, respectively. For all three glasses, failure strains decrease with increasing relative humidity. The humidity dependence of failure strain is plotted in logarithm scales for all three glasses in Figure 4.4.

The Weibull distributions of failure strains for silica measured at a constant humidity but at different faceplate velocities are shown in Figure 4.5. The failure strains increase with increasing faceplate velocity. Table 4.1 lists the average failure strains (± one standard deviation) for all three compositions measured using TPB at the different values of v_{fp}. Also listed are the dynamic fatigue parameters (n) calculated from equation (9) from the slopes of the plots like those shown in Figure 4.6, Figure 4.7 and Figure 4.8.

4.3.1. Dynamic Fatigue. The fatigue parameter for silica measured at room temperature is 22.9±1.7 in 98% RH and 29.2±3.0 in 3.4% RH. The fatigue parameter measured in high humidity compares well with that measured in room temperature distilled water (23.7±1.5, Table 4.1). Table 4.2 summarizes the reported values of fatigue parameter measured in static or dynamic fatigue studies using various techniques. The value we obtained compares favorably with most reported values. By calculating reaction order in a low humidity range using a high humidity (15% to 100% RH) fatigue parameter, Duncan [23] implicitly suggested that the fatigue parameter should be independent of humidity. Our data suggests that this is not necessarily true. Our observation is consistent with Mrotek et al. [22], who reported that the fatigue parameter of silica decreased with increasing humidity (shown in Figure 4.9). This brought up the argument that the power law approach (equation (1)) is deficient in describing fatigue in humid conditions, because it defines A as the environmental constant and n as the materials constant.

The fatigue parameter for E-glass also exhibits a humidity dependence (n=32.3±2.8 in 0.2±0.1% RH vs. n=23.1±1.6 in 43.4±0.2% RH). Both values are greater compared with that measured in room temperature distilled water (16.6±2.8, Table 4.1). There are few reported studies of fatigue for E-glass. A value of 25.8±0.8 was reported for E-glass in 32% RH in a TPB dynamic fatigue study [24]. A value of 20 was reported for E-glass at 20°C and 100% relative humidity from a static fatigue study [42]. Wiederhorn and Bolz [11] reported a value of 27.4 for an aluminosilicate glass (similar to E-glass) in room temperature distilled water from a slow crack growth study.

Room temperature TPB fatigue studies of a calcium aluminosilicate glass (~20% CaO, 20% Al_2O_3, 60% SiO_2, in mole %) and a calcium aluminoborosilicate glass (~20% CaO, 10% Al_2O_3, 10% B_2O_3, 60% SiO_2, in mole %), on the other hand, showed no dependence of n on RH [24]. The fatigue parameter for soda-lime silicate glass also appears independent of humidity (n=16.8±0.2 in 0.7±0.1% RH vs n=16.2±0.4 in 41.8±0.5% RH). The fatigue parameter measure in water was 14.9±2.1, shown in Table 4.1. This is consistent with the findings from a slow crack growth study which showed that the fatigue parameter was also independent of humidity for a soda-lime silicate glass (n=~20 in RH ranging from 0.017%-100%, [12]). Another fatigue study of soda-lime silicate glass indicated that n=16.4 in both 0.2% humidity air and in distilled water [14]. Counterevidence was found in a four-point bend static fatigue study of acid-etched soda-lime silicate glass rods, where n~35±6 in 50% RH vs. n=~30±2 in 100% RH [43], but these values of n are significantly greater than the current study or other studies, raising some uncertainty about the significance of the reported RH dependence.

The environmental fatigue effect is minimized when the strength of glass is measured in dry environments, for example, high vacuum (~10^{-8} Torr) [23]. This implies that the effective fatigue parameter for soda-lime silicate glass should eventually increase at low RH. Actually, the slope of $\log\varepsilon_f$ vs. $\log v_{fp}$ may even decrease to 0 and then to a negative value, considering the inert failure delayed effect (IDFE, [44]). But for some reason, the fatigue reaction for soda-lime silicate was not affected by RH higher than 0.017% [12].

It was discussed in our other paper that depolymerized alkali containing glasses have a different fatigue mechanism than cross-linked glasses, like silica or E-glass [10].

For cross-linked network glasses, the fatigue reaction is mainly the hydrolysis of network bonds [5,8]:

$$\begin{array}{c} | \\ -Si-O- \\ | \end{array} \begin{array}{c} | \\ Si- \\ | \end{array} + H_2O \longrightarrow 2\left[\begin{array}{c} | \\ -Si-OH \\ | \end{array}\right] \qquad (10)$$

The fatigue of depolymerized alkali containing glasses, like soda-lime silicate glass, is initiated by ion-exchange reactions between alkali ions and hydrogen species [8]:

$$\begin{array}{c} | \\ -Si-O^-Na^+ \\ | \end{array} + H_2O \longrightarrow \begin{array}{c} | \\ -Si-OH \\ | \end{array} + Na^+ + OH^- \qquad (11)$$

Depth profile studies of hydrated soda-lime silicate glass showed that three H-atoms replace each Na atom leached from a hydrated glass surface, indicating a Na^+-H_3O^+ exchange mechanism [45, 46]:

$$\begin{array}{c} | \\ -Si-O^-Na^+ \\ | \end{array} + H_3O^+ \longrightarrow \begin{array}{c} | \\ -Si-OH(H_2O) \\ | \end{array} + Na^+ \qquad (12)$$

The ion-exchange reaction occurs faster than the Si-O hydrolysis, so probably the ion exchange kinetics are less affected at low RH, compared to bond hydrolysis.

For soda-lime silicate glass, the fatigue parameter measured in humid air (which is independent of RH) compares well with that measured in water. For silica, the fatigue parameter depends on RH, but the *n* measured in 98% RH compares well with that measured in water. For E-glass, the fatigue parameter also depends on RH, and the *n* measured in 43% RH is greater compared to *n* measured in water (23.1±1.6 vs 16.6±2.8).

4.3.2. Humidity Dependence. Figure 4.4 shows that failure strains decrease with decreasing relative humidity for silica, soda-lime silicate glass and E-glass. The humidity dependence of failure strains is more pronounced in high humidity than in low humidity for all three glasses. Figure 4.10 shows the humidity dependence of failure strains for

silica from the present work and from reported studies. The difference in the absolute values might be due to some experiment uncertainties. For example, Duncan et al. [23] measured polymer coated silica fibers, and Mrotek et al. [22] removed the coatings by hand. But the trend of humidity dependence is consistent. The overall humidity dependence of failure strains appears to be composed of three stages: a strong dependence in the high humidity range (10% to 100%), a small dependence almost like a 'plateau' in the intermediate humidity range (10^{-2}% to 10%), and a medium dependence in the ultra low humidity range (10^{-7}% to 10^{-2}%). Because we were not able to measure failure strains below ~0.1% RH, the three-stage humidity dependence is yet to be confirmed, and we do not intend to deeply discuss the reaction order below ~0.1% RH. But the change in reaction order (humidity dependence) near 10% RH appears to be reproducible. Mrotek et al. [22] attributed the changes in reaction order to the formation of a water monolayer on the glass surface above ~18% RH.

Changes in reaction order are also clear for soda-lime silicate glass and E-glass (shown in Figure 4.4). Such changes were also reported for soda-lime silicate glass in Wiederhorn's slow crack growth study, in which the glass samples were annealed in a chamber with flowing nitrogen gas (RH<0.017%) and tested in the same chamber [12]. It was observed that the reaction order decreased from ~1.3 in the range of 10-100% RH to ~0.5 in the range of 0.017%-1% RH. If the change in reaction order is real, it probably means that more than one reaction is occurring between the water and the glass [12]. Considering the differences between reaction (11) and (12), the two different ion-exchanging water species should depend on the equilibration of the following reaction:

$$2H_2O \longrightarrow H_3O^+ + OH^- \tag{13}$$

In the high humidity environments, the condensed liquid water allows reaction (13) to occur; hence the hydronium is the dominant ion-exchange species. Combining reaction (12) with (13) gives:

$$\begin{array}{c} | \\ -Si-O^{-}Na^{+} \\ | \end{array} + 2H_2O \longrightarrow \begin{array}{c} | \\ -Si-OH(H_2O) \\ | \end{array} + Na^{+} + OH^{-} \qquad (14)$$

In the low humidity environments, there might not be a complete monolayer of water, so reaction (13) is not allowed and reaction (11) is the dominant fatigue reaction (14). Thus, in high humidity, two water molecules are associated with bond hydrolysis, whereas only one water molecule is able to break a bond in low humidity. Additional experiments similar to the depth profile studies [45,46] need to be done to confirm this speculation.

In the high humidity range (RH≥10%), the humidity dependence of failure strains can be fit to straight lines using equation (5). Table 4.3 summarizes the slope (a) of these lines and the reaction order (m) calculated from these slopes and the fatigue parameter (n) measured in the high humidity range. The reaction orders are 2.2±0.3, 1.5±0.2, and 1.7±0.2, for silica, SLS and E-glass, respectively. The reaction order in the high humidity range compares favorably with reported values, including m=~2 for silica [22,23] and m=~1.3 for soda-lime silicate glass [12]. Armstrong et al. [21] suggested that the reaction with water is second order if it is first order with OH^-, and there should be enough OH^- available the at silica surface in the high humidity range. The fatigue reaction mechanism for SLS is more complex than for silica because the ion-exchange reactions (11) and (14) will generate OH^- ions as by-products, causing the local pH to increase, and leading to further attack on Si-O bonds [5]. This is especially true in the case of fatigue in humid conditions because the OH^- will not migrate away from reaction sites as quickly as in liquid water. This might explain qualitatively why the reaction order is lower for SLS than for silica and E-glass.

4.4. SUMMARY

Failure strains as a function of humidity (ranging from ~0.1% to ~100%) were measured for silica, soda-lime silicate and E-glass fibers in room temperature air using the two-point bend technique. Dynamic fatigue behavior was also studied for all three glasses in both low (~0.1-10%) and high (~10-100%) humidity ranges. A humidity dependence of the fatigue parameter for silica and E-glass was observed, whereas the fatigue parameter for soda-lime silicate glasses seems to be independent of humidity, at

least in the range of our test. These observations are consistent with reported fatigue behaviors for both silica and soda-lime silicate glass in humid air. It is suggested that the dominant fatigue reaction for silica is between water and Si-O bonds which greatly relies on the available water, whereas the dominant fatigue reaction for soda-lime silicate glass is an ion-exchange reaction which occurs more rapidly and thus is less affected by the RH within the test range. However, this speculation needs to be confirmed in future studies.

The reaction order for fatigue seems to differ in the low humidity range (0.1% to 10%) and high humidity range (10% to 100%) for all three glasses. In the high humidity range, silica and E-glass have a reaction order around 2, and soda-lime silicate glass has a reaction order around 1.5. These values compare favorably with reported values. The difference in reaction order between cross-linked glasses (silica and E-glass) and depolymerized glasses (soda-lime silicate glass) is attributed to the different fatigue mechanism. For depolymerized glasses, the ion-exchange fatigue reaction forms OH^- ions which can further react with Si-O bonds. Thus the same number of water molecules can break more bonds in depolymerized glasses than in cross-linked glasses. The actual fatigue mechanism is likely to be consisted of different reactions occurring simultaneously and thus is expected to be more complex.

ACKNOWLEDGMENT

We gratefully acknowledge the NSF/I/U CRC Center for Glass Research (CGR) for funding this research. We also wish to thank PPG, Inc. and Owens-Illinois Inc. for providing glass samples. Thanks are also due to Nate Lower for building the two-point bender and the fiber drawing system used in this research.

REFERENCES

[1] L. Grenet, 'Mechanical Strength of glass,' *Bull. Soc. Enc. Industr. Nat. Paris, (Ser. 5)*, 4 838-48 (1899).

[2] T. C. Baker and F. W. Preston, 'Wide Range Static Strength Testing Apparatus for Glass Rods,' *J. Appl. Phys.*, 17 [3] 162-9 (1946).

[3] T. C. Baker and F. W. Preston, 'Fatigue of Glass under Static Loads,' *J. Appl. Phys.*, 17 [3] 170-8 (1946).

[4] T. C. Baker and F. W. Preston, 'The Effect of Water on the Strength of Glass,' *J. Appl. Phys.*, 17 [3] 179-88 (1946).

[5] R. J. Charles, 'Static Fatigue of Glass. I,' *J. Appl. Phys.*, 29 [11] 1549-53 (1958).

[6] R. J. Charles, 'Static Fatigue of Glass. II,' *J. Appl. Phys.*, 29 [11] 1554-60 (1958).

[7] R. J. Charles, 'Dynamic Fatigue of Glass. II,' *J. Appl. Phys.*, 29 [12] 1657-62 (1958).

[8] B. C. Bunker, 'Molecular Mechanisms for Corrosion of Silica and Silicate Glasses,' *J. Non-Cryst. Solids*, 179 300-8 (1994).

[9] R. H. Doremus, 'Interdiffusion of Hydrogen and Alkali Ions in A Glass Surface,' *J. Non-Cryst. Solids*, 19 137-44 (1975).

[10] Z. Tang, C. R. Kurkjian, and Richard K. Brow, 'Two-Point Bend Studies of Fatigue Effects in Silicate Glasses,' to be submitted to *J. Non-Cryst. Solids*, Nov 2011.

[11] S. M. Wiederhorn, L. H. Bolz, 'Stress corrosion and Static Fatigue of Glass,' *J. Am. Ceram. Soc.*, 53 [10] 543-9 (1970).

[12] S. M. Wiederhorn, 'Influence of Water Vapor on Crack Propagation in Soda-Lime Glass,' *J. Am. Ceram. Soc.*, 50 [8] 407-14 (1967).

[13] W. Griffeon, 'Evaluation of Optical Fiber Lifetime Models Based on the Power Law,' *Opt. Eng.*, 33 488-97 (1994).

[14] A. G. Evans, 'Slow Crack Growth in Brittle Materials under Dynamic Loading Conditions,' *Int. J. Fracture*, 10 [2] 251-9 (1974).

[15] G. G. Trantina, 'Strength and Life Prediction for Hot-Pressed Silicon Nitride,' *J. Am. Ceram. Soc.*, 62 [7-8] 377-80 (1979).

[16] B. A. Proctor, I. Whitney, and J. W. Johnson, 'Strength of Fused Silica,' *Proc. Roy Soc. A*, 297 [1451] 534-57 (1967).

[17] S. L. Semjonov, G. S. Glaesemann, D. A. Clark and M. M. Bubnov, 'Fatigue Behavior of Silica Fibers with Different Defects,' *Proc. SPIE*, 4215 28-35 (2001).

[18] J. E. Ritter, Jr., J. M. Sullivan, Jr., and K. Jakus, 'Application of Fracture-Mechanics Theory to Fatigue Failure of Optical Glass Fibers,' *J. Appl. Phys.*, 49 [9] 4779-82 (1978).

[19] D. Kalish and B. K. Tariyal, 'Static and Dynamic Fatigue of a Polymer-Coated Fused Silica Optical Fiber,' *J. Am. Ceram. Soc.*, 61 [11-12] 518-23 (1978).

[20] F. A. Donaghy and D. R. Nicol, 'Evaluation of the Fatigue Constant n in Optical Fibers with Surface Particle Damage,' *J. Am. Ceram. Soc.*, 66 [8] 601-4 (1983).

[21] J. L. Armstrong, M. J. Matthewson, C. R. Kurkjian, 'Humidity Dependence of the Fatigue of High-Strength Fused Silica Optical Fibers,' *J. Am. Ceram. Soc.*, 83 [12] 3100-8 (2000).

[22] J. L. Mrotek, M.J. Matthewson, and C.R. Kurkjian, 'The Fatigue of High-Strength Fused Silica Optical Fibers in Low Humidity,' *J. Non-Cryst. Solids*, 297 91-5 (2002).

[23] W. J. Duncan, P. W. France and S. P. Graig, 'The Effect of Environment on the Strength of Optical Fiber,' in: C. R. Kurkjian (Ed.), *Strength of Inorganic Glass*, Plenum, 1985, p. 309-28.

[24] N. P. Lower, Ph D. Thesis, 'Failure Study of Glass Fibers,' Missouri University of Science and Technology, 2004.

[25] R. E. Mould and R. D. Southwick, 'Strength and Static Fatigue of Abraded Glass Under Controlled Ambient Conditions: I, General Concepts and Apparatus,' *J. Am. Ceram. Soc.*, 42 [11] 542-7 (1959).

[26] J. E. Ritter, Jr. and C. L. Sherburne, 'Dynamic and Static Fatigue of Silicate Glasses,' *J. Am. Ceram. Soc.*, 54 [12] 601-5 (1986).

[27] J. E. Ritter, Jr. and R. P. LaPorte, 'Effect of Test Environment on Stress-Corrosion Susceptibility of Glass,' *J. Am. Ceram. Soc.*, 58 [7-8] 265-7 (1975).

[28] M. H. Krohn, J. R. Hellmann, D. L. Shelleman, C. G. Pantano, and G. E. Sakoske, 'Biaxial Flexure Strength and Dynamic Fatigue of Soda-Lime-Silica Float Glass,' *J. Am. Ceram. Soc.*, 85 [7] 1777-82 (2002).

[29] G. S. Glaesemann, 'The Mechanical Behavior of Large Flaws in Optical Fiber and Their Role in Reliability Predictions,' Corning, Inc. Available from internet:<http://www.new.corning.com/assets/0/433/573/625/631/F6439231-19C5-445B-947C-D5D5CB64951E.pdf>, sited: Jun 29, 2011

[30] R. D. Maurer, 'Behavior of Flaws in Fused Silica Fibers,' in: C. R. Kurkjian (Ed.), *Strength of Inorganic Glass*, Plenum, 1985, p. 291-308.

[31] C. R. Kurkjian, J. T. Krause and U. C. Paek, 'Tensile Strength Characteristics of "Perfect" Silica Fibers,' *J. de. Physque*, C9-585-586 (1982).

[32] T. P. Dabbs and B. R. Lawn, 'Strength and Fatigue Properties of Optical Glass Fibers Containing Microindentation Flaws,' *J. Am. Ceram. Soc.*, 68 [11] 563-9 (1985).

[33] F. Celarie, M. Ciccotti, C. Marliere, 'Stress-Enhanced Ion Diffusion at the Vicinity of a Crack Tip as Evidenced by Atomic Force Microscopy in Silicate Glasses,' *J. Non-Cryst. Solids*, 353 [1] 51-68 (2007).

[34] S. Glasstone, K. J. Laidler, and H. Eyring, *The Theory of Rate Processes*, McGraw-Hill Book Co., New York, 1941, p. 369.

[35] S. W. Freiman, S. M Wiederhorn, and J. J. Mecholsky, Jr., 'Environmentally Enhanced Fracture of Glass: A Historical Perspective,' *J. Am. Ceram. Soc.*, 92 [7] 1371-82 (2009).

[36] P. W. France, M. J. Paradine, and K. J. Beales, 'Ultimate Strengths of Glasses Used for Optical Communication,' *Proc. Int. Congr. Glass*, 12th, 1980.

[37] P. W. France, M. J. Paradine, M. H. Reeve, and G. R. Newns, 'Liquid Nitrogen Strengths of Coated Optical Glass Fibers,' *J. Mater. Sci.*, 15 [4] 825-830 (1980).

[38] M. J. Matthewson, C. R. Kurkjian, and S. T. Gulati, 'Strength Measurement of Optical Fibers by Bending,' *J. Am. Ceram. Soc.*, 69 [11] 815-21 (1986).

[39] V. V. Rondinella, and M. J. Matthewson, 'Effect of Loading Mode and Coating on Dynamic Fatigue of Optical Fiber in Two-Point Bending,' *J. Am. Ceram. Soc.*, 76 [1] 139-44 (1993).

[40] W. Weibull, 'A Statistical Theory of the Strength of Materials,' *Eng. Res. Proc.* 151 1-45 (1939).

[41] W. Weibull, 'A Statistical Distribution of Wide Applicability,' *J. Appl. Mechan.*, 18 293-7 (1951).

[42] G. K. Schmitz and A. G. Metcalfe, 'Stress Corrosion of E-glass Fibers,' *Ind. Eng. Chem. Prod. Res. Dev.*, 5 (1) 1-8 (1966).

[43] J. E. Ritter, Jr. and C. L. Sherburne, 'Dynamic and Static Fatigue of Silicate Glasses,' *J. Am. Ceram. Soc.*, 54 [12] 601-5 (1986).

[44] N. P. Lower, R. K. Brow and C. R. Kurkjian, 'Inert Failure Strain Studies of Sodium Silicate Glass Fibers,' *J. Non-Cryst. Solids*, 349 168-172 (2004).

[45] W. A. Lanford, K. Davis, P. Lamarche, T. Laursen, and R. Groleau, 'Hydration of Soda-Lime Glass,' *J. Non-Cryst. Solids*, 33 249-66 (1979).

[46] T. Fett, J. P. Guin and S. M. Wiederhorn, 'Stress in Ion-Exchange Layers of Soda-Lime-Silicate Glass,' *Fatigue Fract. Engng. Mater. Struct.*, 28 [6] 507-14 (2005).

Table 4.1. Failure strain (ε_f) measured at different faceplate velocities (v_{fp}) in air at 21°C and the corresponding fatigue parameter (n) for silica, soda-lime silicate glass (SLS) and E-glass; the fatigue parameter for the same glasses measured in room temperature distilled water [10] are shown for comparison.

	ε_f (%) in 21˚C humid air				n
v_{fp} (μm/s) =	50	500	4000	10000	
Silica (RH 3.4±0.1%)	7.77±0.14	8.61±0.13	9.14±0.18	9.44±0.10	29.2±3.0
Silica (RH 98±2%)	5.84±0.09	6.58±0.13	7.11±0.09	7.49±0.12	22.9±1.7
Silica (RT distilled water) [10]					23.7±1.5
SLS (RH 0.7±0.1%)	5.77±0.11	6.67±0.15	7.59±0.12	8.10±0.35	16.8±0.2
SLS (RH 41.8±0.5%)	4.80±0.12	5.53±0.08	6.42±0.12	6.76±0.17	16.2±0.4
SLS (RH 92±2%)	4.43±0.06	5.07±0.10	5.80±0.15	6.21±0.07	16.7±0.8
SLS (RT distilled water) [10]					14.9±2.1
E-glass (RH 0.2±0.1%)	6.11±0.09	6.64±0.07	6.98±0.12	7.27±0.06	32.3±2.8
E-glass (RH 43.4±0.2%)	4.96±0.07	5.49±0.06	6.10±0.07	6.23±0.10	23.1±1.6
E-glass (RH 97±2%)	4.45±0.08	4.94±0.08	5.49±0.07	5.84±0.7	20.4±1.4
E-glass (RT distilled water) [10]					16.6±2.8

Table 4.2. A summary of dynamic and static fatigue parameters (n) for silica measured in room temperature humid air using two-point bending (TPB) test, tension test and four-point bending (4PB) test.

Sample Form	Technique	RH	n (dynamic)	n (static)	Ref.
Pristine Fibers	TPB	3.4%	29.2±3.0		Present
Pristine Fibers	TPB	98%	22.9±1.7		Present
Pristine Fibers	TPB	50%	25		[23]
Pristine Fibers	TPB	50%	30.4±1.0		[24]
Pristine Fibers	TPB	0.02%	31±1		[22]
Pristine Fibers	TPB	20%	26±2		[22]
Pristine Fibers	TPB	95%	21±2		[21]
Pristine Fibers	Tension	Not Spec.		19.5	[16]
Pristine Fibers	Tension	50%	20		[17]
Abraded Fibers	Tension	50%	27		[17]
Indented Fibers	Tension	50%	31		[17]
Pristine Fibers	Tension	55%	18.5-22.2		[18]
Pristine Fibers	Tension	97%	15.9	14.3	[19]
Pristine Fibers	Tension	50%	22.1±0.7	19.8±0.8	[20]
Abraded Rods	4PB	Wetted	37.8		[26]

Table 4.3. The fatigue parameter (n) in 90-100% RH, the humidity dependence parameter (a), and the reaction order (m) calculated from equation (5) for silica, soda-lime silicate glass and E-glass in RH≥10%.

	n	a	m
Silica	22.9±1.7	-0.099±0.009	2.2±0.3
SLS	16.7±0.8	-0.095±0.010	1.5±0.2
E-glass	20.4±1.4	-0.090±0.009	1.7±0.2

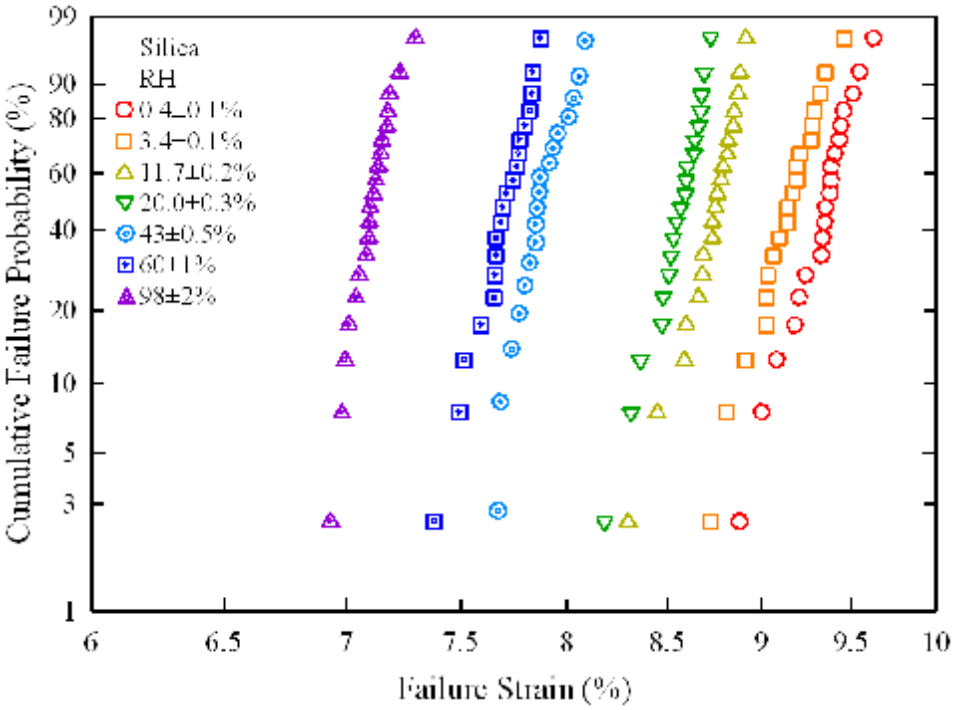

Figure 4.1. Weibull distributions of failure strains for silica measured at room temperature and at different relative humidities, using a faceplate velocity of 4000 μm/s.

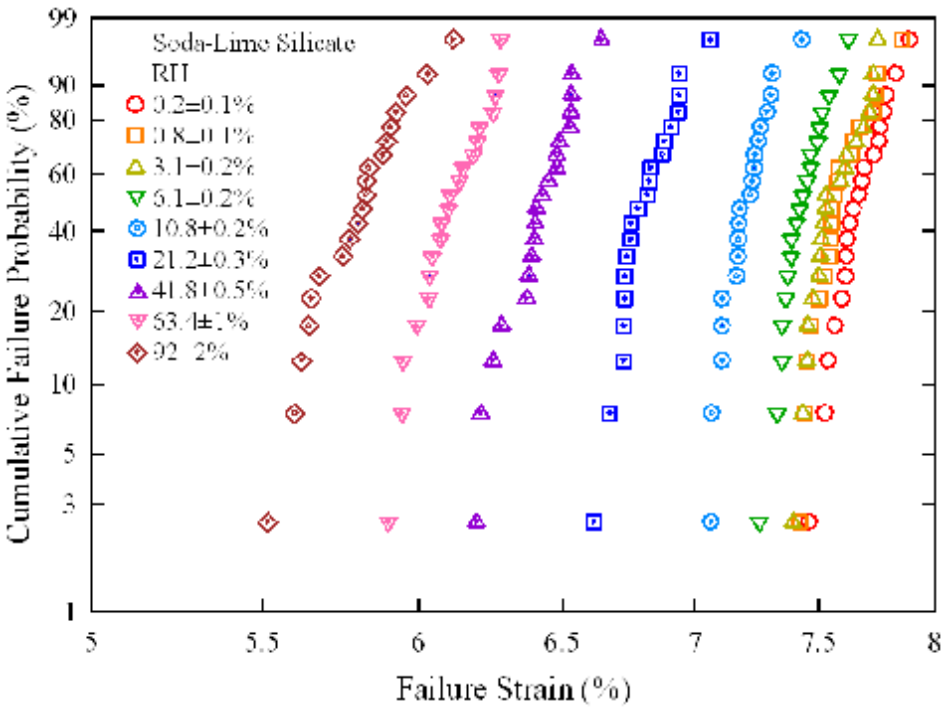

Figure 4.2. Weibull distributions of failure strains for soda-lime silicate glass measured at room temperature and at different relative humidities, using a faceplate velocity of 4000 μm/s.

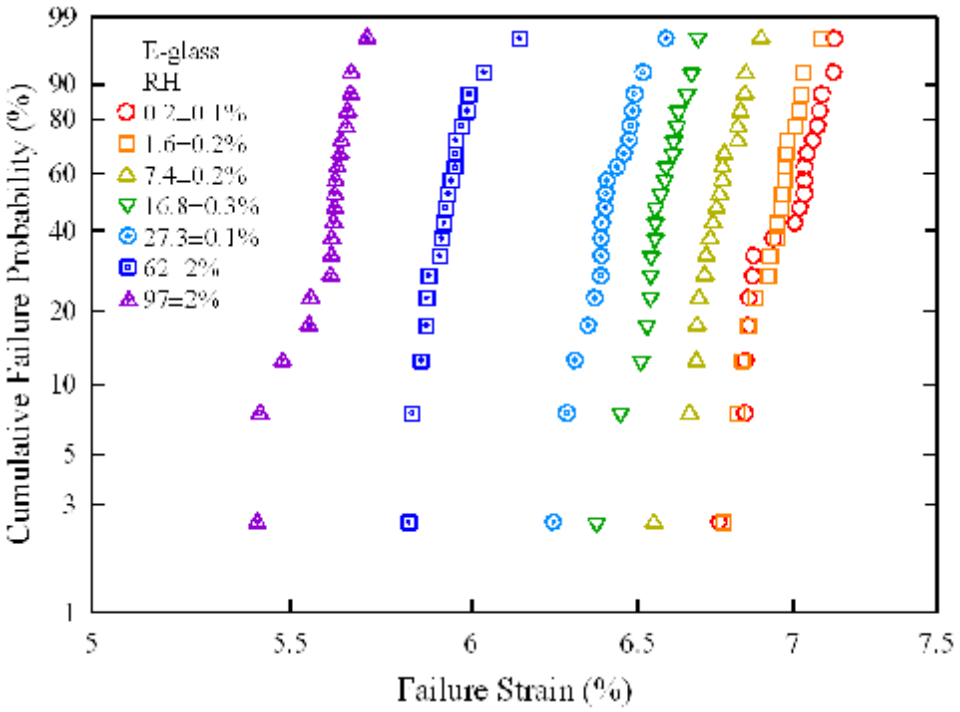

Figure 4.3. Weibull distributions of failure strains for E-glass measured at room temperature and at different relative humidities, using a faceplate velocity of 4000 μm/s.

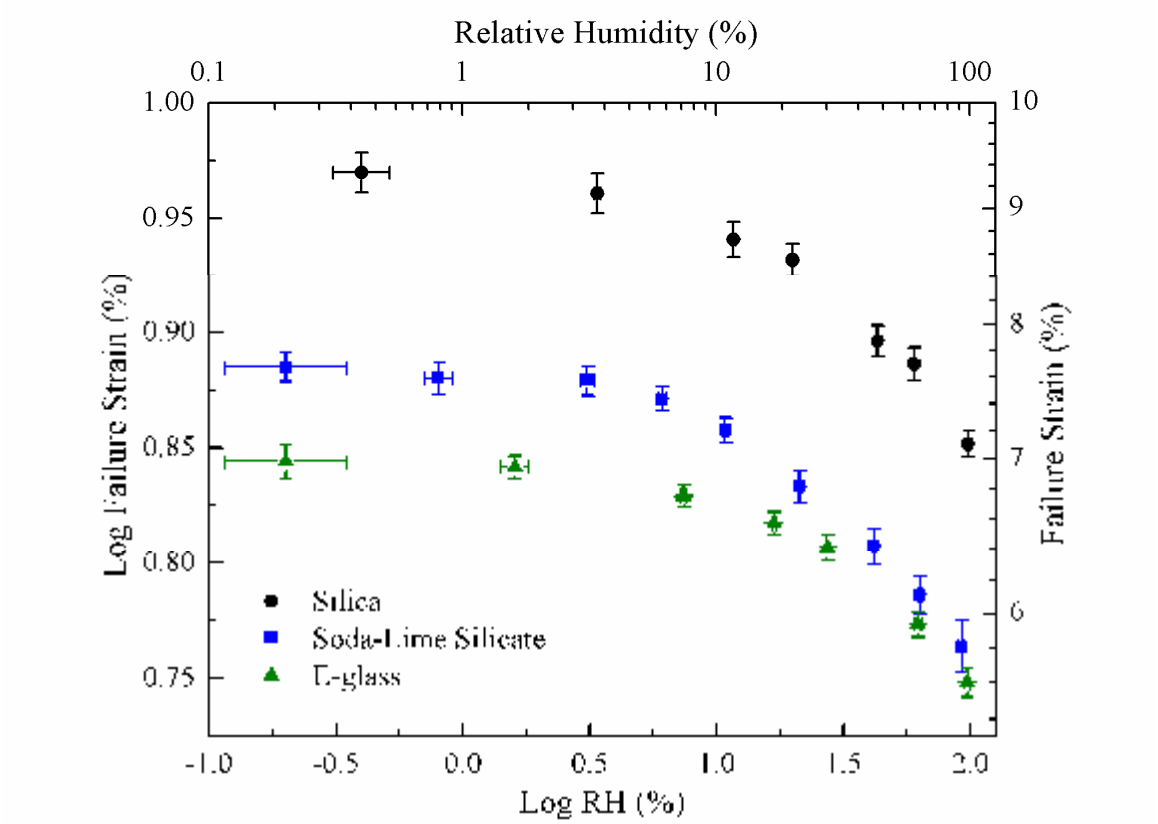

Figure 4.4. Humidity dependence of failure strains for silica, soda-lime silicate glass and E-glass, measured at room temperature

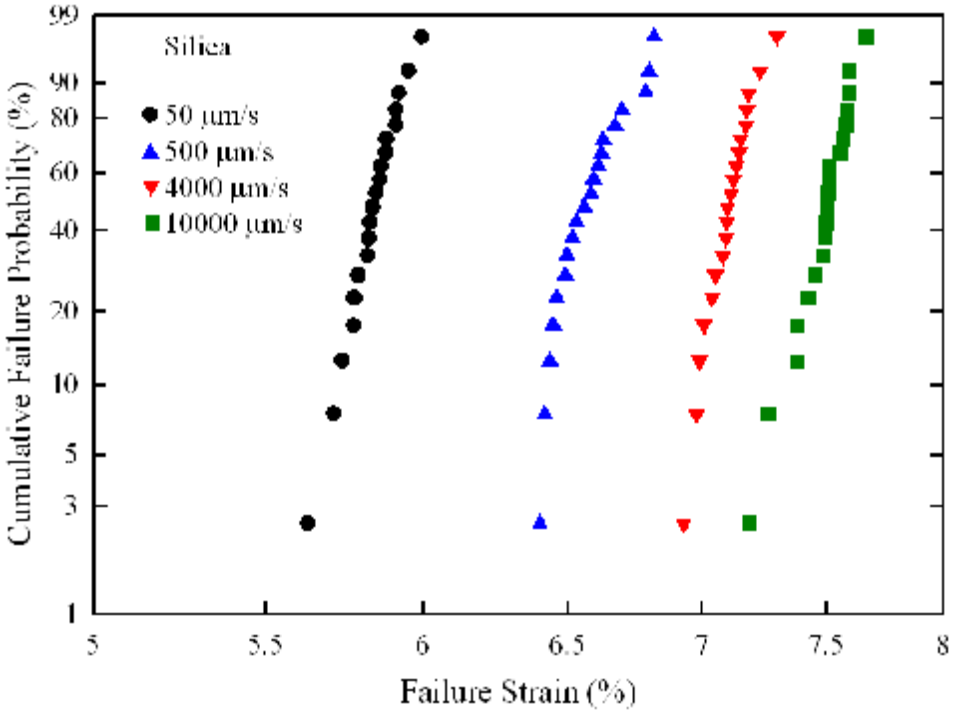

Figure 4.5. Weibull distributions of failure strains for silica measured at room temperature at 43±0.5% RH, using different faceplate velocities.

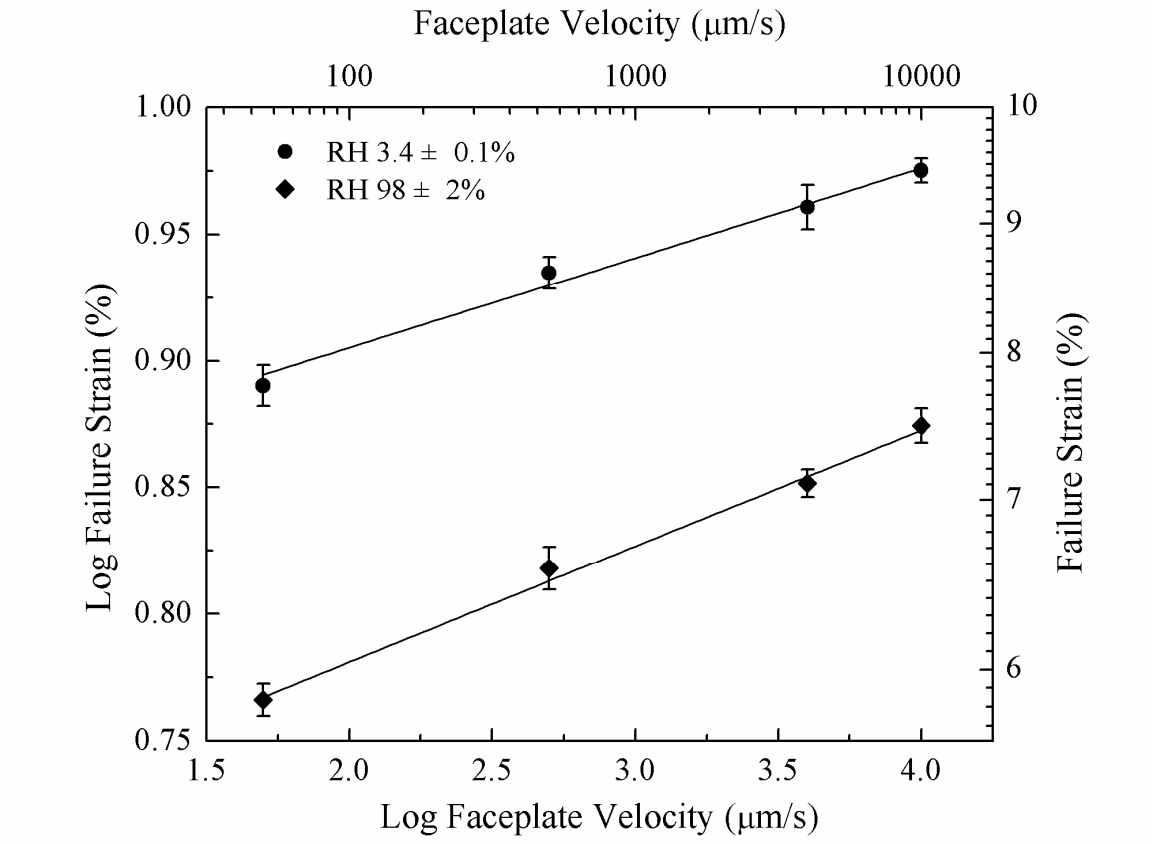

Figure 4.6. Dynamic fatigue for silica measured at room temperature and at different relative humidities.

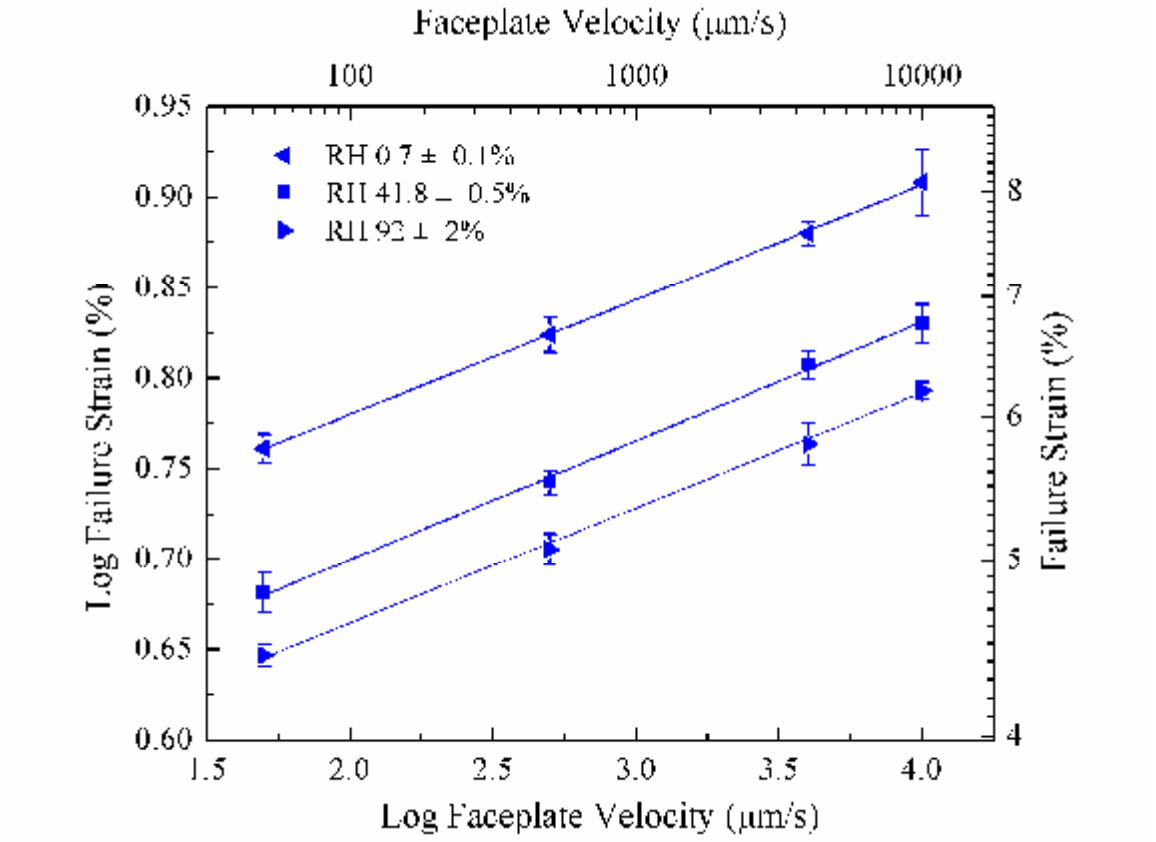

Figure 4.7. Dynamic fatigue for soda-lime silicate glass measured at room temperature and at different relative humidities.

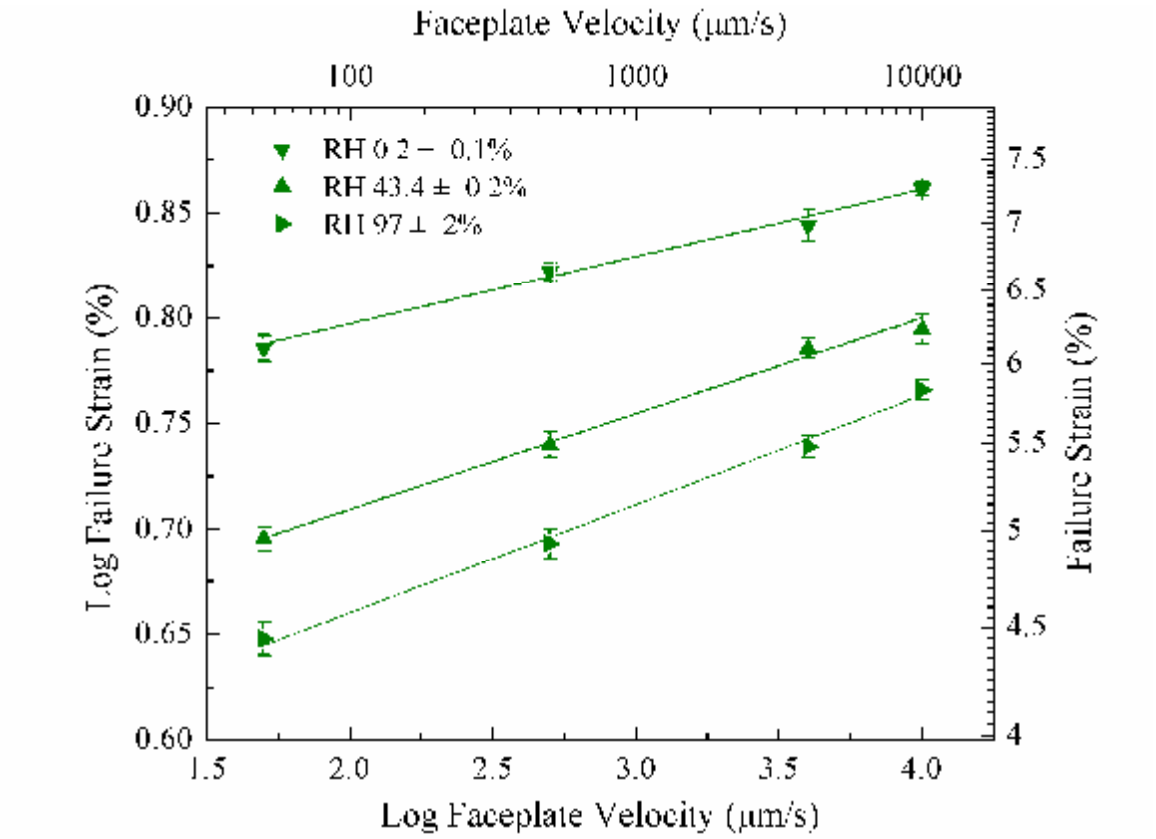

Figure 4.8. Dynamic fatigue for E-glass measured at room temperature and at different relative humidities.

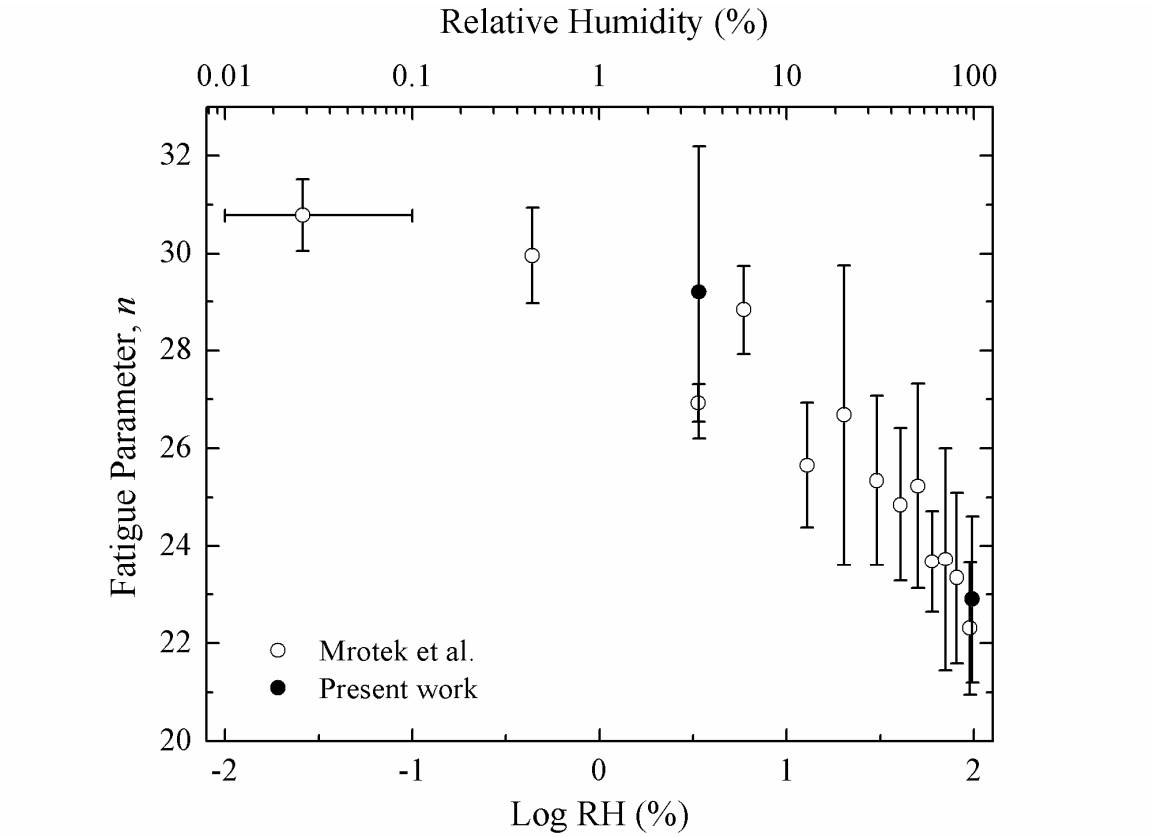

Figure 4.9. Fatigue parameter for silica measured at room temperature and at different relative humidities, data from present work and from Mrotek et al. [22].

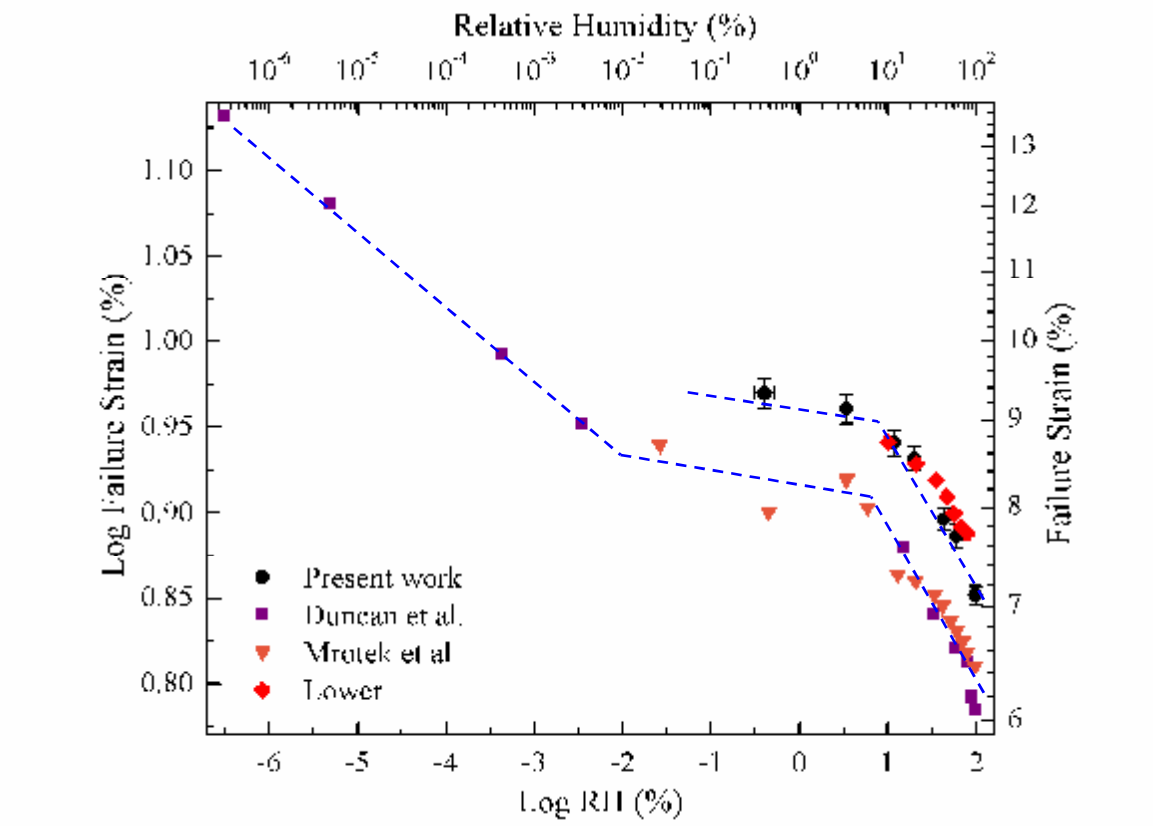

Figure 4.10. Room temperature humidity dependence of failure strains for silica from the present work, and from Duncan et al. [23], Mrotek et al. [22] and Lower [24].

2. SUMMARY AND AFTERWORDS

The failure characteristics of glass are of great interest in both science and technology. This dissertation includes several different aspects of this topic. This chapter serves as a summary of the previous chapters, mixed with some suggestions for future work.

The development of high strength glasses and their applications are an important component to meet the need of today's progressing industry. There are several critical aspects in determining the useful strength of glass: 1. the ultimate strength of glass, which is determined by the bond strength and the glass structure; 2. the presence of flaws or heterogeneities, in the structure, i.e. variation in bond strength, interstice size, ring size, etc; 3. the presence of surface flaws, and 4. the fatigue effect. The first two aspects can be categorized into the intrinsic properties and the last two aspects are extrinsic effects. The two categories are to be discussed in the following texts.

2.1. INTRINSIC ASPECTS OF GLASS STRENGTH

2.1.1. Elastic Deformation of Glasses. As was described in Paper 1, the inert intrinsic failure strains measured by the two-point bend technique represent one approach to measure the ultimate strength of glass, and thus are related to the atomic structure and bond strength of glass. It was shown in Paper 1 that the inert strength of silica glass can be as high as ~12 GPa (failure stress), which is the greatest among the glasses studied, including E-glass, soda-lime silicate glass, sodium aluminosilicate glass, sodium silicate glass and sodium aluminosilicate glasses. This is attributed to the cross-linked network and high bond strength of silica. However, silica does not exhibit the greatest inert failure strain. The strain-to-stress relationship (elastic modulus) is important in determining the ultimate strength of glass.

Young's modulus is often used to predict the ultimate strength. For example, the ultimate strength of glass is estimated to range from $E/10$ to E/π, where E is Young's modulus, since Young's modulus represents the bond strength [1]. In Paper 2, it was discussed that for sodium silicate glasses, sodium aluminosilicate glasses, and sodium borate glasses, the inert failure strain decreases with increasing Young's modulus. Similar correlations were observed for many other glasses [2]. This indicates that glasses

with greater bond strength exhibits smaller inert failure strains. It is suggested that the elastic modulus increases with increasing connectivity and dimensionality of the glass structure [3]. A cross-linked strong glass that exhibits great ultimate strength will at the same time fail at a small strain. You can't sell the cow and drink the milk. An intuitive reason for this phenomenon would be that the weak structure allows the glass network to deform more prior to failure [4]. However, this explanation merely describes the question but does not actually answer it. It would be interesting to further study the structural changes that occur before and at the crack initiation.

The molecular dynamic (MD) simulation could be a useful tool to study the structural dynamics of a strained fiber [5]. The MD simulation provides the possibility to directly observe the simulated atom movement and bond breaking under tension or compression stress. The energy dissipation mechanism can also be examined. The information of failure process can be compared to the measurement from real materials.

2.1.2. Inert Fatigue and IDFE. The inert fatigue [6] and IDFE (inert delayed failure effect) [7] also strongly depend on the glass structure. It was summarized in Paper 1 that most cross-linked glasses exhibit inert fatigue while depolymerized glasses exhibit IDFE. The inert fatigue is attributed to thermal fluctuations of bond strength under high stress [6], whereas IDFE is possibly due to the reorganization or relaxation of glass structure, perhaps in processes similar to those that account for low-temperature internal friction [8,9]. These speculations need to be confirmed in further research.

It would be interesting to study the inert failure behavior at different temperatures. For example, room temperature high vacuum (~20°C), elevated temperature high vacuum (>100°C), immersion in liquid helium (~4K), liquid nitrogen (~77K), liquid oxygen (~90K) and some appropriate water-insoluble liquid mixed with dry ice (~-79°C). If inert fatigue is due to thermal fluctuations associated with individual bonds, it should be an activated process and change systematically with increasing temperature, following an Arrhenius relationship. If IDFE is due to internal friction, it can be correlated to the inertial friction peaks at different temperatures [8].

In Paper 1, IDFE is correlated with the deformation mechanisms associated with indentation. It will be interesting to study the indentation behavior in inert conditions for

several different glasses that exhibit IDFE to different degrees. Shear flow under indentation possibly accounts for the IDFE behavior.

Another important piece of information that can be studied in indentation experiments is 'brittleness' [10], which was discussed in Paper 2. Compared to the toughness, which describes how easily a crack can grow on the glass surface, the brittleness describes how easily a crack can form on the glass surface, thus can help understanding crack initiation processes.

2.2. EXTRINSIC ASPECTS OF GLASS STRENGTH

The practice strength of glass is lower than the ultimate strength of glass due to flaws and fatigue. Surface damage is minimized by testing freshly-drawn fibers. During the failure strain measurements, extra care was used to avoid any contact on the fiber surface; otherwise the failure strain will be much smaller. The failure strain of glass fibers is found to depend on the surface topology (see Appendix E). The relationship between the flaw size and strength is well established in fracture mechanics [12,11]. Other than surface flaws, there are also 'Griffith's flaws' in the bulk of the glass.

2.2.1. Melt History Effect. The melt history effect is discussed in Appendix C. For some glass fibers, the inert failure strain distribution is tight, showing that the glass is 'homogeneous' in structure; for other glass fibers, prepared from melts with different melt histories, the inert failure strain distribution is broad, showing that there are some heterogeneities serving as 'weak points' or 'Griffith flaws' [12] in the glass bulk or on the glass surface (discussed in Appendix F). To understand the broad failure strain distributions, it is important to study the sources of the heterogeneities and hopefully their sizes, shapes and distribution. The presence of these critical flaws is difficult to detect due to their small size [2]; however, it is possible to grow crystals on the flaws and then they can be detected (see Appendix D).

2.2.2. Environmental Fatigue Effect. The other major enemy of the useful strength of glass is the environmental fatigue effect, which was discussed in Paper 3 and 4. It was found that the fatigue mechanism and the fatigue susceptibility vary with glass compositions and structures. The dominant fatigue reaction for cross-linked silicate glasses is Si-O bond hydrolysis, whereas for alkali modified silicate glasses, the ion-exchange reaction with water species is dominant. The power law model [13,14] is used

to predict the fatigue behavior, including reaction order and fatigue parameter (reaction rate). The fatigue parameter is found to depend on the relative humidity, whereas power law suggests that fatigue parameter should be independent of environment. This suggests that the power law has some deficiency describing the fatigue of freshly-drawn fibers. A further study might be focused on the modeling of the fatigue. The change in fatigue reaction order at around ~10% RH suggests that the fatigue reaction is complex and it is likely that more than one reaction occurs at the strained surface of glass. The fatigue reactions of silica were thoroughly studied by Matthewson's group [15,16,17,18]. It would be interesting to study the fatigue of one of the simple compositions of alkali modified silicate glasses, for example $33\%Na_2O{\cdot}67\%SiO_2$ glass. The understanding of different fatigue mechanism might contribute to help develop glasses with greater useful strength in different environments.

REFERENCES

[1] E. Orowan, 'The Mechanical Strength Properties and the Real Structure of Crystals,' ***Z. Krist.***, A89 327-43 (1934).

[2] N. P. Lower, Ph D. Thesis, 'Failure Study of Glass Fibers,' Missouri University of Science and Technology, 2004.

[3] E. Latif, 'Ultrasonic Study on the Role of Na_2O on the structure of Na_2O-B_2O_3 and Na_2O-B_2O_3-SiO_2 glasses,' ***J. Pure Appl. Ultrason.***, 27 80-91 (2005).

[4] N. P. Lower, R. K. Brow and C. R. Kurkjian, 'Inert Failure Strain Studies of Sodium Aluminosilicate Glass Fibers,' ***J. Non-Cryst. Solids***, 344 [1-2] 17-21 (2004).

[5] L. Adkins, A. Cormack, 'Large-Scale Simulations of Sodium Silicate Glasses,' ***J. Non-Cryst. Solids***, 357 [14] 2538-41 (2011).

[6] C. R. Kurkjian, P. K. Gupta, R. K. Brow, and N. P. Lower, 'The Intrinsic Strength and Fatigue of Oxide Glasses,' ***J. Non-Cryst. Solids***, 316 [1] 114-24 (2003).

[7] N. P. Lower, R. K. Brow and C. R. Kurkjian, 'Inert Failure Strain Studies of Sodium Silicate Glass Fibers,' ***J. Non-Cryst. Solids***, 349 168-172 (2004).

[8] D. E. Day, and G. E. Rindone, 'Properties of soda aluminosilicate glasses. II. Internal Friction,' ***J. Am. Ceram. Soc.***, 45 496-504 (1962).

[9] J. E. Shelby. Jr., and D. E. Day, 'Mechanical Relaxations in Mixed-Alkali Silicate Glasses: I, Results,' ***J. Am. Ceram. Soc.***, 52 [4] 169-74 (1969).

[10] B. R. Lawn, D. B. Marshall, 'Hardness, Toughness, and Brittleness: an Indentation Analysis,' ***J. Am. Ceram. Soc.***, 62 [7] 347-50 (1979).

[11] C. E. Inglis, 'Stress in a Plate due to the Presence of Cracks and Sharp Corners,' ***Trans. Inst. Naval Archit.***, 55, 219-30 (1913).

[12] A. A. Griffith, 'The Phenomena of Rupture and Flow in Solids,' ***Phil. Trans. Roy. Soc.***, 22 163-198 (1921).

[13] W. Griffeon, 'Evaluation of Optical Fiber Lifetime Models Based on the Power Law,' ***Opt. Eng.***, 33 488-97 (1994).

[14] A. G. Evans, 'Slow Crack Growth in Brittle Materials under Dynamic Loading Conditions,' ***Int. J. Fracture***, 10 251 (1974).

[15] Y. S. Shiue and M. J. Matthewson, 'Stress Dependent Activation Entropy for Dynamic Fatigue of Pristine Silica Optical Fibers,' ***J. Appl. Phys.***, 89 [9] 4787-93 (2001).

[16] V. V. Rondinella and M. J. Matthewson, 'Effect of Loading Mode and Coating on Dynamic Fatigue of Optical Fiber in Two-Point Bending,' ***J. Am. Ceram. Soc.***, 76 [1] 139-44 (1993).

[17] V. V. Rondinella, M. J. Matthewson and C. R. Kurkjian, 'Coating Additives for Improved Mechanical Reliability of Optical Fiber,' ***J. Am. Ceram. Soc.***, 77 [1] 73-80 (1994).

[18] M. J. Matthewson and C. R. Kurkjian, ‘Static Fatigue of Optical Fibers in Bending,’ *J. Am. Ceram. Soc.*, 70 [9] 662-8 (1987).

APPENDIX A
VISCOSITY MEASUREMENTS FOR COMMERCIAL GLASSES

VISCOSITY MEASUREMENTS FOR COMMERCIAL GLASSES

The viscosity-temperature characteristics for glass melts were determined with a standard method described in ASTM C1276-94 and C965-96 using a Haake high temperature viscometer (Model: ME-1700, shown in Figure A.1).

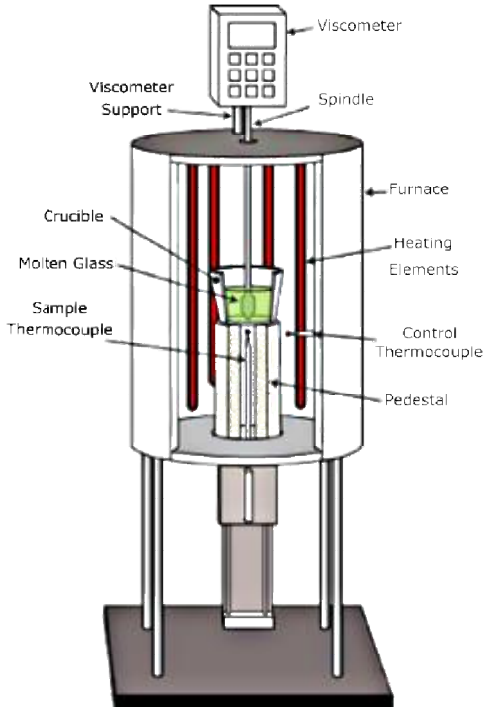

Figure A.1. Schematic diagram of a high temperature viscometer measuring system

The viscometer features a platinum crucible (diameter *R*) and spindle (length *L* and diameter *r*), and viscosity (h) is determined by measuring the torque (T) required to maintain a constant spindle spinning speed (w) as a function of melt temperature (Equation (1)).

$$\eta = \frac{1}{4\pi L}\left(\frac{1}{r^2} - \frac{1}{R^2}\right)\frac{T}{\omega} \quad (1)$$

In a particular experiment, a glass sample is crushed to small pieces and about 50 grams of crushed glass were re-melted in the viscometer platinum crucible in the viscometer at about 1400°C for at least 4 hours to produce bubble free melt. After a homogeneous melt was obtained, the platinum spindle was lowered into the melt and rotated. The rotation speed is adjusted so the corresponding torque is in the detect range of the viscometer. The furnace was cooled to about 1000°C at the rate of 10°C/min, when the torque and the spindle speed were recorded and used to calculate the melt viscosity. Each melt was then re-heated at 10°C/min and the viscosity was again recorded as a function of temperature. The temperature was cycled several times for each melt and an average viscosity-temperature was determined.

This viscometer is calibrated using several different glasses with known viscosity-temperature characteristics, including SRM717a, a standard borosilicate glass provided by NIST, and BK-7, a commercial borosilicate optical glass provided by Schott Glass North America. Figure A.2 shows an excellent agreement between the melt viscosity-temperature curve for BK-7 measured at Missouri S&T and that reported by Schott. Figure A.3 shows similar curves obtained for the SRM717a glass.

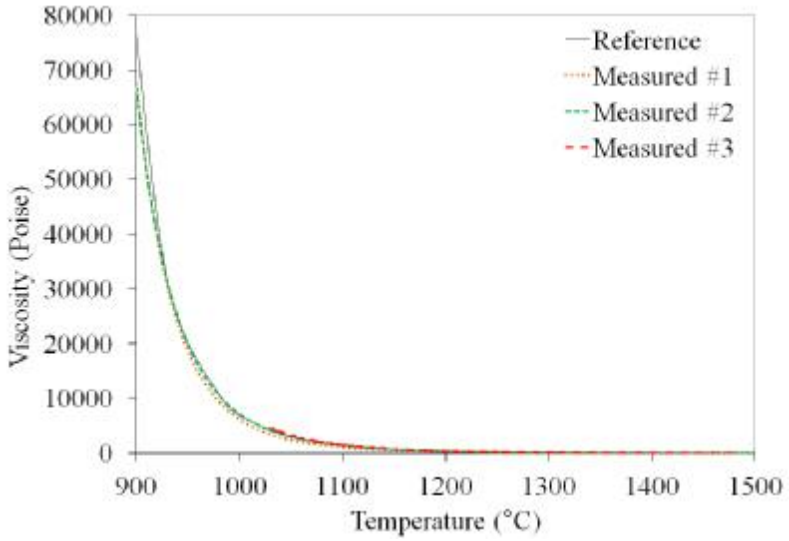

Figure A.2. Viscosity-temperature curves for BK-7 glass, measured at Missouri S&T and reported by Schott Glass North America (reference).

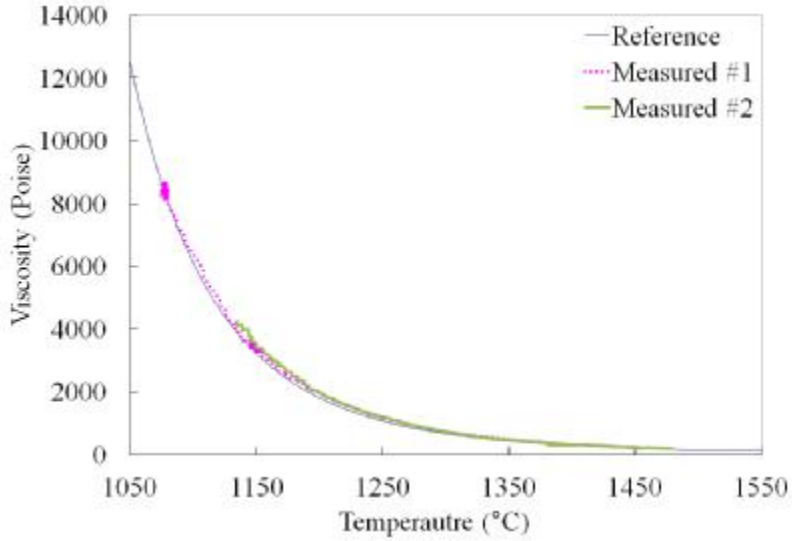

Figure A.3. Viscosity-temperature curves for NIST SRM717a glass, measured at Missouri S&T and reported by NIST.

The viscosity curve provides valuable information for glass manufacturing in industry, and also benefits this research. The isokom temperature of 1000 Poise is referred to as the forming temperature (T_F), due to the ease of manufacturing glass at this temperature. It is also used as the "well-conditioned" melting temperature baseline in the thermal history study.

Figure A.4 to Figure A.7 show the viscosity-temperature curves collected for each of the four OI samples. These curves were fit using the Vogel–Fulcher–Tammann (VFT) equation (Equation (2)):

$$\log \eta = a + \frac{b}{T - c} \tag{2}$$

where a, b and c are VFT fitting parameters. Table A.1 lists the VFT parameters for each respective average data set.

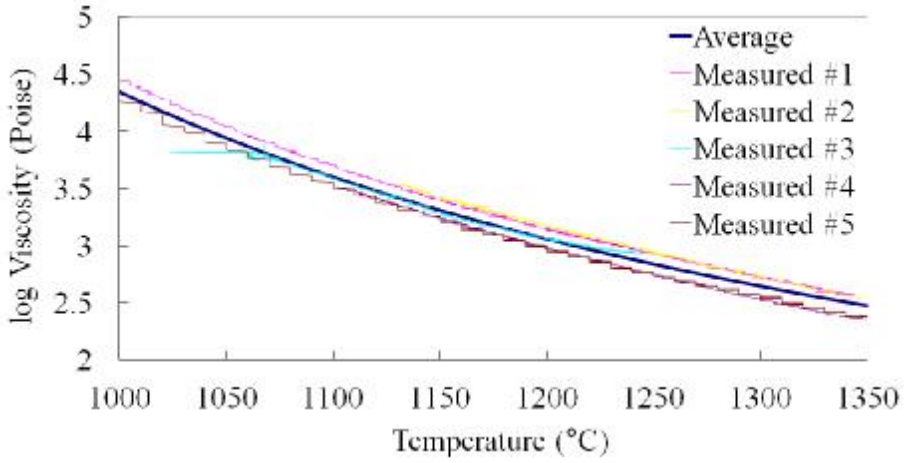

Figure A.4. Viscosity-temperature curve of OI-A clear SLS bottle glass.

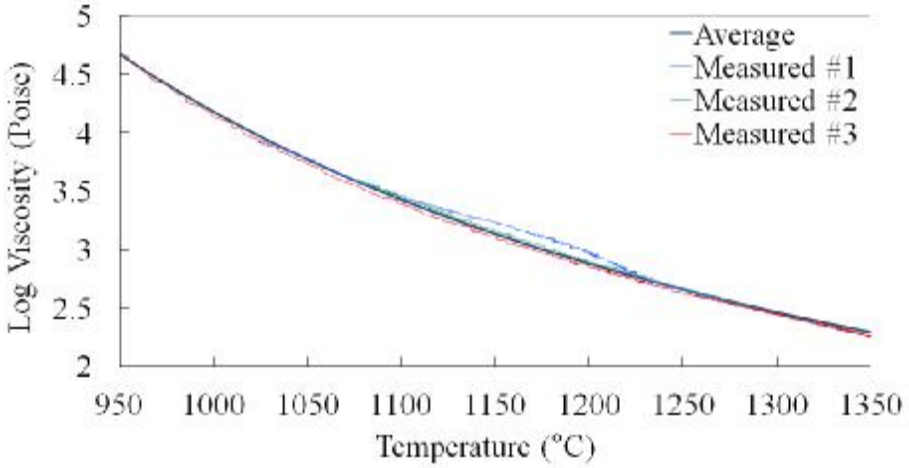

Figure A.5. Viscosity-temperature curve of OI-B emerald green SLS bottle glass.

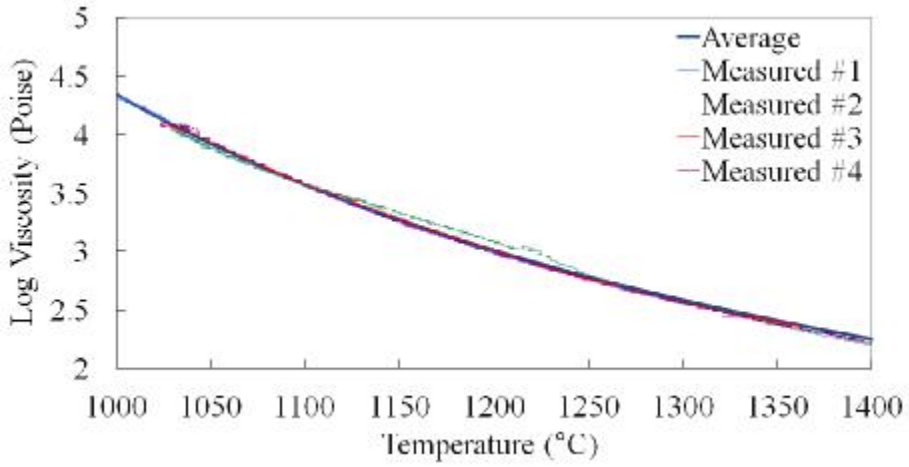

Figure A.6. Viscosity-temperature curve of OI-C amber SLS bottle glass.

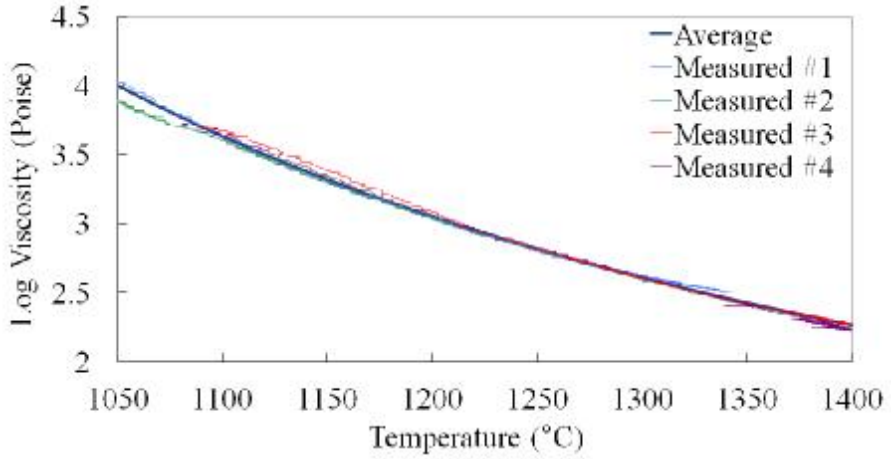

Figure A.7. Viscosity-temperature curves of OI-D dead leaf green SLS bottle glass.

Table A.1. VFT parameters and 1000 P isokom temperatures for four OI SLS bottle glass samples.

Glass Samples provided by Owens-Illinois	VFT parameters			Forming Temperature 10^3 P isokom (°C)
	a	b	c	
OI-A (clear)	-0.41	2549	463	1220 ±19
OI-B (emerald green)	-0.586	2550	465	1175 ± 5
OI-C (amber)	-0.504	2550	474	1202 ± 4
OI-D (dead leaf green)	-0.529	2553	487	1210 ± 5

Figure A.8 to Figure A.11 show the viscosity-temperature curves collected for four of the five PPG samples, except for PPG-E glass, for which the viscosity curve provided by PPG is used. The VFT parameters and the 1000 P isokom temperatures (Forming temperatures) for each sample are listed in Table A.2. The measured values for the Forming temperatures are very close to reported values provided by PPG.

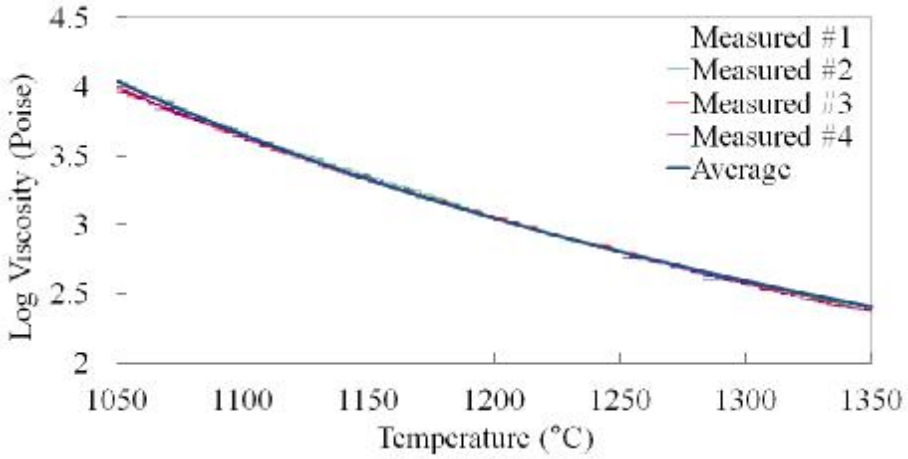

Figure A.8. Viscosity-temperature curve of PPG-C glass.

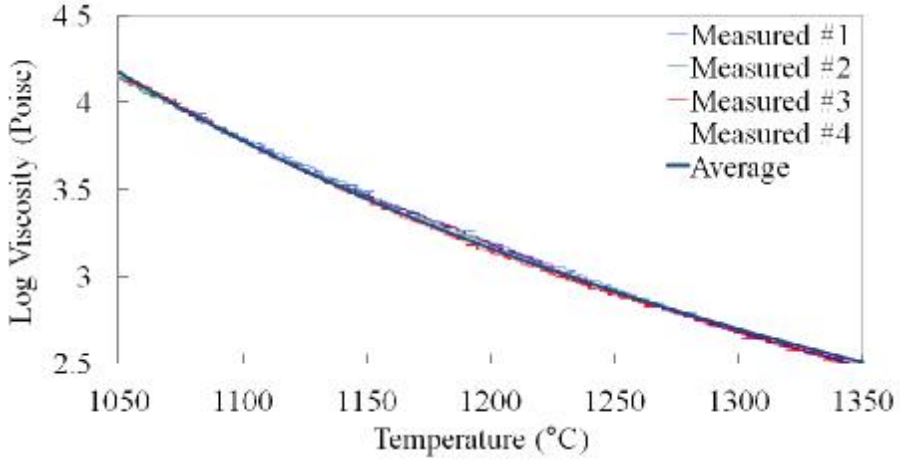

Figure A.9. Viscosity-temperature curve of PPG-P glass.

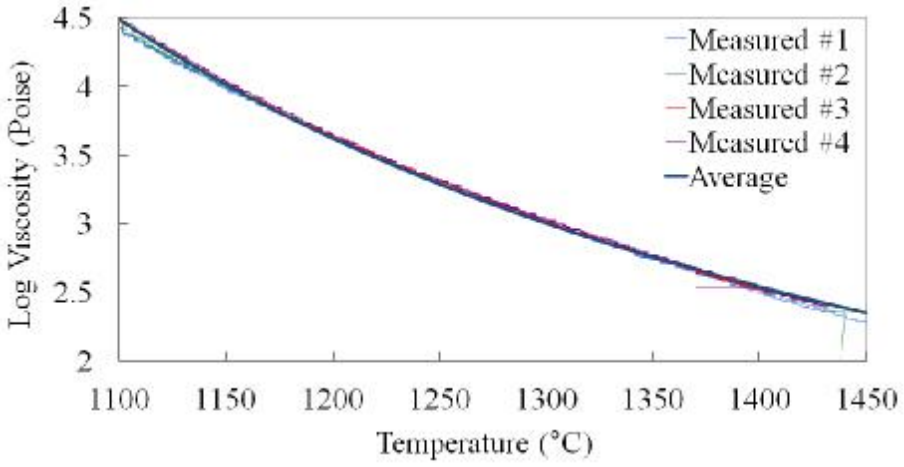

Figure A.10. Viscosity-temperature curve of PPG-D glass.

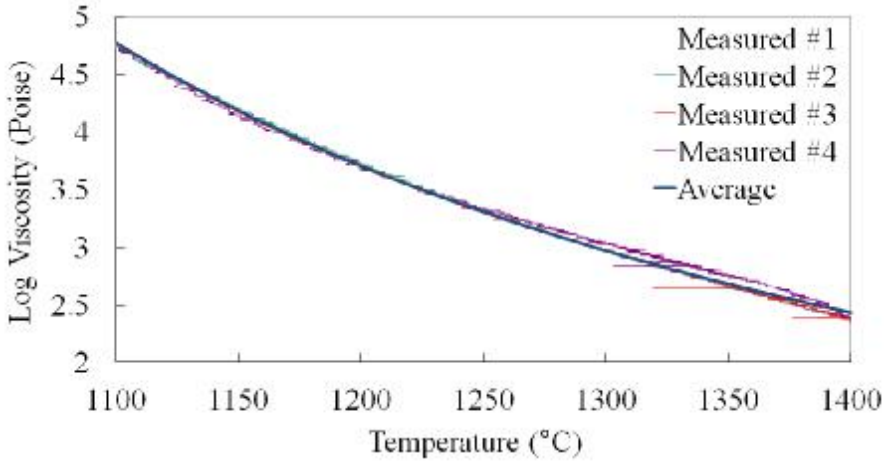

Figure A.11. Viscosity-temperature curve of PPG-H glass.

Table A.2. VFT parameters and 10^3 P isokom temperatures for four PPG glass samples.

Glasses provided by PPG	VFT parameters			Forming Temp.10^3 P isokom (°C)	
	a	b	c	Measured	Reported (PPG)
C-glass	-0.597	2554.2	498.8	1209 ± 3	1217
P-glass	-0.520	2555.3	506.2	1232 ± 6	1223
D-glass	-0.684	2569.2	603.4	1301 ± 3	1288
H-glass	-1.027	2567.1	555.7	1295 ± 8	1293

APPENDIX B

LIQUIDUS TEMPERATURE MEASUREMENTS FOR COMMERCIAL GLASSES

LIQUIDUS TEMPERATURE MEASUREMENTS FOR COMMERCIAL GLASSES

The liquidus temperature (T_L) of a melt is the maximum temperature at which the primary crystalline phase is in equilibrium with the melt. T_L is measured using the gradient furnace technique described in ASTM C829-81. In a particular experiment, approximately 40 grams of glass powder was spread evenly onto a ten-inch-long platinum foil boat. The boat was kept in the gradient furnace with a temperature range from ~800 to ~1100°C in air for 24 hours. During this period, the temperature profile of the furnace was recorded at 0.25 inch intervals. After 24 hours, the boat was removed from the furnace and the sample quenched in air to room temperature. The sample was then examined under a light microscope to identify the position of the crystal/melt interface. From the recorded temperature profile, the liquidus temperature was determined. Based on the precision of the position measurement and the uncertainty in the temperature profile, the experimental uncertainty of this measurement is about ±10°C.

Figure B.1 shows a photograph of the platinum strip with a sample of OI-A after 24 hours in the gradient furnace. Superimposed on this photograph is the temperature gradient recorded for this sample. The distinct line between the crystallized portion of the sample and the clear (glassy) portion corresponds to 999 ± 10°C, and this is defined as T_L for this glass.

The liquidus temperatures measured in this study are listed in Table B.1. Also listed are reported values from glass provider. The liquidus temperature of PPG-C glass is 1092°C, compared favorable to reported value of 1095°C. for PPG-P glass the measured value is 1110°C, compared favorable to reported value of 1118°C. The difference is within error of this experiment.

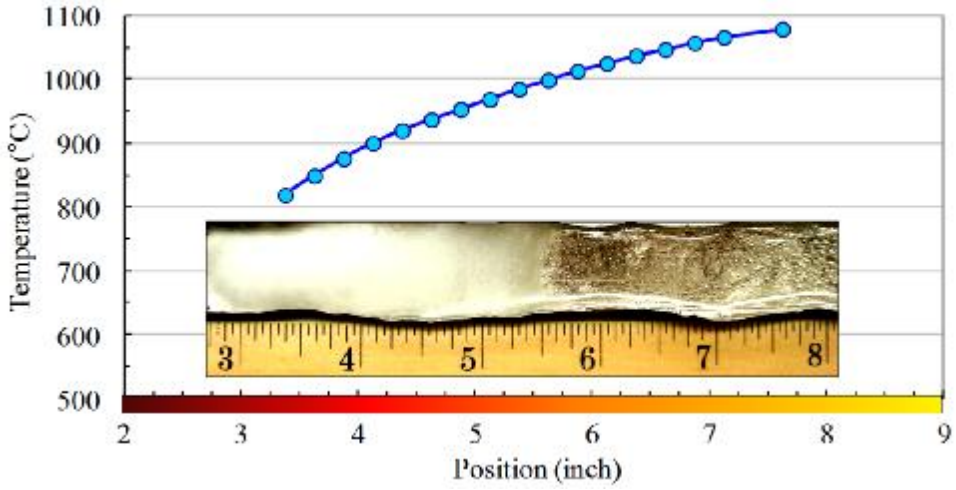

Figure B.1. Liquidus temperature measurement for SLS glass OI-A.

Table B.1. Liquidus Temperatures for OI and PPG glass samples.

Glass Samples	T_L measured (±10°C)	T_L reported by glass provider (°C)
OI-A	999	N/A
OI-B	1005	N/A
OI-C	1018	N/A
OI-D	1050	N/A
PPG-C	1092	1095
PPG-P	1110	1118

APPENDIX C

MELT HISTORY EFFECT ON FAILURE STRAINS FOR COMMERCIAL SODA-LIME SILICATE GLASSES

MELT HISTORY EFFECT ON FAILURE STRAINS FOR COMMERCIAL SODA-LIME SILICATE GLASSES

Strength of glass was considered an extrinsic property for a long time, because extrinsic flaws are the most decisive factors in determining the strength of glass [1]. Measured strength can vary several orders of magnitude according to the surface conditions of the sample [2]. Attempts have been made to measure intrinsic strength of glass by testing 'flaw-free' pristine samples [3]. Some reports of strength measurement have approached the theoretical values of strength by measuring pristine samples in inert conditions [4,5,6], whereas others found that strength distribution of glass can be broad, and that is related to the melt history of the glass[7,8]. Otto [9] measured tensile strength of pristine calcium aluminoborosilicate glass fibers with different diameters and with different forming conditions. He found that the strength of fibers of different diameters were identical within the experimental limits, as long as the forming conditions are nearly identical, and that fibers of same diameter exhibited greater strength when formed at higher temperatures. This indicates that, when the effects of surface flaws are minimized, some other imperfections that are generated during the forming process limit the ultimate strength of glass. Griffith [1] suggested that, other than extrinsic flaws on the surface of the samples, melt preparation and conditioning play an important role in glass strength. Batch purities, melting temperature and forming temperature, etc. have influences on the measured strength of glass.

Lower et al. [10,11] showed that in general, longer melting times and greater melting temperatures ensure greater average failure strain and narrower strain distribution. Nuclear Magnetic Resonance (NMR), Atomic Force Microscopy (AFM) and Scanning Electron Microscopy (SEM) were used to characterize sources of broad failure distribution of the fibers, but no distinct sources for strength-limiting flaws were detected. If the broad strength distributions are due to some heterogeneity from the melt, they are expected to be so small in size (nanometer scale) that they are beyond the delectability of these techniques.

In the present work, failure strains of a commercial soda-lime silicate glass are measured and the melt history effects on the strength distribution are studied.

Commercial flint soda-lime silicate (SLS) clear glass bottles (termed 'OI-A') provided by Owens-Illinois were remelted in platinum crucibles in air. Fibers were drawn from the surface of the melt onto a rotating cage which was designed to prevent fiber overlap and damage. Fiber diameter was monitored by eye and controlled by the fiber pulling temperature and the drawing speed. All fibers are drawn into a diameter of 125 ± 20 μm.

Failure strains of freshly drawn fibers were measured using the two-point bending (TPB) technique [12] with fibers either immersed in liquid nitrogen or tested in air at room temperature (21±2°C) with a relative humidity of 50±2%. The relative humidity is controlled by blowing a mixture of wet and dry air onto the surfaces of the fibers, and is monitored using a digital psychrometer (Extech RH305). The fibers drawn from melts were tested immediately after they were formed. No aging effects were observed.

In a TPB test, a pristine section of glass fiber, diameter d, is bent into a U-shape between two parallel face plates, one of which travels towards the second at a constant faceplate velocity (v_{fp}), compressing the 'U' until failure. The gap distance at failure (D) is recorded, and the failure strain (ε_f) is then calculated from: [13]

$$\varepsilon_f = \frac{1.198 \times d}{(D - d)} \tag{1}$$

OI-A SLS glass bottles were crushed and remelted in platinum crucible in air at 1120°C, 1220°C (1000 Poise isokom temperature) and 1320°C for different lengths of time. Inert failure strains of fibers drawn from each melt with different melt time were measured using TPB technique under liquid nitrogen. For glass melted at 1120°C, failure strains were also measured in room temperature air (21±2°C) with 66±2% relative humidity. The Weibull distributions for these failure strains were shown from Figure C.1 to Figure C.3.

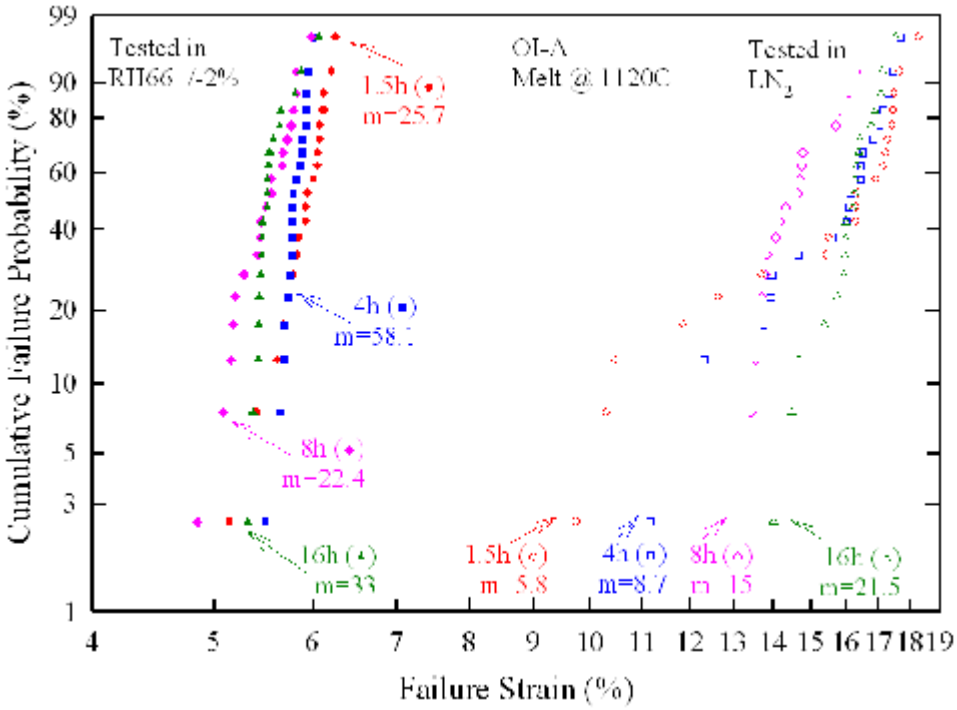

Figure C.1. Failure strain distribution of OI-A SLS glass fibers measured using TPB technique. The glass was melted at 1120°C for different lengths of time prior to fiber pulling. Open data points are measured in liquid nitrogen, solid data points are measured in air at room temperature (21±2°C) with a relative humidity of 66±2%.

From Figure C.1, it can be seen that when melted at 1120°C, the inert failure strain distributions for OI-A glasses tighten as the melting time increases from 1.5 to 16 hours. The failure strains measured in humid air do not show such distinct dependence on melting time dependence.

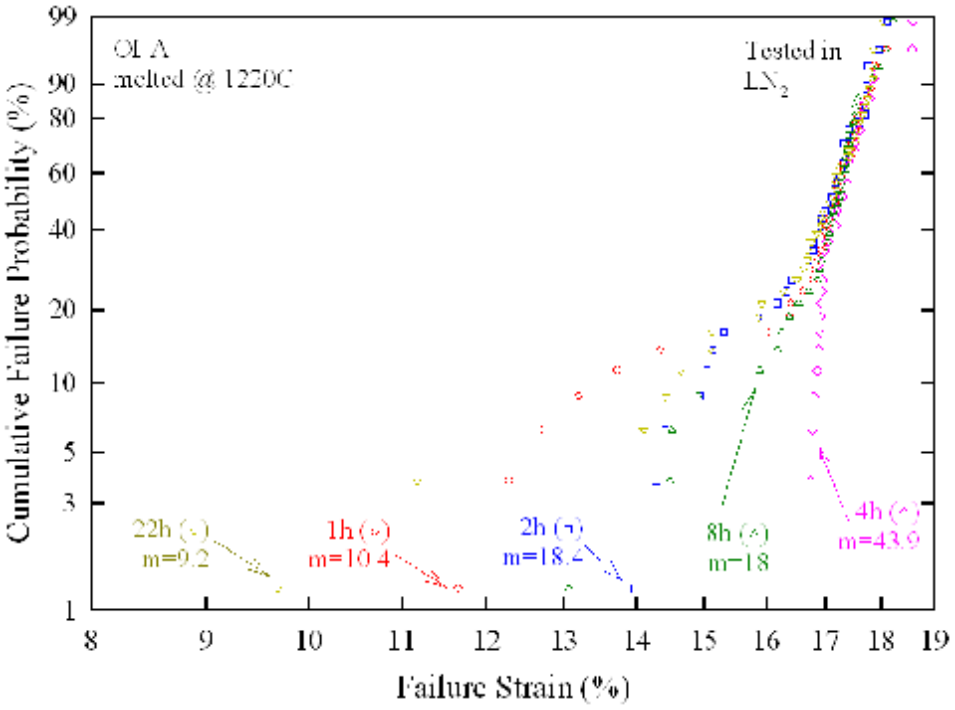

Figure C.2. Inert failure strain distribution of OI-A SLS glass fibers measured in liquid nitrogen using TPB technique. The glass was melted at 1220°C for different length of time prior to fiber pulling.

When melted at 1220°C, the failure strain distribution initially starts to tighten as the melting time increases. The tightest failure strain distribution is from glasses melted for 4 hours at 1120°C, and then the failure strain distribution starts to broaden for longer melting time. The tightest distribution in Figure C.2 is tighter than the tightest distribution in Figure C.1, and it takes shorter time, indicating that melting at 1220°C makes the glass melt reach its homogeneous state faster than melted at 1120°C. But for some reason, this homogeneous state discontinued after longer melting time.

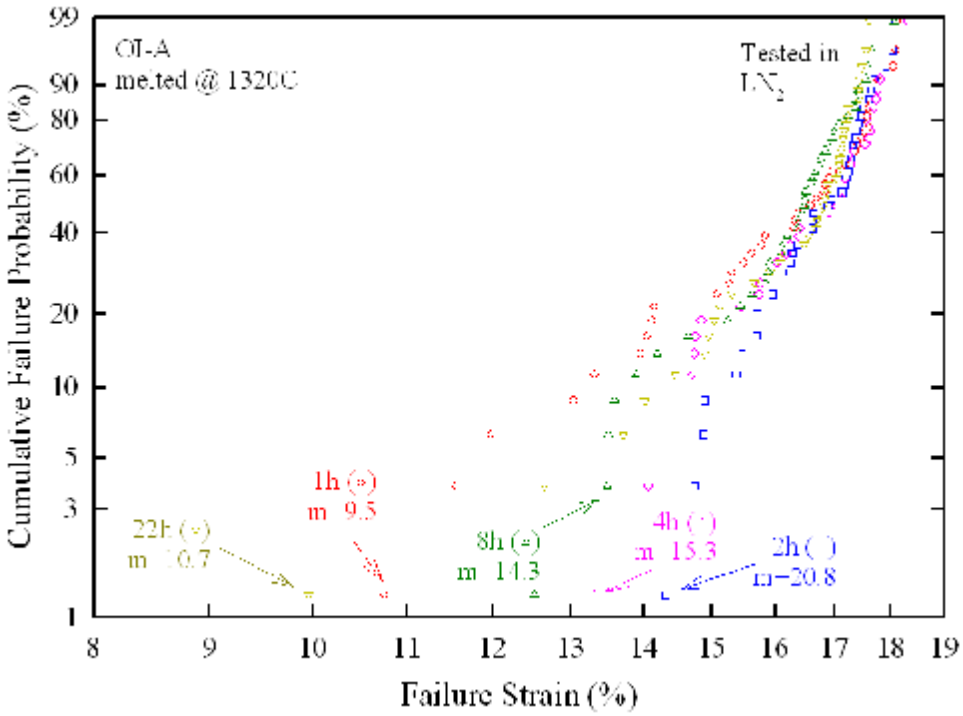

Figure C.3. Inert failure strain distribution of OI-A SLS glass fibers measured in liquid nitrogen using TPB technique. The glass was melted at 1320°C for different lengths of time prior to fiber pulling.

Melting time dependence of inert failure strain distributions for 1320°C melt (Figure C.3) is similar to that for 1220°C melt (Figure C.2). The failure strain distribution tightens at first than broadens after longer time of melting.

A summary of melt history and corresponding failure strains are listed in Table C. to Table C.3, where ε_{max} is the average of 3 maximum failure strain measured for a particular set of fibers, ε_{mid} is the medium failure strain, ε_{min} is the average of 3 minimum failure strain, and m is the Weibull modulus, which is the slope of data in the Weibull plot. The Weibull modulus is a measure of the tightness of a distribution. The tighter the distribution is, the steeper the slope is, and the greater value of m is.

Table C.1. Melt history (1120°C) study on OI-A glass.

Melt History	Pull#, Condition	ε_{max} (%)	ε_{mid} (%)	ε_{min} (%)	m
1120°C 1.5h	P1, RH 66%	6.20	5.94	5.40	25.7
	P1, LN	17.82	16.32	10.18	5.8
1120°C 4h	P2, RH 66%	5.97	5.79	5.61	58.1
	P2, LN	17.48	16.13	11.68	8.7
1120°C 8h	P3, RH 66%	5.88	5.53	5.04	22.4
	P3, LN	16.64	14.50	13.39	15
1120°C 16h	P4, RH 66%	5.91	5.52	5.38	33
	P4, LN	17.24	16.23	14.39	21.5

Table C.2. Melt history (1220°C) study on OI-A glass.

Melt History	Pull#, Condition	ε_{max} (%)	ε_{mid} (%)	ε_{min} (%)	m
1220°C 1h	P1, LN	18.03	17.18	12.22	10.4
1220°C 2h	P2, LN	17.94	17.07	14.22	18.4
1220°C 4h	P3, LN	18.34	17.27	16.69	43.9
1220°C 8h	P4, LN	18.08	17.22	14.02	18
1220°C 22h	P5, LN	17.91	17.11	11.65	9.2

Table C.3. Melt history (1320°C) study on OI-A glass.

Melt History	Pull#, Condition	ε_{max} (%)	ε_{mid} (%)	ε_{min} (%)	m
1320°C 1h	P1, LN	18.08	16.65	11.43	9.5
1320°C 2h	P2, LN	18.02	16.92	14.65	20.8
1320°C 4h	P3, LN	18.23	17.08	13.96	15.3
1320°C 8h	P4, LN	17.77	16.49	13.18	14.3
1320°C 22h	P5, LN	17.54	16.83	12.10	10.7

Figure C.4 plots failure strain and Weibull modulus as a function of melting time at 1120°C, for both in liquid nitrogen (LN) and in relative humidity (RH). Inert failure strain distribution tightened as melting time increases. A clear trend of increase can be found in Weibull modulus. However, failure strain distribution in RH does not seem to have a melting time dependence, except that the Weibull modului of failure data at 4 hours is abnormally high. It can also be seen that the inert failure strains are much greater than failure strains measured in RH, whereas the Weibull modulus is smaller in LN than in RH. This indicates that the failure mechanisms for the two conditions are different.

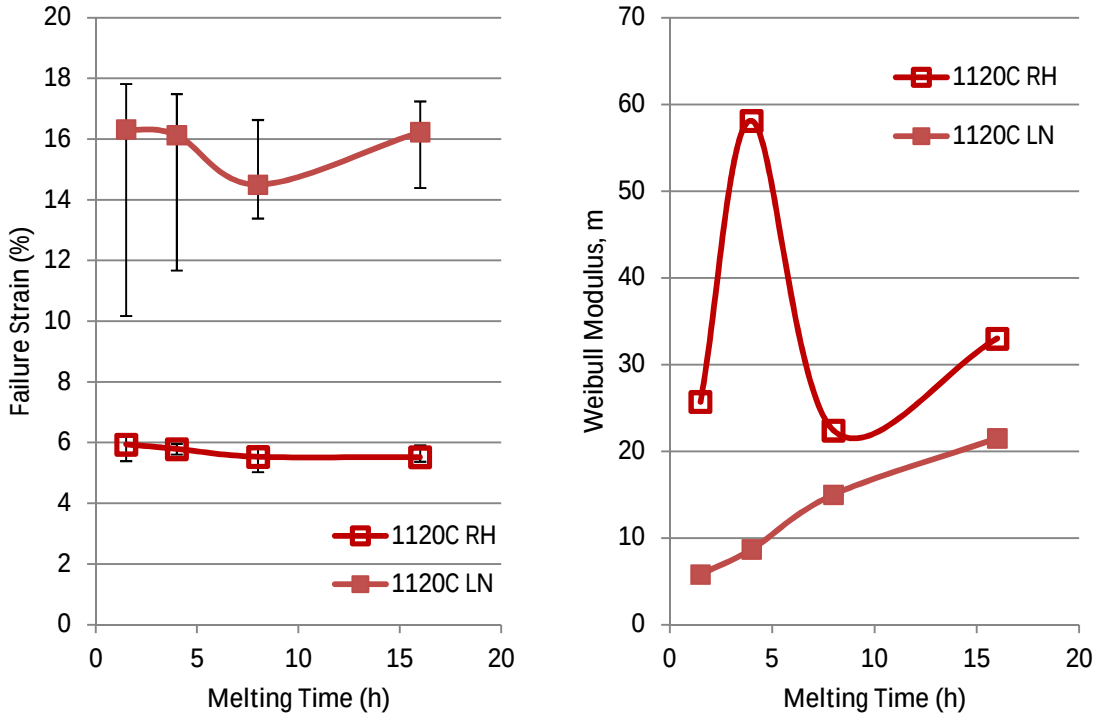

(a) (b)

Figure C.4. Melt history study for OI-A SLS glass melted at 1120°C, (a) Failure strain; (b) Weibull modulus of OI-A SLS glass fibers measured using TPB technique. Solid data points are measured in liquid nitrogen, open data points are measured in air at room temperature (21±2°C) with a relative humidity of 66±2%.

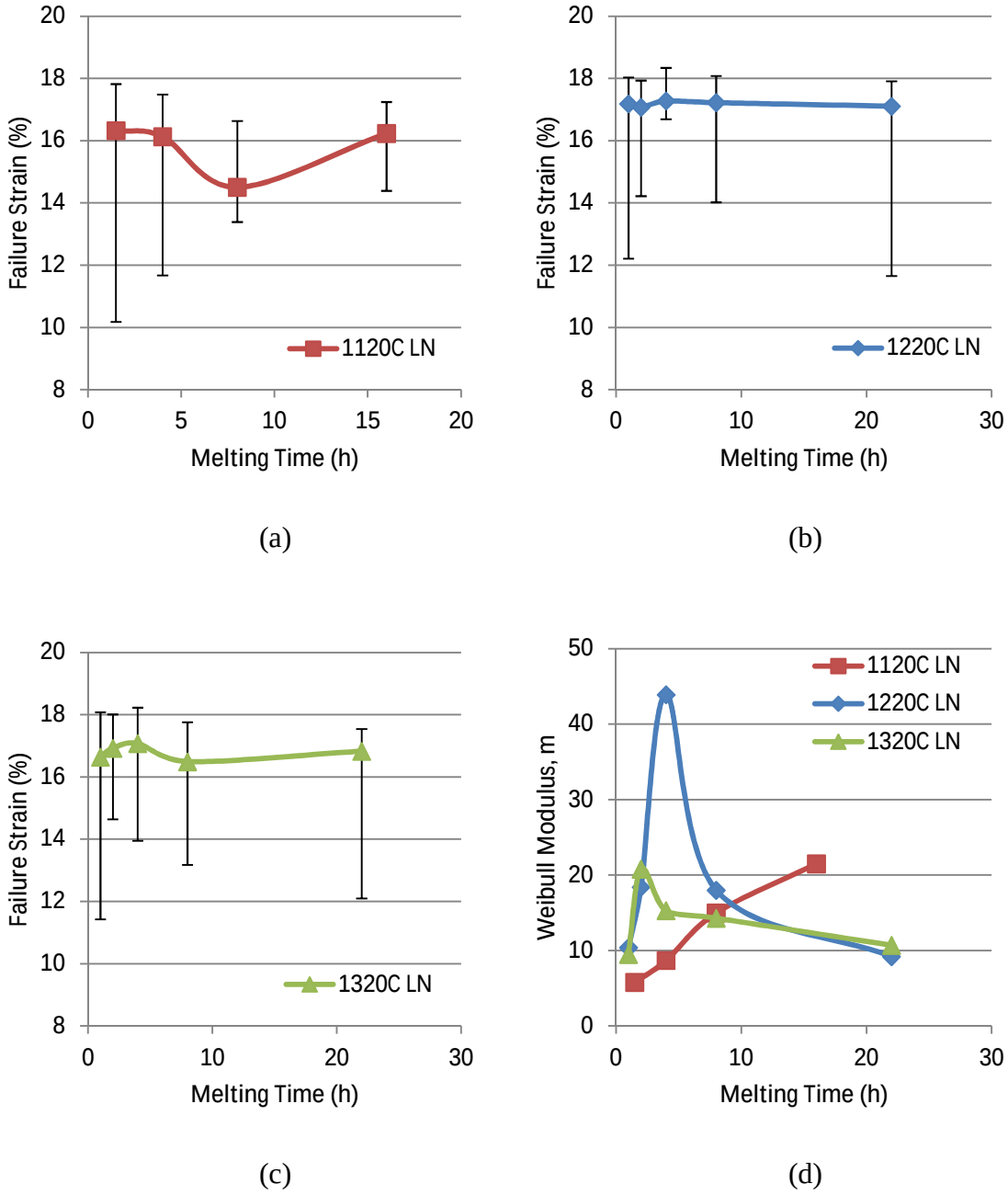

Figure C.5. Failure strain of OI-A SLS glass fibers measured in liquid nitrogen using TPB technique. Glass were melted at 1120°C (a), 1220°C (b), and 1320°C (c), for a certain period of time prior to fiber pulling. (d) Weibull modulus of corresponding data.

Figure C.5 shows the melting time dependence of the inert failure strains and the Weibull modulus for OI-A glass melted at 1120°C, 1220°C and 1320°C. The greatst failure strain in every distribution is lying at about 18%, which is probably the greatest

TPB failure strain for OI-A glass measured at this condition (LN, 4000 μm/s). If this value represents the inert failure strain of a 'perfect' homogeneous OI-A glass fiber, then any failure strain which is smaller than 18% is due to some structural flaw present in the bent region of a fiber.

The Weibull moduli at 1120°C increase with increasing melting time, while for 1220°C and 1320°C melts, the Weibull modulus reach their highest values at 4 and 2 hours respectively. The reason for the decreasing Weibull modulus is unknown.

A continuous melt history study is shown in Figure C.6. Fibers were drawn from the same melt held at different temperature for different length of time. Generally, the average failure strains pulled from melts conditioned at T_F or above T_L increased with increasing melting time. Air quench of melt resulted in a decrease in failure strain. The average failure strain melted below T_F decreased with increasing melting time.

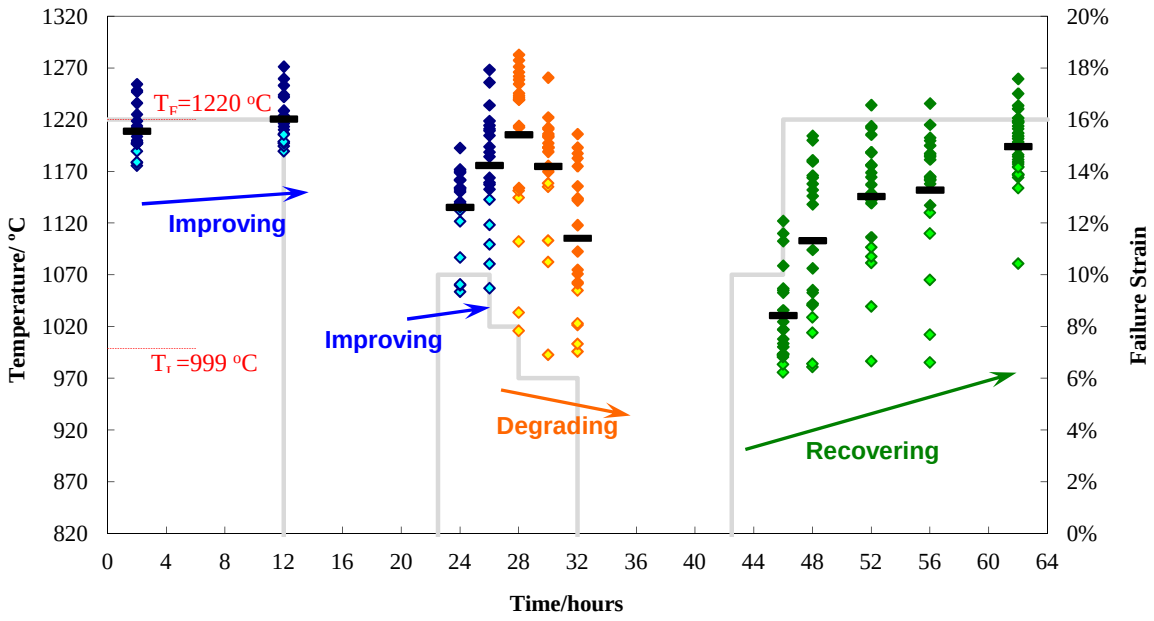

Figure C.6. Thermal history study of SLS container glass OI-A (grey lines show melt history, corresponding to left Y-axis; Colored symbols show failure strains, corresponding to right Y-axis; black bars represent average number of each set of data; highlighted open symbols represent five worst failure strains from each set of data).

The viscosity-temperature curves for 4 OI bottle glasses and 4 PPG fiber glasses were determined using a high temperature rotational viscometer. The 1000 P isokom temperatures, or the forming temperatures (T_F) are comparable to the available reported values from the glass providers. The liquidus temperatures (T_L) for 4 OI bottle glasses and 2 PPG fiber glasses were determined using a gradient furnace, and they are comparable to the available reported values from the glass providers.

Failure strains for OI-A soda-lime silicate glass fibers were determined using two-point bending technique. The failure strain distributions are dependent on the melt history of the glass prior to the fiber drawing. Melt history study are performed based on T_F and T_L for OI-A glass. It was observed that the inert failure strain distribution tightens with increasing melting time at a temperature close to T_F at the beginning, then the failure strain distribution starts to broaden. The reason for the broadening of the failure strain distribution is unknown. The melting history effect on inert failure strains was not observed on failure strains measured in room humidity. The small failure strains in broad inert failure strain distributions might due to some structural flaws which are not big enough to have an effect on failure strains measured in room humidity. When the glass is melted below T_L, inert failure strains decrease with increasing melting time. This degradation can be recovered by melting the glass above T_L.

Fibers drawn from glasses melted at T_F and below T_L are heat treated at its crystallization temperature. 'Bad' fibers (melted below T_L and yielded a broad failure strain distribution) grow more and bigger crystals on the surface than 'good' fibers (melted at T_F and yielded a tight failure strain distribution). This might indicates that the heterogeneities that are responsible for broad failure strain distribution can serve as nuclei in crystallization behavior. Further study has to be done to confirm this speculation.

Fibers etched in acid has smaller inert failure strains and tighter failure strain distribution, indicating that the etching process produced similar sized and evenly distributed flaws on the fiber surfaces. The existence of the 'low strain tail' suggests that the heterogeneities which are responsible for the broad failure strain distribution are located in the fiber instead of on the fiber surface.

REFERENCES

[1] A. A. Griffith, 'The Phenomena of Rupture and Flow in Solids,' *Phil. Trans. Roy. Soc.*, 22 163-198 (1921).

[2] R. E. Mould, "The Strength of Inorganic Glasses," pp. 119 to 149 in *Fundamental Phenomena in the Materials Sciences, V. 4: Fracture of Metals Polymers and Glasses,* by L. J. Bonis, J. J. Duga and J. J. Gilman (Ed.), PlenumPress, New York (1967).

[3] P. K. Gupta and C. R. Kurkjian, 'Intrinsic failure and nonlinear elastic behavior of glass,' *J. Non-Cryst. Solids*, 351 2324-8 (2005).

[4] B. A. Proctor, I. Whitney and J. W. Johnson, 'The Strength of Fused Silica,' *Proc. Roy Soc. A*, 297 534 (1967).

[5] V. P. Pukh, L. G. Baikova, M. F. Kireenko, L. V. Tikhonova, T. P. Kazannikova and A. B. Sinani, 'Atomic Structure and Strength of Inorganic Glasses,' *Phys. Solid State,* 47 [5] 850-5 (2005).

[6] W.A. Smith, T.M. Michalske, 'Inert Strength of Pristine Glass Fibers,' *Sandia Report*, SAND92-1107 (1993).

[7] N. M. Cameron, 'Relation Between Melt Treatment and Glass Fiber Strength,' *J. Am. Ceram. Soc.*, 49 [3] 144-8 (1966).

[8] C. L. McKinnis, and J. W. Sutton, 'The Glassmelting Process: II, Glass Structure and the Effects of "Melting History" on Glass Properties,' *J. Am. Ceram. Soc.*, 42 [5] 250-3 (1959).

[9] W. H. Otto, 'Relationship of Tensile Strength of Glass Fibers to Diameter,' *J. Am. Ceram. Soc.*, 38 [3] 122-4 (1955).

[10] R. K. Brow, N. P. Lower, C. R. Kurkjian, H. Li, "The Effects of Melt History on the Failure Characteristics of Pristine Glass Fibers," *Phys. Chem. Glasses, Eur. J. Glass Sci. Tech.*, 50 [1] 31-33 (2009).

[11] N. P. Lower, Ph D. Thesis, 'Failure Study of Glass Fibers,' Missouri University of Science and Technology, 2004.

[12] P. W. France, M. J. Paradine, M. H. Reeve, and G. R. Newns, "Liquid Nitrogen Strengths of Coated Optical Glass Fibers," *J. Mater. Sci.*, 15 825-830 (1980).

[13] M. J. Matthewson, C. R. Kurkjian, S. T. Gulati, "Strength Measurement of Optical Fibers by Bending" *J. Am. Ceram. Soc.*, 69 [1] 815-20 (1986).

APPENDIX D
FIBER HEAT TREATMENT

FIBER HEAT TREATMENT

It is discussed in Appendix C that the inert failure strain distributions are dependent on the melt history of the glass. It is possible that these weak points are due to 'Griffith' flaws [1] that are too small to be detected using nuclear magnetic resonance (NMR), atomic force microscopy (AFM) or scanning electron microscopy (SEM) [2].

A hypothesis is that such heterogeneities can serve as nucleation cites in crystallization process. If so, crystals can grow on these heterogeneities upon an appropriate heat treatment. A differential thermal analysis (DTA, Perkin-Elmer DTA7) is performed on about 100 mg of commercial soda-lime silicate flint clear bottle glass (OI-A) powders (<150 μm). Samples were heated in air in an alumina crucible at 2°C/min from 700°C to 1100°C in a . Figure D.1 shows that an exothermal peak at 880°C was detected and it is expected to be the crystallization peak.

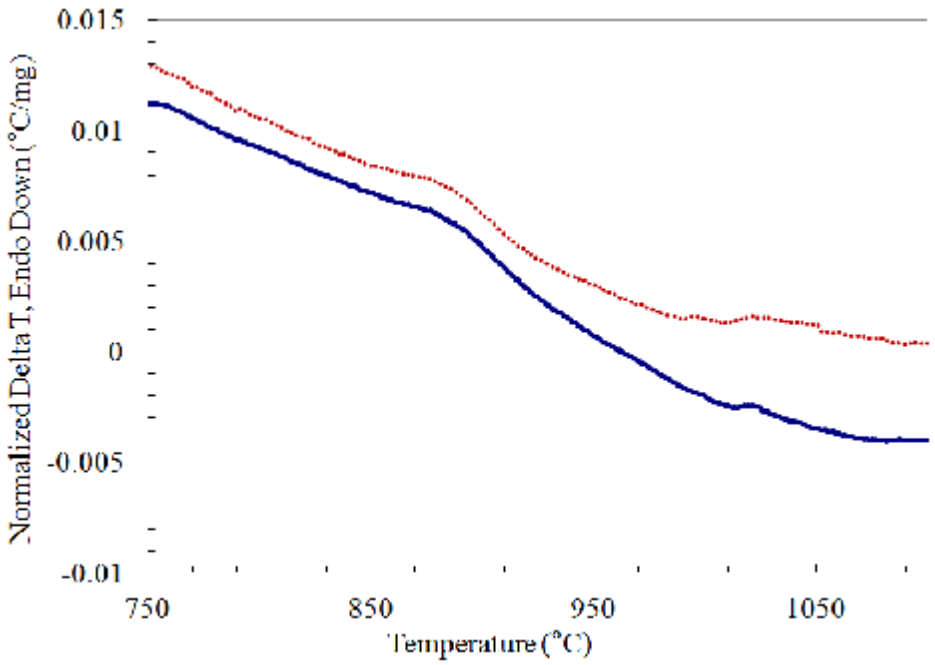

Figure D.1. DTA patterns of OI-A soda-lime silicate glass heated in air at 2°C/min (two identical runs).

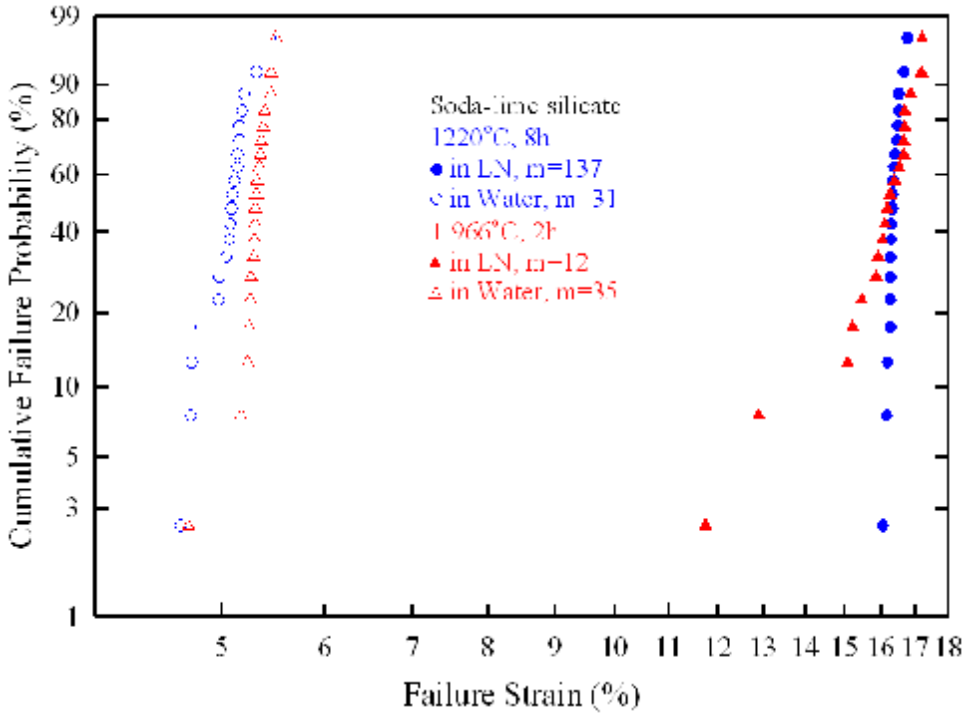

Figure D.2. Weibull distributions failure strains for OI-A soda-lime silicate glasses with different melting histories, failure strains were measured using two-point bend technique in 21°C distilled water and in liquid nitrogen (LN) at a faceplate velocity of 4000 μm/s.

Fibers with different melt histories and different failure strains were heat treated in a tube furnace at 880±2°C for 1 hour. The temperature is examined using a second thermocouple at the location of the fibers. Fibers are arranged in alternate way so that 'good' fibers and 'bad' fiber are scattered. Heat treated fibers were examined using an optical microscope (Nikon Optiphot-POL) (shown in Figure D.3).

Before heat treatment, there is no difference for 'good' fibers and 'bad' fibers under microscope. Both fibers look immaculate. After 1 hour of heat treatment, there are more crystals grown on the surface of 'bad' fibers and less on 'good' fibers, shown in Figure D.3. If these crystals are grown from the nuclei that are responsible for weaker fibers, this may indicate that the Griffith flaws are on the surface of the fibers. Assuming all Griffith flaws are on the surface of the fibers, such flaws can be eliminated by etching the fiber surface before failure test.

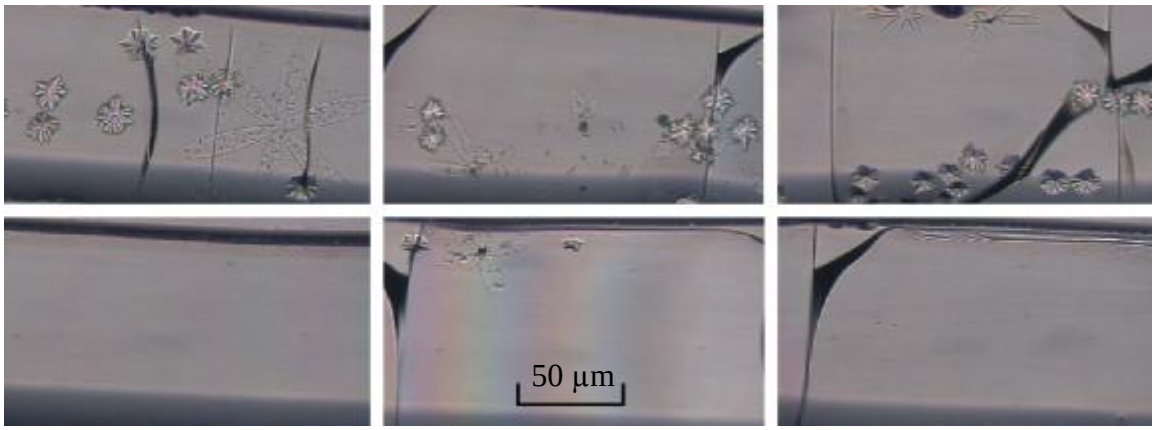

Figure D.3. Optical microscope images for heat treated fibers, upper three images from ‘bad’ fibers and bottom three images from ‘good’ fibers.

REFERENCES

[1] A. A. Griffith, ‘The Phenomena of Rupture and Flow in Solids’ *Phil. Trans. Roy. Soc.*, 22 163-198 (1921).

[2] N. P. Lower, Ph D. Thesis, ‘Failure Study of Glass Fibers,’ Missouri University of Science and Technology, 2004.

APPENDIX E
FAILURE STRAINS FOR ACID ETCHED FIBERS

FAILURE STRAINS FOR ACID ETCHED FIBERS

Etching test was performed on soda-lime silicate glass provided by Asahi Glass. The SLS glass sample was remelted in air in a platinum crucible at 1450°C for 4 hours. Fibers with a diameter of 125±20 μm were pulled from the surface of the melt at 1170°C using a fiber drawing system. After the fibers are drawn from the melt, they are etched in an acid solution (8% HF and 10% HCl in weight) for 30 seconds. After the etching, the fibers were washed by dipping in distilled water in the #1 bottle for 10 seconds, dipping in distilled water in the #2 bottle for 10 seconds, dipping in distilled water in the #3 bottle for 10 seconds, dipping in ethanol in the #4 bottle for 10 second, dipping in acetone in the #5 bottle for 10 seconds, and drying in the air. By dipping several times, acid on the surface can be removed. Water on the fiber surface is removed in ethanol and acetone. A control group of fiber were 'etched' using the same process but with distilled water replacing the acid solution, in order to rule out the effect of the extra handling effect on the fibers. Fiber diameters were measured before and after etching. An average of 3.3±0.5 μm decrease in diameter is recorded. Inert failure strains for etched fibers are shown in Figure E.1.

The failure strains for the original fibers and fibers 'etched' in water are almost identical, indicating that the extra handling does not have much effect on the inert failure strain. The greatest failure strain decreases from 18.0% to 13.4% after etching, and the medium failure strain decreases from 16.7% to 12.7%. It is suggested that the pristine surface of the fibers become etched and relatively coarse, after dipping in the acid. It is interesting that after etching, there are still 10% data points fall in the weak tail of the failure strain distribution, and the failure strain distribution below 10% probability for three sets of data are almost identical. This probably suggests that the Griffith flaws are in the body of the fibers.

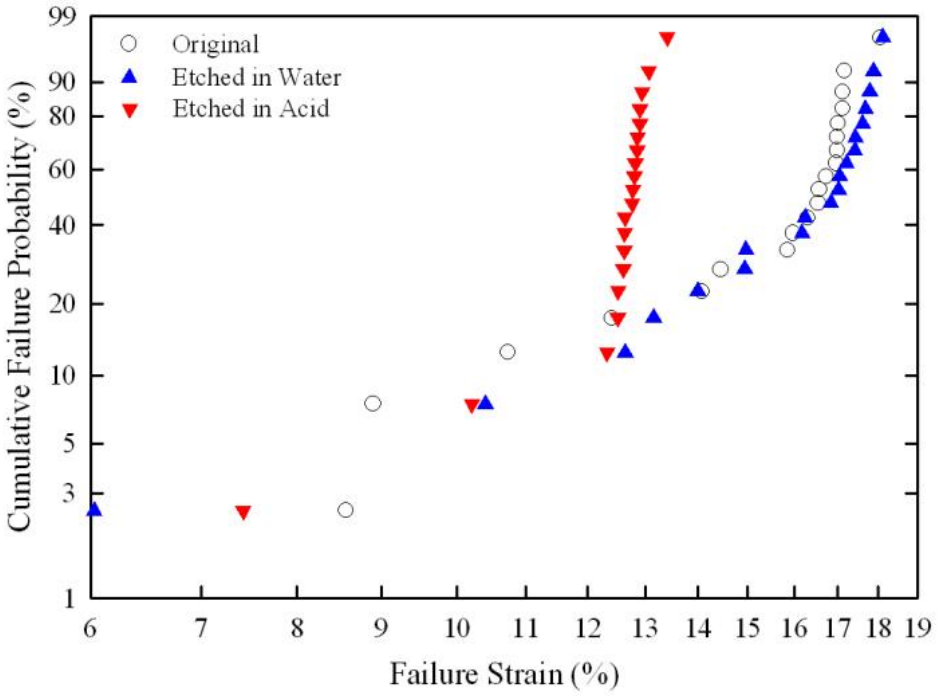

Figure E.1. Inert failure strains for etched soda-lime silicate glass fibers

APPENDIX F
RAMAN STUDY OF BENT FIBERS

RAMAN STUDY OF BENT FIBERS

The glass structure is believed to change when the glass is under stress. Using Raman (Horiba Jobin Yvon, LabRAM ARAMIS Confocal Raman Microscope) to exam a bent fiber which is under both positive and negative stress, a shift of the structure peak is expected to be discovered. A new custom-built two-point bending apparatus was designed to examine the bent fibers under micro Raman spectrometer (shown in Figure F.1). This apparatus is working as a small-sized two-point bender, with two polished parallel faceplates bending the fiber into U-shape.

Figure F.1. Two-point bend apparatus design for Raman spectroscopy.

In this study, a silica fiber with a diameter of 124 microns was bent into U-shape and tested under Raman spectroscope in air. The distance between two faceplates was 3.08 mm, providing a strain of 5.17% and a maximum stress of 3.7 GPa. Diode laser was focused on the stress-concentrated regions and the stress free region.

Figure F.2 shows Raman spectra of the stress-free, tensile, and compressive region of a bent fiber. We were able to observe peak shift in the 423 cm^{-1}, 482 cm^{-1}, 596 cm^{-1}, and 802 cm^{-1} bands. No significant shift observed at 1050 cm^{-1}. Generally, in tensile region, the Raman peak shifted to lower frequency; in compressive region, the Raman peak wave number shifted to higher frequency. Central force models predict that

under tensile stress, Si-O-Si angle increase, with decreasing frequency of 440 cm^{-1} and 800 cm^{-1} band, whereas under compressive stress, Si-O-Si angle decreases, with increasing frequency of 440 cm^{-1} and 800 cm^{-1} band.

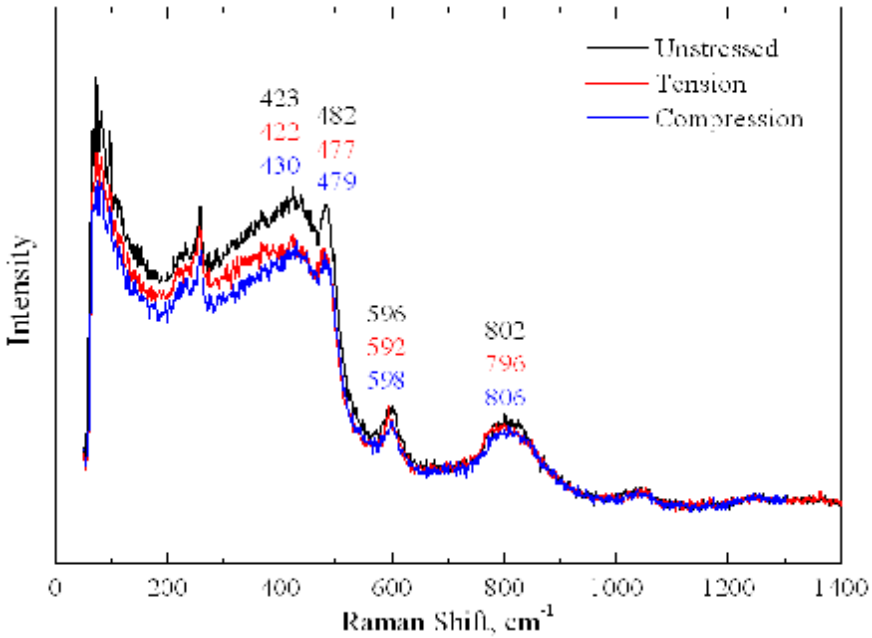

Figure F.2. Raman spectrum for silica fiber under stress.

This apparatus does not allow bending in liquid nitrogen or other inert conditions, thus the highest strain for silica without failure is ~5%. If it can be improved to allow bending in liquid nitrogen or other conditions, a silica fiber can be bent to >15% strain, and much more significant Raman peak shifts are expected.

VITA

Zhongzhi Tang was born in 1984 in Fuzhou, Fujian, China to Xiaozhong Ye and Dian Tang. He graduated from Fuzhou No. 1 Middle School in the spring of 2003. He attended Tianjin University in Tianjin China and graduated with his B.S. with the major in Applied Physics in the spring of 2007. He began his graduate study in August of 2007 at Missouri University of Science and Technology, under the supervision of Dr. Richard K. Brow. He worked mainly on the mechanical properties of glass and collaborated with several leading companies in the U.S. glass industry. He received a Ph.D degree in Materials Science and Engineering in December of 2011.